Vol. 293, No. 3, July 29, 1994
Completing Volume 293

ISSN 0003-2670

ANALYTICA CHIMICA ACTA

An international journal devoted to all branches of analytical chemistry

ELSEVIER

ANALYTICA CHIMICA ACTA

Scope. *Analytica Chimica Acta* publishes original papers, rapid publication letters and reviews dealing with every aspect of modern analytical chemistry. Reviews are normally written by invitation of the editors, who welcome suggestions for subjects. Letters can be published within **four months** of submission. For information on the Letters section, see inside back cover.

Submission of Papers

Americas

Prof. Harry L. Pardue
Department of Chemistry
1393 BRWN Bldg, Purdue University
West Lafayette, IN 47907-1393
USA

Tel:(+1-317) 494 5320
Fax:(+1-317) 496 1200

Computer Techniques

Prof. J.T. Clerc
Universität Bern
Pharmazeutisches Institut
Baltzerstrasse 5, CH-3012 Bern
Switzerland

Tel:(+41-31) 6314191
Fax:(+41-31) 6314198

Prof. Sarah C. Rutan
Department of Chemistry
Virginia Commonwealth University
P.O. Box 2006
Richmond, VA 23284-2006
USA
Tel:(+1-804) 367 7517
Fax:(+1-804) 367 8599

Other Papers

Prof. Alan Townshend
Department of Chemistry
The University
Hull HU6 7RX
Great Britain

Tel:(+44-482) 465027
Fax:(+44-482) 466410

Prof. Willem E. van der Linden
Laboratory for Chemical Analysis
Department of Chemical Technology
Twente University of Technology
P.O. Box 217, 7500 AE Enschede
The Netherlands
Tel:(+31-53) 892629
Fax:(+31-53) 356024

Prof. Paul Worsfold
Dept. of Environmental Sciences
University of Plymouth
Plymouth PL4 8AA
Great Britain

Tel:(+44-752) 233006
Fax:(+44-752) 233009

Submission of an article is understood to imply that the article is original and unpublished and is not being considered for publication elsewhere. *Anal. Chim. Acta* accepts papers in English only. There are no page charges. Manuscripts should conform in layout and style to the papers published in this issue. See inside back cover for "Information for Authors".

Publication. *Analytica Chimica Acta* appears in 16 volumes in 1994 (Vols. 281-296). *Vibrational Spectroscopy* appears in 2 volumes in 1994 (Vols. 6 and 7). Subscriptions are accepted on a prepaid basis only, unless different terms have been previously agreed upon. It is possible to order a combined subscription (*Anal. Chim. Acta* **and** *Vib. Spectrosc.*).
Our p.p.h. (postage, packing and handling) charge includes surface delivery of all issues, except to subscribers in the U.S.A., Canada, Australia, New Zealand, China, India, Israel, South Africa, Malaysia, Thailand, Singapore, South Korea, Taiwan, Pakistan, Hong Kong, Brazil, Argentina and Mexico, who receive all issues by air delivery (S.A.L.-Surface Air Lifted) at no extra cost. For Japan, air delivery requires 25% additional charge of the normal postage and handling charge; for all other countries airmail and S.A.L. charges are available upon request.

Subscription orders. Subscription prices are available upon request from the publisher. Subscription orders can be entered only by calendar year and should be sent to: Elsevier Science B.V., Journals Department, P.O. Box 211, 1000 AE Amsterdam, The Netherlands. Tel: (+31-20) 5803 642, Telex: 18582, Telefax: (+31-20) 5803598, to which requests for sample copies can also be sent. Claims for issues not received should be made within six months of publication of the issues. If not they cannot be honoured free of charge. Readers in the U.S.A. and Canada can contact the following address: Elsevier Science Inc., Journal Information Center, 655 Avenue of the Americas, New York, NY 10010, U.S.A. Tel: (+1-212) 6333750, Telefax: (+1-212) 6333990, for further information, or a free sample copy of this or any other Elsevier Science journal.
Advertisements. Advertisement rates are available from the publisher on request.

US mailing notice - Analytica Chimica Acta (ISSN 0003-2670) is published 3 times a month (total 48 issues) by Elsevier Science B.V. (Molenwerf 1, Postbus 211, 1000 AE Amsterdam). Annual subscription price in the USA US$ 3035.75 (valid in North, Central and South America), including air speed delivery. Second class postage paid at Jamaica, NY 11431. *USA Postmasters*: Send address changes to Anal. Chim. Acta, Publications Expediting, Inc., 200 Meacham Av., Elmont, NY 11003. Airfreight and mailing in the USA by Publication Expediting.

ANALYTICA CHIMICA ACTA

An international journal devoted to all branches of analytical chemistry

(Full texts are incorporated in CJELSEVIER, a file in the Chemical Journals Online database available on STN International; Abstracted, indexed in: Aluminum Abstracts; Anal. Abstr.; Biol. Abstr.; BIOSIS; Chem. Abstr.; Curr. Contents Phys. Chem. Earth Sci.; Engineered Materials Abstracts; Excerpta Medica; Index Med.; Life Sci.; Mass Spectrom. Bull.; Material Business Alerts; Metals Abstracts; Sci. Citation Index)

VOL. 293 NO. 3 CONTENTS JULY 29, 1994

(Continued overleaf)

Contents (continued)

ELSEVIER

Analytica Chimica Acta 293 (1994) 219–235

ANALYTICA CHIMICA ACTA

Performance advances in ion mobility spectrometry through combination with high speed vapor sampling, preconcentration and separation techniques

Jacek P. Dworzanski *, Man-Goo Kim [1], A. Peter Snyder [2], Neil S. Arnold [3], Henk L.C. Meuzelaar

Center for Micro Analysis and Reaction Chemistry, University of Utah, Salt Lake City, UT 84112, USA

(Received 20th October 1993; revised manuscript received 28th February 1994)

Abstract

Rugged, low weight, hand-held ion mobility spectrometry devices, initially developed for chemical warfare detection purposes, possess attractive characteristics as field-portable instruments for paramilitary (treaty verification, chemical demilitarization, drug interdiction, counterterrorism operations) and civilian (environmental monitoring, forensic characterization, process control) applications. Generally, however, such devices tend to exhibit limited resolution, narrow dynamic range, nonlinear response and long clearance times which severely limit their usefulness for qualitative and quantitative analysis of mixtures. To overcome these restrictions a prototype combined gas chromatography–ion mobility spectrometry (GC–IMS) unit was constructed by replacing the membrane inlet of a military IMS device known as the CAM (chemical agent monitor) with suitable front-end modules. These modules enable high speed automated vapor sampling (AVS), microvolume preconcentration/thermal desorption, and isothermal GC preseparation of analytes using a short capillary column while operating the IMS source and cell at subambient pressures as low as 0.5 atm. The AVS-GC–IMS methodology sharply reduces competitive ionization and facilitates identification of mixture components, thereby enabling quantitation of volatile and semivolatile compounds over a broad range of concentrations in air. At higher concentration levels (e.g. > 1 ppm) using the AVS inlet in automatic attenuation control (AAC) mode maintains excellent linear response. At ultralow concentration levels, e.g. < 10 ppb, a microvolume, trap-and-desorb type preconcentration module, maintains adequate signal to noise levels, thereby expanding the effective dynamic range of the method to approx. 6 orders of magnitude (100

* Correspondence to: J.P. Dworzanski, Center for Micro Analysis and Reaction Chemistry, University of Utah, 214 EMRL, Salt Lake City, UT 84112, USA.

[1] Present address: Department of Environmental Science, Kangweon National University, Chuncheon, 200-701 South Korea.

[2] U.S. Army Edgewood Research, Development and Engineering Center, Aberdeen Proving Ground, MD 21010, USA.

[3] Present address: FemtoScan Corporation, Salt Lake City, UT 84118, USA.

SSDI 0003-2670(94)00127-8

ppt–100 ppm). The resulting "hyphenated" GC–IMS technique has the potential of evolving into the first hand-portable, combined chromatography–spectroscopy instruments for field screening applications.

Key words: Chromatography; Ion mobility spectrometry; High speed vapor sampling; Preconcentration; Field-portable instruments

1. Introduction

In recent years the growing demand for rapid on-site screening of volatiles in air, headspace or fluegas samples with portable, rugged, user-friendly instruments capable of yielding at least semiquantitative results has revived the interest in ion mobility spectrometry (IMS).

In the 1980s military needs for defense against chemical agents spurred the development of rugged, hand-held IMS instruments characterized by low weight, small size and minimal power consumption. The relatively small cost of such instruments combined with their high sensitivity and speed of operation have made it possible for IMS based systems, such as embodied in the Graseby Ionics (Watford, UK) hand-held chemical agent monitor (CAM) to become the mainstay of military detection and monitoring strategies for chemical agents [1,2]. Presently, there is a widespread interest in extending the capabilities of such type of IMS instruments to various paramilitary (chemical demilitarization, treaty verification, drug interdiction, explosives detection) as well as civilian fields including forensic characterization [3], environmental monitoring [4] and process control applications. IMS devices operate at atmospheric pressure and rely on separation of ions in a uniform electric field on the basis of differences in their mobility. Most IMS technologies rely on ionization of vapor phase analytes by β-emitters such as ^{63}Ni due to the inherent simplicity and reliability of such sources. In the ^{63}Ni source a reservoir of reactant ions, both positive and negative, is formed that reflect the composition of the gas supplied to the ionization region. In purified nitrogen or air protonated water clusters $H^+(H_2O)_n$ as well as ions derived from some impurities, e.g., ammonium ions obtained by proton transfer, compose reactant ions [1,2,5] observed in IMS spectra during positive mode of operation as a strong signal, the so called reactant ion peak (RIP). Conversely, negatively charged molecular ions or their clusters with anions (e.g., superoxide, chloride), originating from the negative ion reservoir represented mainly by O_2^-, $O_2^-(CO_2)_n$ and $O_2^-(H_2O)_n$, are detected in the negative ion mode of IMS operation [1,2,5]. Ion–molecule clusters are formed at high efficiency, as the rate constants for the underlying atmospheric pressure ion–molecule reactions are generally proportional to the collision rates of the reagents. Ions formed in the reaction region are injected as a short pulse (ca. 200 μs) into a drift tube where they acquire constant velocities under the influence of a weak electrical field and collisions with a counterflowing neutral drift gas (air or nitrogen). Various ions injected into the IMS drift region will arrive at the Faraday cup detector at different times, as determined by their mass, charge and collisional cross section with a drift gas. Hence, the average velocities of ion species exposed to the same electrical field reflect the combined properties of the species and the drift gas. Consequently, different ion species, even if characterized by the same mass, may arrive at the detector at different times [6].

In their current form, CAM type devices (including related civilian or para-military IMS versions) are hand-held instruments equipped with a heated membrane inlet protecting the IMS cell from becoming contaminated with background constituents and reducing clustering complications from ambient water and ammonia. This inlet design provides some degree of control over both the type and amount of sample introduced into the detector but simultaneously reduces the scope of analytes to those compounds which can pass through a heated silicone membrane. Moreover, since silicone membranes undergo increasingly rapid air oxidation at temperatures above 150°C, this limits the size and polarity of the molecules which can be detected. In addition to

the restrictions imposed by the membrane, several inherent limitations of IMS itself become apparent when trying to analyze complex mixtures of atmospheric vapors, namely: (1) relatively low resolution, (2) mutual interference between analytes and/or background components, and (3) limited dynamic range [1,2,4–8]. However, the rugged design of the Graseby Ionics CAM as well as its nonmilitary "incarnations" makes this type of instrument especially attractive for a broad range of field-portable applications. Hence, the use of a gas chromatography (GC) based preseparation step offers a potential way to overcome the limitations of IMS systems imposed by the silicone membrane interface as well as the inherently low resolution and the mutual interference between analytes [9,10].

As early as in 1970 Cohen and Karasek [11] described a combined GC–IMS system. Although the earliest GC–IMS work depended on the use of packed GC columns, most of the studies published after 1980 have made use of capillary GC columns [12–16]. In the past few years Hill and co-workers [5,8], Eiceman [1] and, recently, Eiceman and Karpas [2] prepared comprehensive overviews of recent advances in IMS, including GC–IMS techniques.

Besides improving overall system resolution by providing a second dimension of separation while markedly decreasing the likelihood of interference between analytes and/or background components, the use of a short capillary GC column may enable detection of larger and/or more polar molecules than hitherto accessible to CAM technology provided that the silicone membrane is removed and the column outlet has direct access to the IMS ion source. In order to sample larger, and especially more polar, molecules directly from ambient air it is important to avoid contact with potential adsorption sites; e.g., relatively cold and/or otherwise strongly adsorbing surfaces. This may be facilitated by using a newly developed automated vapor sampling (AVS) device in which only deactivated fused silica and/or glass surfaces are present in the sample path. This type of inlet, which has been described in more detail elsewhere [17], has proved its efficiency in combination with transfer line GC–MS and GC–IR methods [17–19].

The concept of a compact air sampling GC–IMS system based upon the combination and integration of the Graseby Ionics CAM and short column GC has been developed in our laboratories and several prototype instruments were constructed and tested [9,10]. A prototype fabricated by Graseby Ionics (Watford, UK) is known as the environmental vapour monitor (EVM). The results of these initial studies indicate the effectiveness of such system for separation and identification of diverse chemical classes of compounds such as amines, alcohols, ketones, ethers, volatile carboxylic acids and their anhydrides, as well as phosphonates and polychlorophenols [9,10].

Responses of IMS detectors are characterized by relatively narrow linear ranges that usually do not exceed two orders of magnitude. Although, this phenomenon was recognized in the early days of analytical IMS the only solution proposed was based on the so called servo-inlet principle [20]. In the opinion of Eiceman and Karpas "this concept presents the best opportunity of all the proposals for extending the linear range in IMS response" [2]. However, to the best of our knowledge, results of experimental demonstrations of this concept have never been published.

In this paper we are reporting new modifications capable of improving the overall performance of the GC–IMS system, especially by expanding its apparent dynamic range for quantitative assessment of detected analytes. The enhancements described in this paper include: (1) a new GC–IMS interface module that improves GC separations; (2) a microvolume preconcentrator/thermal desorption module to achieve sensitivities in the mid ppt range; and (3) expansion of the apparent dynamic range to higher concentrations of analytes through a computer controlled variable sampling time technique, known as "automatic attenuation control" (AAC).

2. Experimental

2.1. Instrumental development

The main building blocks of the transfer line GC–IMS system are presented schematically in Fig. 1 and comprise: (1) microvolume preconcen-

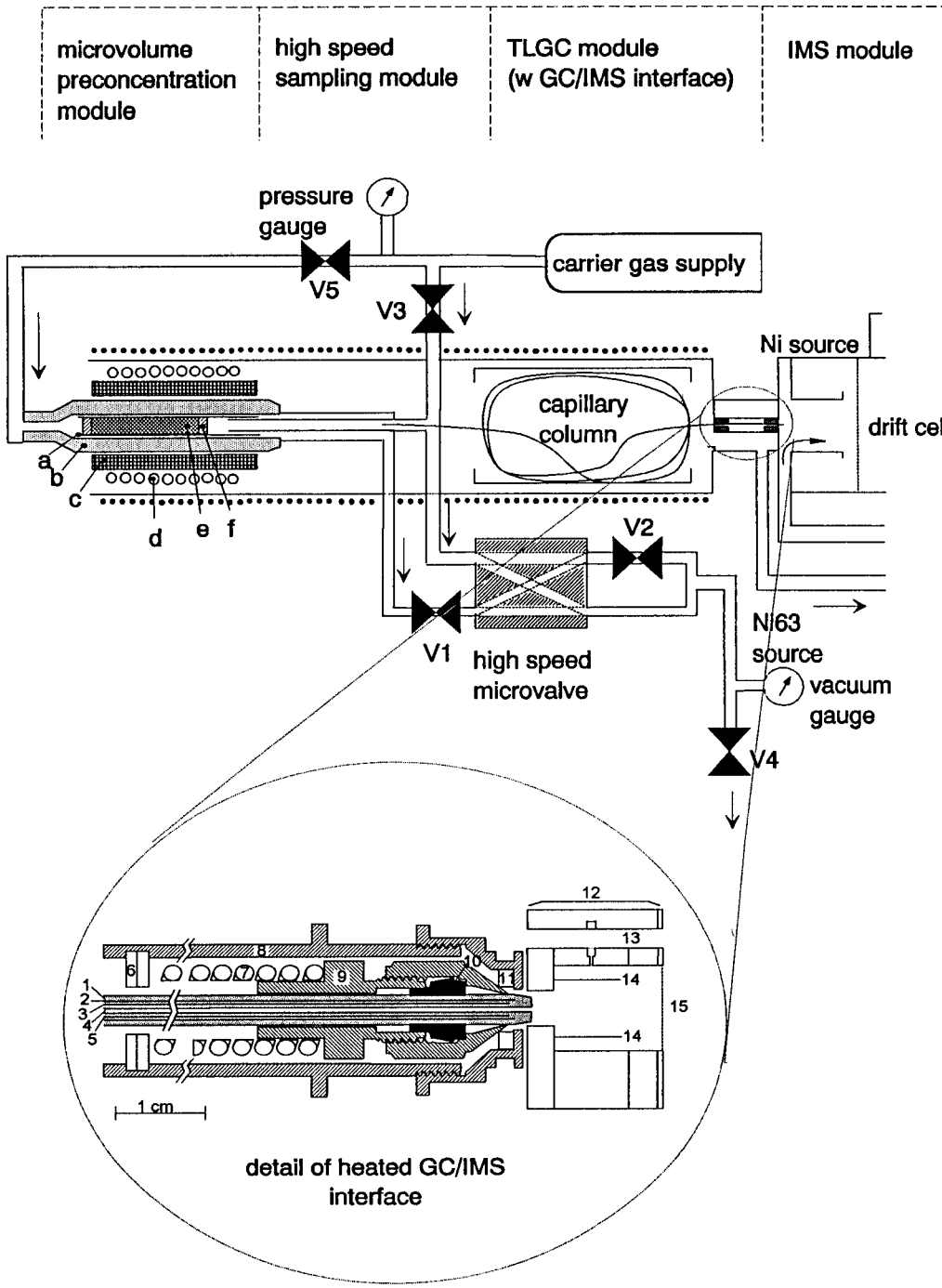

Fig. 1. Highly schematized cross-section through the AVS-TLGC–IMS prototype: (a) pyrofoil 315°C; (b) glass tube; (c) tungsten wire/ceramic tube heater; (d) high frequency induction coil; (e) Tenax-GR or -TA; (f) quartz wool; and schematic cross-section of GC/IMS interface: (1) heat shrink Teflon (TFE/FEP) tube; (2) glass tube; (3) thermocouple for measuring temperature of the column tip; (4) capillary GC column (transfer line); (5) thermocouple for resistive heating of the column tip; (6) spring clip; (7) spring; (8) stainless steel housing; (9) modified Swagelok union; (10) ferrule; (11) Kalrez O-ring; (12) PTFE ion source enclosure; (13) sweep gas flow channel; (14) ^{63}Ni foil; (15) ion gating grid.

trator/thermal desorption module, (2) automated vapor sampling (AVS) inlet module; (3) transfer line GC (TLGC) module with GC–IMS interface; and (4) modified (CAM-type) IMS module.

Microvolume preconcentrator / thermal desorption module

To achieve sensitivities in the low ppb and sub-ppb concentration range a microvolume preconcentrator was constructed and integrated with the remaining modules of the GC–IMS system. A borosilicate glass tube (i.d., 1.5 mm) was modified by insertion of a thin foil of a ferromagnetic alloy, characterized by a Curie-point temperature of 315°C (Pyrofoil, Japan Analytical Industry, Tokyo). Both ends of the insert were cylindrical and the middle region v-shaped. The latter region was filled with an adsorbent immobilized by two quartz wool plugs. About 8 mg of Tenax-TA (or 15 mg of Tenax-GR) from Chrompack (Raritan, NJ), previously conditioned at 350°C under flow of helium, were applied as adsorbents. The adsorption tube is surrounded by a ceramic heater and a high-frequency induction coil powered by a Fisher Labortechnik power supply (model 0310, 1 MHz, 1.5 kW) enabling fast heating rates of the foil and the adsorbent to the required temperature, as specified by the Curie-point of the metal foil. The solid-phase enriched analytes were thermally desorbed by inductive heating of the ferromagnetic foil, thus providing: (a) preheating of the carrier gas, (b) fast heating of the adsorbent, and (c) elimination of cold spots by heating the space between the adsorbent and the AVS inlet.

Automated vapor sampling inlet module

Analysis of gases or vapors of compounds that are present in the medium ppm(v) to ppb(v) range may be performed without a preconcentration step. Under such conditions the adsorption tube is replaced by an empty one that is directly exposed to the analyzed atmosphere and usually kept above 100°C to minimize adsorption phenomena during sampling. As shown in Fig. 1, the AVS device developed at the University of Utah (U.S. Patent 4,970,905) consists of three concentric tubes which function as a virtual (pneumatically switched) inlet valve. The AVS inlet operates at the same temperature as the "transfer line" module. The principle of the AVS approach has been described in more detail elsewhere [17]. Briefly, the 1.5 mm i.d. borosilicate glass tube represents the outermost tube while the intermediate tube consists of a 0.53 mm i.d., deactivated fused silica capillary column (Supelco) cut to extend beyond the end of the outer tube and approximately 2 cm beyond the end of the innermost tube, which represents the initial part of the capillary transfer line column (0.25–0.32 mm i.d., fused silica) to the ion mobility spectrometer. All fittings are standard or in-house modified stainless steel Swagelok-type connectors. The AVS technique enables rapid, repetitive introduction of ambient air and vapor samples into capillary GC columns operating at subambient outlet pressures, e.g., connected to an IMS cell operating at 50–300 Torr below ambient pressure. Moreover, sampling times of ambient air or vapors can be varied from 20 ms to 4 s by using a pulse timer and fast switching (5 ms) solenoid micro valve (Model K4M, Honeywell, Skinner Valve Division, New Britain, CT). The duration and repetition frequency of the injection pulses admitting sample aliquots onto the column are controlled by a software or hardware programmable power supply. The system is typically run with 10–30 ml min^{-1} of gas sampled through the large-diameter outermost tube and controlled by valve "V1". Between injections 12–15 ml min^{-1} of helium carrier gas flow, supplied via valve "V3", is expelled from the intermediate-diameter (0.53 mm) tube into this flow in order to prevent access of atmospheric components to the capillary column. During the injection the direction of the intermediate tube flow is reversed by a high speed microvalve to provide direct access to the head of the capillary GC column by gas atmospheres analyzed.

Transfer line GC module and GC–IMS interface

The "transfer line" GC module consists of a heated, cylindrical aluminum housing, which functions as an isothermal GC oven and a 2–3 m long fused silica capillary column (SPB-5 or DB-1, 320 μm i.d., 0.25 μm film thickness). The capillary column, also functioning as the transfer line

between AVS inlet and IMS module, is folded into a 3×8 cm cartridge positioned across the center of the aluminum housing. The short capillary column was operated under isothermal conditions at temperatures ranging from 25°C to 150°C, depending upon the type of target analytes. With a pressure drop ca. 50–300 Torr, the flow rates of helium as a carrier gas were in the 4–12 ml min^{-1} range for a 2 m column at 25°C. In order to make use of the existing nozzle connector design of the CAM while providing adequate support for the TLGC module, a special mechanical interface module was designed as shown in Fig. 1. To avoid cold spots in the TLGC column the interface has to be carefully heated. Unfortunately, due to space limitations, materials limitations and the necessity to minimize stray electrical fields, the choice of heating methods for the column tip was limited. The newly designed interface module, shown in Fig. 1 uses a 0.51 mm o.d. stainless steel sheathed, K-type thermocouple (Omega Engineering, Stamford, CT) for resistive heating of the column tip whereas a second thermocouple of the same type is used to monitor the temperature. Column and thermocouples are inserted into a 1.5 mm i.d. glass capillary tube and kept in place with a short length of a tube composed of heat shrink poly(tetrafluoroethylene)/fluorinated copolymer of ethylene and propylene (TFE/FEP; Small Parts Inc., Miami Lakes, FL). The column tip is generally operated a few degrees above the temperature of the isothermal GC module.

Ion mobility spectrometry module

The IMS instrument used in this study was a CAM (chemical agent monitor) type IMS device manufactured by Graseby Ionics, and especially modified by the removal of the regular inlet nozzle, the silicone membrane and the membrane heater unit, as shown in Fig. 1. Secondly, the flow paths of the 10 mCi ^{63}Ni source sweep gas and the cell drift gas were separated from each other (contrary to the original design) and flow meters were inserted into each flow path. Sweep and drift gas flows were not recirculated as in a regular CAM, but each gas stream was supplied separately from an external nitrogen cylinder equipped with molecular sieve and silica gel purification traps. Thirdly, the acetone dopant container and molecular sieve pack were removed, therefore, the ionization chemistry of the modified CAM was no longer based on acetone but simply on residual water from nitrogen. The small pneumatic pump unit controlling the membrane inlet flow was used instead as a vacuum pump for achieving pressures in the IMS cell in the range 50–300 Torr below the ambient pressure, which in our laboratory was usually about 650 Torr (about 1500 m above sea level). The reduced pressure is needed in order to maintain a sufficient pressure gradient across the GC column to provide an adequate driving force for a carrier gas flow. Naturally, as a consequence of the subambient IMS cell pressures, ion drift times were substantially shortened.

The drift tube was kept at room temperature. The remaining operating parameters for the modified CAM were established by the manufacturer and included a 12 mm long reaction region, a 39 mm long drift region, field gradient ca. 200 V cm^{-1}, shutter pulse width (180 μs), and shutter repetition rate (50 Hz). Signals were processed using digital signal averaging and all spectra were recorded using a 386-type IBM compatible PC equipped with a Graseby Ionics advanced signal processing (ASP) board and software. The number of scans and samples per spectrum were varied, depending on the requirements of the particular type of analysis.

2.2. Procedures

Generation of vapors

Vapor standards were prepared by dilution of the headspace vapors of studied compounds with a stream of clean air. Saturated vapors were obtained under temperature and pressure controlled conditions in a helium atmosphere and delivered via a short, deactivated 0.53 mm i.d. fused silica capillary column into an air stream inside of an all glass manifold. A ternary mixture of alkylphosphonates was prepared by mixing constituents, i.e., DMMP–DEMP–DIMP in a volummetric ratio of 2:4:5 to obtain equimolar concentrations of vapors in a head space. Vapor phase concentrations were changed by either varying the flow rate of a saturated vapor or the

flow rate of air, and were kept in the ppt–ppm range. The dilution system was allowed to equilibrate for a period of approximately 1 h before sampling was initiated. Vapor levels calculated on the basis of the known vapor pressure and the dilution factor applied were regarded as approximations and were confirmed by GC–MS analyses with a Hewlett-Packard model 5890 gas chromatograph (Palo Alto, CA) interfaced to a model 700 Ion Trap Detector (ITD, Finnigan-MAT, San Jose, CA).

Analysis of vapors using microvolume preconcentration / thermal desorption-GC–IMS

During the adsorption process the entrance to the borosilicate glass tube, designated as "b" in Fig. 1, was directly exposed to the atmospheric environment analyzed. That is, valve "V5" was closed and a carrier gas line disconnected from the preconcentration module. Flows through the adsorption tube during this stage were set in the range of 30–300 ml min^{-1} using a needle valve "V1" connected to a small vacuum pump. The microvolume preconcentrator tubes were generally kept at room temperature during the enrichment step. To protect the GC–IMS system during this stage against any compound, that could potentially be released from the preconcentrator, a carrier gas flow regulated by a needle valve "V3" was set at a level exceeding the flow through the GC column. Under such conditions that extra flow (ca. 5 ml min^{-1}) of a carrier gas is backflushed into a stream from the adsorbent, regulated by valve "V1". An additional part of the carrier gas released from valve "V3" was directed through valve "V2" and kept at a level of 0.5 ml min^{-1} to eliminate dead volumes and to purge the connections of the inlet. After completion of the enrichment process the inlet of the glass adsorption tube was coupled with a line of a carrier gas supplied via needle valve "V5" (as shown in Fig. 1), while valves "V1" and "V3" were closed, and the enriched analytes were thermally desorbed and analyzed by means of the GC–IMS technique.

Microvolume preconcentrator efficacy study

In order to test the efficacy of the microvolume preconcentration module used in the GC–IMS studies, the GC column exit was inserted via a heated transfer line directly to the vacuum of the ITD mass spectrometer instead of the IMS instrument. The adsorption tube of the microvolume preconcentrator/thermal desorption module was inserted into the sampling port of a dilution manifold and a known volume (up to 1.0 l) of air containing a known concentration of the analyte was passed through the tube at the rate of 30–150 ml min^{-1}. The adsorption tube was subsequently inserted into a Curie-point desorption "reactor" coupled to a GC capillary column and the analytes desorbed using a 10 s period of inductive heating.

Desorption step recoveries were tested with 1 μl injections of the same standard solutions in dichloromethane into a quartz wool plug on the head of the sorbent bed of the adsorption cartridge that was inserted in the Curie-point reactor and kept at room temperature under the flow of the carrier gas. To purge the solvent the flow of the carrier gas through the sorbent was increased to about 20 ml min^{-1} for a few minutes by a needle valve controlled splitter. After initial purging the splitter flow was set to 2 ml min^{-1} to keep the carrier flow through the desorption cartridge at 4 ml min^{-1}, and analytes were desorbed at 315°C by triggering power supply to the high frequency induction coil surrounding the tube. The whole process from the point of an injection up to arrival of an analyte was monitored by ITD. Usually, a short (5 m × 0.25 mm i.d.) fused silica capillary column coated with a 0.25 μm DB-5 phase (J&W Scientific, Folsom, CA) and highly purified helium as a carrier gas were used for analysis. The ITD was scanned from m/z 35 up to the mass of a molecular ion region of tested compounds at the rate of 4–8 scans per second and the total ion current chromatogram or selected m/z values were used for quantitations. The GC–MS system had been calibrated previously using a series of known concentrations of reference compounds in dichloromethane.

Direct GC–IMS analysis of vapors

Analysis of vapors in the ppb–ppm range of concentrations were performed using the system shown in Fig. 1 after closing valve "V5" and

replacing the preconcentrator with an empty glass tube. The entrance to this tube was directly exposed to the atmosphere analyzed that was sampled on the GC column by changing the flow direction in the intermediate tube of the AVS module using a high speed microvalve. The AAC experiments were performed using the computer controlled pulse duration and repetition frequency of the sampling sequence. The repetition frequency was selected on the basis of the time required to perform a GC analysis, i.e., to elute all sample components. The pulse duration, that can be varied from 20 ms to 4 s, was adjusted to avoid saturation of the IMS detector. The duration of vapor sample pulses entering the GC column can be selected manually, e.g., on the basis of the degree of RIP depletion in the IMS spectrum or automatically. In the latter case a special software written in FORTH and Assembler languages to control the vapor sampling timing of the AVS module [17] has been modified to receive IMS signal information from the Graseby Ionics software and hardware via D/A output from the ASP board and input back into the same personal computer via a Metrabyte DAS 16 data acquisition board. After an initial sample is admitted on the column using the shortest sampling time IMS responses are stored as background subtracted heights of the reactant and product (analyte) ion peaks during the chromatographic process, using preselected windows of drift times. As total detector response, integrated intensities of reactant ions depletion as well as direct product ions formed were utilized by a computer for setting the pulse duration of the next vapor sample. Such process is repeated automatically to reach a targeted level of detector responses by selecting an appropriate sampling time.

2.3. Chemicals and standards used

Chemicals were obtained directly from chemical suppliers and used without further purification. Dimethyl methylphosphonate (DMMP) and diethyl methylphosphonate (DEMP) were purchased from Aldrich (Milwaukee, WI), diisopropyl methylphosphonate (DIMP), dibutyl butylphosphonate (DBBP) and diethyl ethylphosphonate (DEEP) from Lancaster Synthesis (Windham, NH), and *o*-chlorophenol, 2,4-dichlorophenol, 2,4,5-trichlorophenol and phosdrin were purchased from Chem Service (West Chester, PA).

3. Results and discussion

3.1. Optimization of chromatographic conditions

Chromatographic preseparation using a short capillary GC column facilitates the removal of background contaminants from target compound signals while maintaining response times in the 10–30 s range [9,10]. The primary GC parameters for separation of potential contaminants interfering with the determination of a given target compound were optimized by mathematical modeling techniques [21] using the Golay equation [22]. Also, the more complex the mixture analyzed and the higher the concentrations and/or ionization efficiencies of the contaminants, the higher the average column resolving power is required to separate all interfering contaminants and/or analytes.

The relationship between column plate number (N) and the resolution of two adjacent GC peaks of similar intensity as a function of the ratio of their retention factors (k_2/k_1) is depicted in Fig. 2, illustrating the column performance needed to separate the target compound from potential contaminants before reaching the IMS ionization source. For example, only 10000 and 3000 plates are needed to separate two adjacent peaks representing compounds with a ratio of retention factors $k_2/k_1 = 1.04$ at the peak resolution levels of 1.0 and 0.5, respectively. As shown in Fig. 3b, such plate numbers are obtainable by using only 1–2 m long capillary columns. Relationships between key separation parameters at three different column radii are shown in Fig. 3a–c and indicate that a 3 m × 320 μm i.d column operated at an outlet pressure of 0.77 atm with nitrogen as a carrier gas can achieve the separation efficiency of about 3000 plates. Under these conditions, the retention time of a com-

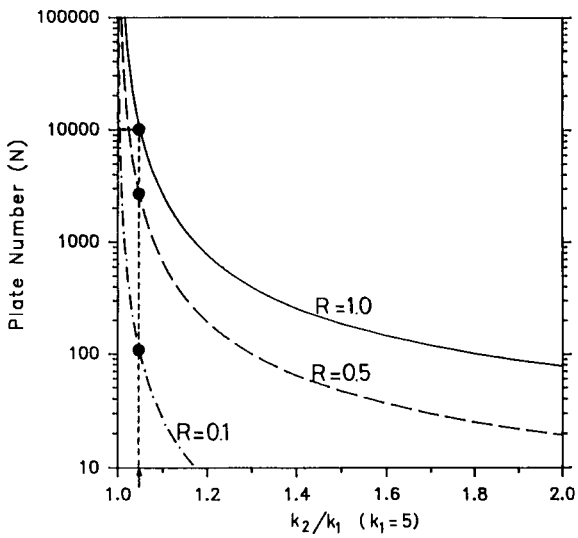

Fig. 2. Relationship between column efficiency (as expressed by the plate number, N) and the resolution (R) of two adjacent GC peaks as a function of the ratio of their retention factors (k_2/k_1).

pound with the retention factor $k = 5$ will be less than 20 s and the volumetric column flow will be about 6 ml min^{-1}. However, in order to achieve optimal sensitivity and response times, it is important to keep column flows above 5 ml min^{-1}. Nevertheless, it should be pointed out that the maximum of the column performance can only be reached by using a relatively short sampling time. Theoretical analyses indicate [21] that sampling times longer by a factor 2.35 than the intrinsic width (σ) of the GC peak, (where $\sigma = t_r/N^{1/2}$, t_r represents retention time and N is the plate number), will cause extra peak broadening, diminishing the theoretically achievable efficiency of the column. However, too short sampling times will lead to reduced detection limits caused by intrinsic column broadening [23].

3.2. *Qualitative and quantitative aspects of the AVS-GC inlet mode for IMS*

IMS has been shown to be a selective and very sensitive detection technique for monitoring vapors of air pollutants. However, systems with membrane type inlets, such as the CAM, are subject to serious limitations with regard to both qualitative and quantitative performance. Moreover, an ion mobility spectrometer, as any secondary ionization detector, exhibits nonlinear response with respect to the concentration of analytes introduced into the ionization chamber. Such response increases exponentially up to the depletion of the reactant ions that is observed as disappearance of the RIP peak in IMS spectra [1,2,5]. As shown in Fig. 4a, standard IMS sys-

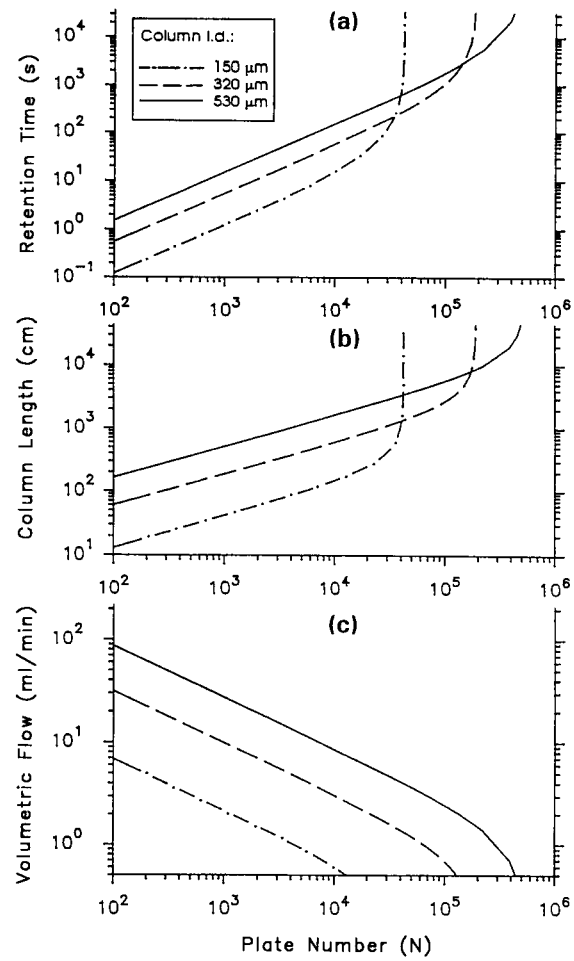

Fig. 3. Theoretical relationships between column plate number (N) and (a) retention time; (b) column length; and (c) volummetric flow rate for a model compound with the retention factor of 5, using 3 different internal diameters of the column and nitrogen as a carrier gas. Calculations are based on approximate values for N_2 carrier gas, using a diffusion coefficient of 0.1 cm^2/s and dynamic viscosity of 200 μpoise, while column inlet and outlet pressures are kept at 760 and 585.5 Torr, respectively.

tems are easily overloaded with analyte and have narrow linear response ranges. Each IMS spectrum in Fig. 4a was obtained at a different concentration of DMMP with 4 s sampling time in the positive ion mode. DMMP vapor concentrations of 20 and 60 ppb produce only peaks of the monomer ions. However, signals for the dimer and trimer ions of DMMP appear above 130 ppb. Furthermore, the intensities of the monomer and dimer ions are proportional to the DMMP concentration between 20 and 280 ppb, and between 130 to 1700 ppb, respectively. The intensity of the trimer ions shows a very narrow linear response range. In other words, high sample concentrations produce both dimer and trimer ion peaks which not only reduce the useful linear response range, but also produce more complex IMS spectra. Consequently, sample concentrations must be controlled with care in direct inlet IMS.

These results suggest that improvements in quantitative performance of IMS could be obtained by more precise control of the analyte amount submitted to the detector. It appeared that the AVS module could be used not only to secure an appropriate GC column performance but also to prevent the IMS source from overloading. Hence, we attempted to use an AVS module in a so called automatic attenuation control (AAC) mode of operation, i.e., to modify sampling time in relationship to the analyte concentration in the analyzed sample. The AAC concept of air monitoring by IMS takes advantage of short analysis times using TLGC–IMS and the computer controlled duration of the air sampling pulse by the AVS module. Assuming relatively slow concentration changes of analytes under real outdoor or indoor environmental monitoring conditions, a series of analyses may be performed using different amounts of an analyte, i.e., changing the volume of air "injected" on the column in order to find the optimum value and to protect the system from overloading. Thus, standard ionization conditions for an analyte in the ion source can be kept constant and are independent of the real analyte concentration for a broad range of concentrations.

In Fig. 4b IMS spectra for various concentrations of DMMP in air and at different sampling

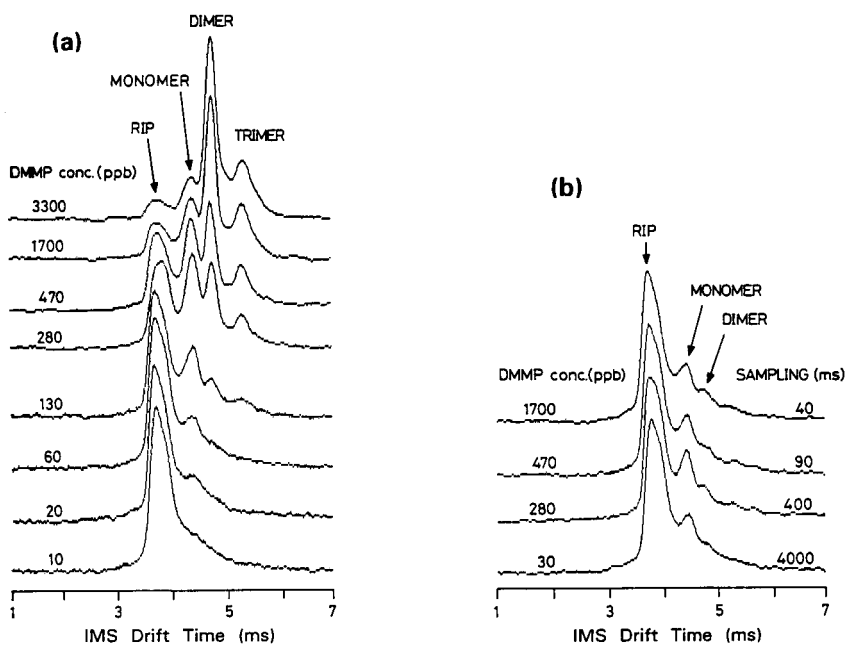

Fig. 4. (a) Variations in IMS spectra due to changes in DMMP sample concentration; (b) control of IMS overload by varying sample size as a function of AVS pulse length (AAC approach). RIP = Reactant ion peak.

pulse durations are gathered and contrasted with spectra taken at a constant sampling time (Fig. 4a). The IMS spectra of DMMP at 280, 470 and 1700 ppb, as shown in Fig. 4a, not only reveal monomer ion peaks, but also display strong intensities of dimer and trimer ion peaks when obtained at a fixed sampling pulse length of 4 s. However, in Fig. 4b only the monomer ions contribute to the major peak for DMMP vapor concentrations up to 1700 ppb when using the AAC type mode of operation for the AVS module.

Fig. 4 illustrates the nature of the AAC approach based on manual variation of sampling time to maintain a fixed IMS spectral response. The automation of such responses requires a peak height detection algorithm which will limit sampling time for concentrations exceeding a preset intensity level. In practice, a targeted response level is determined by specifying the depletion level of the RIP peak, which in our case was selected as 50% of its background level, and a sampling time that should be shorter than the intrinsic broadening caused by the GC–IMS system, as discussed earlier in this paper. Using DMMP in air at the concentration of 900 ppb(v) as a reference calibration standard, our system met the above criteria by selecting 1 s long sampling time that was equivalent to a reference sampling volume (V_{ref}) of 150 μl under the conditions used for construction of the response curves presented in Fig. 5. So, the sampling volumes for higher DMMP concentrations could be automatically selected on the basis of sequential sampling and analysis trials, and responses (R^*) calculated using the following formula:

$$R^* = RV_{ref}/V$$

where R is the "real" detector response and V represents the volume chosen by the computer on the basis of consecutive analysis and computations to obtain the desired targeted response level. Hence, in our approach, responses (R^*) include both the real IMS signal for the analyte as well as a volume of the air "injected" for analysis determined by the AAC algorithm.

The results shown in Fig. 5 illustrate the extended linear response curves for higher concentrations of DMMP constructed on the basis of

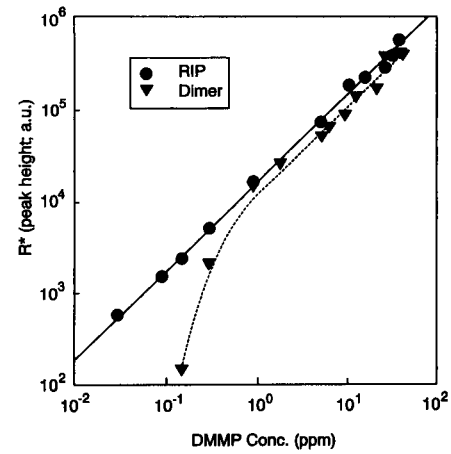

Fig. 5. Response curves for DMMP in air illustrating the use of reduced sampling time (AAC principle) at higher analyte concentrations to prevent IMS overloading. Experimental points represent corrected peak heights, expressed in arbitrary units (a.u.), for $[(DMMP)_2H]^+$ signals (dimer) and the depletion of the reactant ion peak (RIP) heights obtained by averaging of 7–15 determinations. * For calculation of corrected responses (R^*) and explanations, see text.

such automatic attenuation control procedure. The lower, dashed curve represents responses recorded in the window of drift times characteristic for DMMP dimer ions, i.e., $[(DMMP)_2H]^+$, while the upper, solid line reflects the responses calculated for the RIP. Both curves are linear and exhibit an acceptable level of reproducibility and accuracy above ca. 0.9 ppm(v) level, where decreasing of the sampling time up to 40 ms is applied to prevent overloading of the IMS instrument and allows to expand its practical dynamic range. However, for lower concentrations of DMMP only RIP responses remain linear up to the determination level, i.e., ca. 20 ppb(v), while dimer signals rapidly disappear because they are replaced by monomer ions that dominate DMMP spectrum in this range of concentrations (Fig. 4a).

Recent tests with CAM type IMS systems indicated that lower detection limits for alkylphosphonates are in the 10–100 ppb range using the regular heated membrane inlet mode [22]. In this mode, total inlet flows on the outside of the membrane are typically around 500 ml min^{-1}. Assuming a 3–5% collection efficiency of organic vapor molecules through the heated (70°C) mem-

brane, this amounts to an effective air sampling rate of 15–25 ml min^{-1}. In the membraneless capillary GC mode, total column flows are approximately 10 ml min^{-1} when using a 2 m × 320 μm i.d. column at an inlet/outlet pressure ratio of 1.8, corresponding to approximately half of the effective air sampling rate in the membrane sampling mode. Minimum detectable alkylphosphonate (DMMP) concentrations in the GC inlet mode were found to be in the 20–40 ppb range (Fig. 4a), which agrees quite well with the relative effective sampling rates.

Fig. 6 illustrates some advantages of operating an IMS in the AVS-TLGC mode in comparison to the membrane inlet for air analysis of equimolar mixture of model alkylphosphonates. The IMS spectrum of the ternary mixture of alkylphosphonates without GC preseparation, i.e., in the case of a membrane type inlet reveals several mixed ion peaks (e.g., DMMP + DEMP and DEMP + DIMP, etc.) in addition to monomer, dimer and trimer formation by particular components as shown in Fig. 6a. It should be noted that β-radiation induced ambient pressure ionization processes are concentration dependent, as illustrated by the phenomena shown in Fig. 4a, as well as competitive with respect to sequestering of charge by analytes. The latter property is especially manifested at lower reactant ion concentrations. Hence, taking into account the existing differences in proton affinities of the various alkylphosphonates and the resulting changes in proton transfer equilibria for mixed samples, particular mixture components are not necessarily ionized at rates proportional to their relative concentrations.

In Fig. 6b the IMS spectrum of the same mixture as in Fig. 5a is presented, however, this time obtained by averaging 32 scans recorded after AVS "injection" on a 2 m long capillary column. Preseparation by TLGC introduces each mixture component separately into the ion source. Therefore, relative intensities of particular component signals clearly reflect the composition of the original mixture since no mixed ion peaks or competitive ionization processes are observed. All individual IMS spectra recorded after sampling the analyte mixture are presented in Fig. 6c in

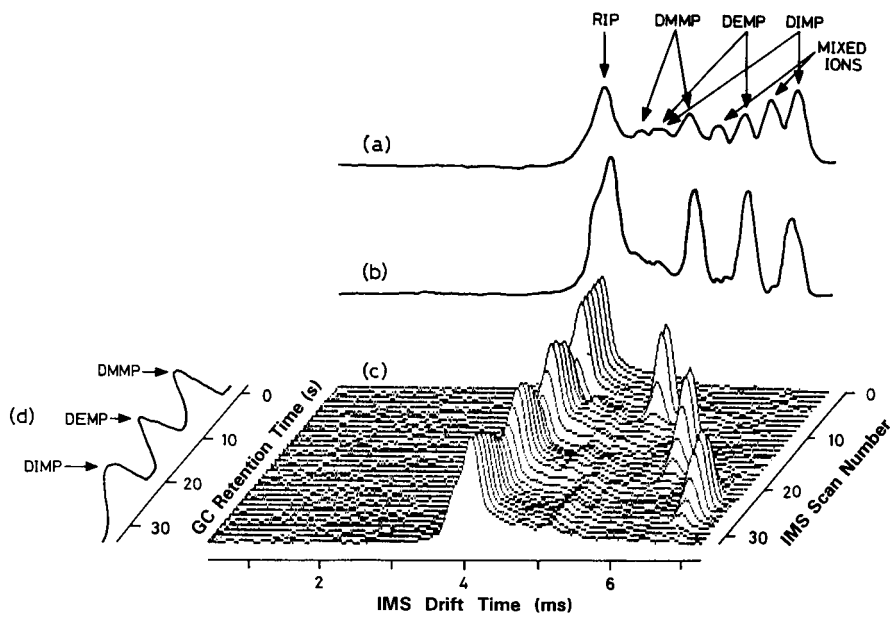

Fig. 6. Comparison of a direct and an AVS-GC–IMS inlet mode: (a) direct inlet IMS spectrum of three methylphosphonates (without TLGC preseparation); (b) sum of the 32 ion mobility scans from the GC–IMS spectra of the methylphosphonates shown in (c); (c) quasi 3-dimensional "waterfall" display of a GC–IMS profile; (d) chromatogram of the GC run shown in (c).

the form of a pseudo-three dimensional "waterfall" graph. Furthermore, a reconstructed transfer line gas chromatogram of this ternary mixture, obtained by summing all ion current intensities at drift times between 5 and 7 ms is shown in Fig. 6d. It is clear that a 2 m long capillary column provides sufficient resolving power to produce base line separation of the ternary mixture components within 30 s, simplifying ionization processes and dramatically improving qualitative and quantitative capabilities of the CAM for analysis of mixtures.

The use of short, fast separation columns reduces many problems associated with analysis of complex mixtures, however, under "real world" conditions coeluting compounds will be inevitable in the IMS. Although IMS responses to coeluting compounds represent a complex issue, that is out of the scope of this paper and require further studies; in many cases IMS demonstrates its potential for dealing with such situations. An example of GC–IMS analysis of a quaternary alkyl phosphonate mixture shown in Fig. 7 indicates that despite successful separation of DMMP, DEMP and DIMP, the latter compound coelutes with the fourth component, i.e., DEEP. Nevertheless, in this case both monomer as well as dimer ions formed from coeluted components are characterized by different mobilities, caused by differences in collision cross sections and can be easily distinguished.

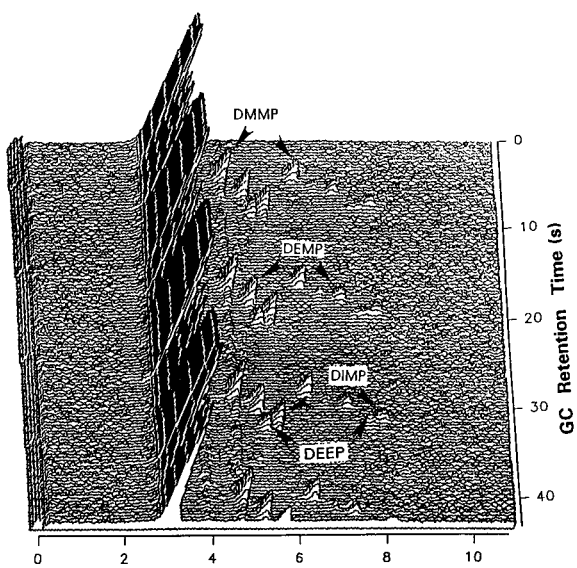

Fig. 7. Quasi 3-dimensional ("waterfall") display of GC–IMS profiles of a mixture of four alkylphosphonates analyzed repetitively at 12 s intervals.

3.3. Adsorption / thermal desorption with microvolume Tenax cartridges

Adsorption with microvolume (ca. 40 μl) Tenax cartridges followed by direct desorption to a fused silica capillary column without any refocusing on the thin film of the column represents a very demanding approach because both adsorption and especially desorption parameters must be carefully optimized to achieve desired results, i.e., good recoveries and narrow desorption profiles of analytes. However, when the sample volume is of the order of a liter or less, a small bed volume of the adsorbent may often suffice. Moreover, a microvolume cartridge alleviate the need for the high temperature and comparatively long desorption times required for larger cartridges. Naturally, careful attention must be paid to the sampling conditions to achieve full recoveries of analytes.

Taking into account that we are using 60–80 mesh Tenax particles with a column bed length of ca. 20 mm, with a volummetric flow up to 150 ml min^{-1} during the enrichment step, an approximate plate number can be calculated from the dimensionless Knox equation [24]: $h_r = A\nu^{1/3} + B/\nu + C\nu$, where h_r and ν represent the reduced plate height and the reduced velocity, respectively, and values for constants A, B, and C according to Guiochon [25] are $A = 3$, $B = 1.5$, and $C = 0.05$ under typical conditions. The reduced plate height, h_r, is defined as $h_r = h/d_p$, where h and d_p represent plate height and the diameter of Tenax particles, respectively, and the reduced velocity (ν) represents the following expression, $\nu = ud_p/D_M$, where u is the linear velocity, and D_M is the diffusion coefficient of analyte in the mobile phase (air). The results obtained indicate that under the described sampling conditions, the Tenax cartridges have about 6–12 theoretical plates.

Lovkvist and Jonsson [26] have shown that for preconcentration columns with low plate numbers (N), the breakthrough volume (V_B) as a function of the retention volume (V_R), the breakthrough level (b), and the plate number can be to a good approximation described by the expression $V_B = V_R[(1-b)^2 + a_1/N + a_2/N^2]^{-1/2}$. Numerical values for coefficients a_1 and a_2 in this equation, which are complicated functions of the breakthrough level, were tabulated [26] and (assuming 1% as a reasonable value for the breakthrough level) should be taken as $a_1 = 13.59$, and $a_2 = 17.60$. Hence, we can calculate the breakthrough volume for our cartridges as ca. 0.52–0.67 of the retention volume for a given analyte. The calculated retention volumes of the alkylphosphonates were in the range of 7–14 l at room temperature, hence, we were unable to detect any breakthrough by sampling only up to 1.0 l of vapors in air.

The initial tests were performed with a GC–MS system to confirm the accuracy of air concentrations of studied compounds and allowed for verification of desorption profiles generated by Curie-point flash heating of the microvolume preconcentrators. The accuracy of DMMP concentrations in air was determined on the basis of recovery studies and indicated that for the ppb–ppm range of concentrations recoveries were characterized by an average value of 103%. The relative standard deviation (R.S.D.) which expresses the precision was 4.6%. For the ppt range of concentrations differences between values expected on the basis of known vapor pressures and dilution factors applied were even higher than 200%, however, R.S.D.s were still below 10%. Hence, all values of DMMP air concentrations

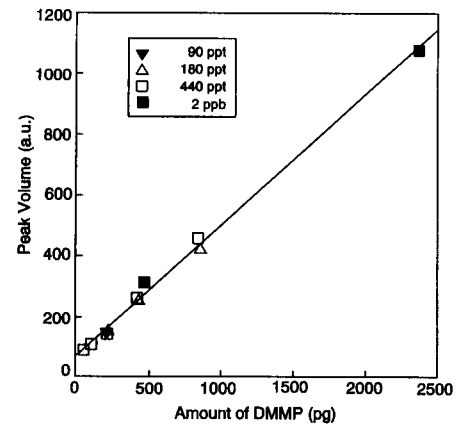

Fig. 8. Response curve for dimethyl methylphosphonate (DMMP) obtained via GC–IMS with the Tenax-GR microvolume preconcentration module and rapid desorption at 315°C. Responses represent peak volumes (using arbitrary units, a.u.) and the amounts of DMMP were determined from the sampling volume for each concentration of the analyte in air.

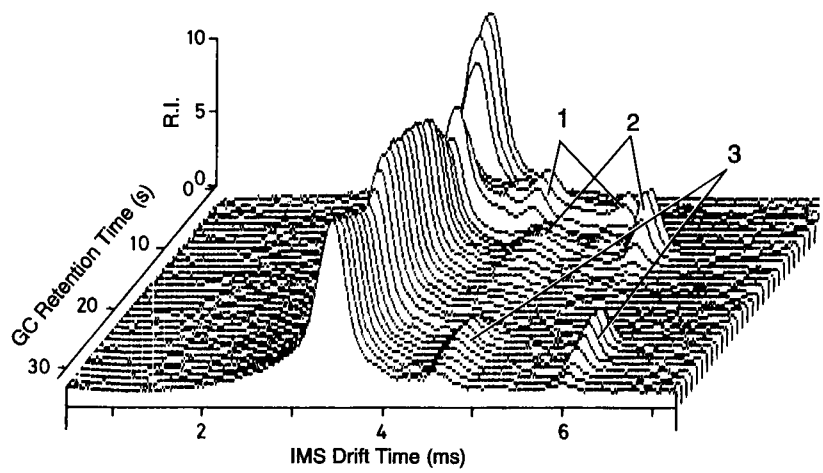

Fig. 9. Quasi 3-dimensional display of TLGC–IMS profiles of the chlorophenol mixture: 1 = *o*-chlorophenol; 2 = 2,4-dichlorophenol; 3 = 2,4,5-trichlorophenol. Conditions: negative ion mode; drift tube pressure 360 Torr; drift gas: air at 400 ml min^{-1}; column: 2 m × 0.32 mm i.d., 0.25 μm DB-1, temperature, 80°C.

and amounts adsorbed by the microvolume preconcentrator presented here are based only on GC–MS determinations. The studied compounds were desorbed in less than 2 s under flow conditions identical to the desorption setup used for the GC–IMS system, using a 5 m long capillary column kept at 200°C and coupled to the ITD.

In Fig. 8 a response curve for DMMP is presented that was constructed by plotting volumes of peaks recorded, using the positive mode of IMS operation, by desorption of picogram quantities of the analyte. Known amounts of this phosphonate, which is frequently used as a simulant of chemical warfare agents, were preconcentrated through sampling at the rate of 150 ml min^{-1} using various volumes of DMMP vapors in air and generated at four different concentration levels in the range 90 ppt(v) to 2 ppb(v). Responses of the IMS detector were linear from 40 to 2200 pg of DMMP desorbed from the Tenax-GR cartridges ($r = 0.998$, $n = 11$) and detector sensitivities (S), calculated per unit concentration of DMMP in the mobile phase, were characterized by the relative standard deviation of 10.9%. The results obtained demonstrate satisfactory precision and good repeatability of the proposed method, based on preconcentration followed by fast thermal desorption and GC–IMS determination, for trace analysis of DMMP vapors.

3.4. Application examples of TLGC–IMS

Fig. 9 shows a pseudo-three dimensional plot of TLGC–IMS data for a ternary mixture of chlorophenols (*o*-chlorophenol, 2,4-dichlorophenol and 2,4,5-trichlorophenol) in the negative ion detection mode. *o*-Chlorophenol and 2,4-dichlorophenol were eluted from the TLGC module with GC retention times of 5 and 10 s, respectively. Although, peak tailing was observed for 2,4,5-trichlorophenol, due to its relatively high polarity, elution from the TLGC column was observed within 35 s at an isothermal column temperature of 80°C and the relative pressure (P) of 1.9. These toxic chlorophenols are usually analyzed by GC-ECD or GC–MS [27] which requires long analysis times and thus tends to be relatively expensive. However, as demonstrated here these types of chlorophenols can be analyzed rapidly by means of TLGC–IMS.

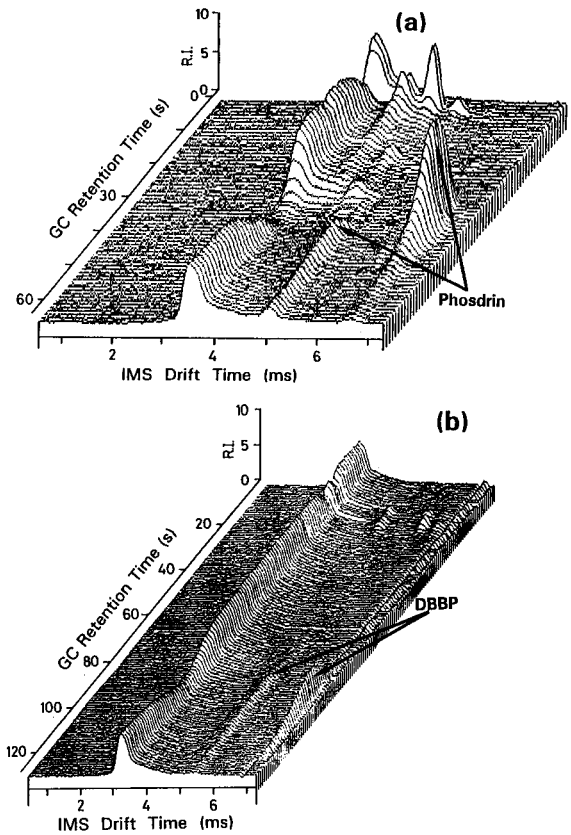

Fig. 10. Pseudo 3-dimensional display of TLGC–IMS spectra of (a) phosdrin; (b) dibutyl butylphosphonate (DBBP). Both analyses were performed under the following conditions: positive ion mode; drift tube pressure 340 Torr; drift gas: nitrogen at 400 ml min^{-1}; GC column: 2 m×0.32 mm i.d., 0.25 μm DB-1; temperature, 80°C.

Organophosphorus type insecticides are used throughout the world, and are known to persist for up to several weeks or months in the environment [28]. Vapors of organophosphorus pesticides are generally known as toxic. Vapors of phosdrin, an organophosphorus pesticide with an molecular weight of 224, were analyzed by short column GC–IMS at a column temperature of 80°C and the relative pressure (P) of 1.9, and the results are shown in Fig. 10a. The IMS intensities at the GC retention times shorter than 27 s

probably represent decomposition products of phosdrin. The predominant IMS intensities were observed at a GC retention time of 30 s and appear to represent ions of the monomer/dimer pair of phosdrin. GC–IMS spectra of dibutyl butylphosphonate (DBBP) are shown in Fig. 10b. DBBP is a vapor pressure matched simulant for *O*-ethyl-*S*-2-diisopropylaminoethyl methylphosphonothiolate (VX), which is the largest and least volatile of the common nerve agents. IMS signals representing contaminants of the commercial sample of DBBP were observed at GC retention times of approximately 20 s, whereas the monomer and dimer peaks for DBBP completely eluted from the TLGC column (80°C, $P = 1.9$) within 2 min. Although the monomers of DBBP and phosdrin have different GC retention times, they exhibit nearly identical IMS drift times (approx. 5 ms) under similar conditions ($P = 1.9$, 100 ml min^{-1} of drift gas flow). Obviously, without GC preseparation phosdrin can interfere with IMS analysis of DBBP (simulant of VX).

4. Conclusion

Preseparation by TLGC greatly enhances the capability of IMS to distinguish between different chemical compounds, especially when present in a mixture. In combination with high speed vapor sampling, using the AVS method, TLGC preseparation markedly reduces the nonlinear effects of competitive ionization phenomena while expanding the dynamic range of IMS into higher concentration levels, especially when the IMS module is used in AAC mode. Furthermore, use of a microvolume preconcentration module enables the use of GC–IMS methods at sub-ppb concentration levels. Altogether, an effective dynamic range spanning 6 orders of magnitude (100 ppt–100 ppm) appears achievable.

Although considerable further work needs to be done to integrate the various modules into a compact, reliable, user-friendly system no significant scientific or technological hurdles appear to prevent AVS-TLGC–IMS from developing into the first generation of handportable, "hyphenated" analytical instruments.

Acknowledgments

The authors wish to thank Steve Harden, Dave Blyth and Gary Eiceman for helpful discussions and advice and John Parsons, Rob Howard and Dennis Davis for professional technical assistance. This work was funded by CRDEC (contract No. DAAA15-90-C-1014) and Battelle (contract No. 2732).

References

[1] G.A. Eiceman, CRC Crit. Rev. Anal. Chem., 22 (1991) 471.
[2] G.A. Eiceman and Z. Karpas, Ion Mobility Spectrometry, CRC Press, Boca Raton, FL, 1993.
[3] Z. Karpas, Forensic Sci. Rev., 1 (1990) 103.
[4] E.J. Poziomek and G.A. Eiceman, Environ. Sci. Technol., 26 (1992) 1313.
[5] R.H. St. Louis and H.H. Hill, Jr., CRC Crit. Rev. Anal. Chem., 21 (1990) 321.
[6] S.H. Kim and G.E. Spangler, Anal. Chem., 57 (1985) 567.
[7] L. Kolaitis and D.M. Lubman, Anal. Chem., 58 (1986) 1993.
[8] H.H. Hill, Jr., W.F. Siems, R.H. St. Louis and D.G. McMinn, Anal. Chem., 62 (1990) 1201 A.
[9] A.P. Snyder, C.S. Harden, A.H. Brittain, M.-G. Kim, N.S. Arnold and H.L.C. Meuzelaar, Anal. Chem., 65 (1993) 299.
[10] A.P. Snyder, C.S. Harden, A.H. Brittain, M.-G. Kim, N.S. Arnold and H.L.C. Meuzelaar, Am. Lab., 24(15) (1992) 32B.
[11] M.J. Cohen and F.W. Karasek, J. Chromatogr. Sci., 8 (1970) 330.
[12] M.A. Baim and H.H. Hill, Jr., Anal. Chem., 54 (1982) 38.
[13] M.A. Baim and H.H. Hill, Jr., J. Chromatogr., 279 (1983) 631.
[14] M.A. Baim and H.H. Hill, Jr., J. High Resolut. Chromatogr. Chromatogr. Commun., 6 (1983) 4.
[15] R.H. St. Louis, W.F. Siems and H.H. Hill, Jr., J. Chromatogr., 479 (1989) 221.
[16] R.H. St. Louis and H.H. Hill, Jr., J. High Res. Chromatogr., 13 (1990) 628.
[17] N.S. Arnold, W.H. McClennen and H.L.C. Meuzelaar, Anal. Chem., 63 (1991) 299.
[18] K.M. Holbrook, R.M. Buchanan and H.L.C. Meuzelaar, Proc. 38th ASMS Conf. Mass Spectr. All. Top., ASMS, East Lansing, 1990, p. 900.
[19] W.H. McClennen, R.M. Buchanan, N.S. Arnold, J.P. Dworzanski and H.L.C. Meuzelaar, Anal. Chem., 65 (1993) 2819.
[20] S.P. Cram and S.N. Chesler, J. Chromatogr., 99 (1974) 267.
[21] N.S. Arnold, M.-G. Kim, W.H. McClennen, J.P. Dworzanski and H.L.C. Meuzelaar, in G.A. Eiceman

(Ed.), Proceedings of the 1992 Workshop on Ion Mobility Spectrometry, U.S. Army CRDEC, Aberdeen Proving Ground, 1993, p. 11.
[22] M.J. Golay, in P.M. Desty (Ed.), Gas Chromatography, Butterworths, London, 1958, p. 89.
[23] L.S. Ettre, Chromatographia, 18 (1984) 447.
[24] G.J. Kennedy and J.H. Knox, J. Chromatogr. Sci., 10 (1972) 549.
[25] G. Guiochon, Anal. Chem., 52 (1980) 2002.
[26] P. Lovkvist and J.A. Jonsson, Anal. Chem., 59 (1987) 818.
[27] B.K. Afghan and A.S.K. Chan (Eds.), Analysis of Trace Organics in the Aquatic Environment, CRC Press, Boca Raton, FL, 1989, p. 119.
[28] B.P. Howard (Ed.), Handbook of Environmental Degradation Rates, Lewis Publishers, Michigan, 1991, p. 478.

ELSEVIER

Analytica Chimica Acta 293 (1994) 237–243

ANALYTICA CHIMICA ACTA

Investigation of chromium(III) and chromium(VI) speciation in water by ion chromatography with chemiluminescence detection

H.G. Beere, P. Jones *

Department of Environmental Sciences, University of Plymouth, Drake Circus, Plymouth PL4 8AA, UK

(Received 6th December 1993; revised manuscript received 28th February 1994)

Abstract

This paper describes the development of an ion chromatography system for the separation and determination of Cr(III) and Cr(VI) species in aqueous samples. The separation was carried out on a Dionex AS4A anion exchange column containing a small proportion of cation exchange groups. Very high sensitivity was achieved using a chemiluminescence post-column reaction detector based on the catalytic oxidation of luminol. Linear calibrations were obtained over the range 0.1 to 500 $\mu g\ l^{-1}$. Reproducibility was better than $\pm 5\%$ at the 10 $\mu g\ l^{-1}$ level with detection limits of 0.05 and 0.1 $\mu g\ l^{-1}$ for Cr(III) and Cr(VI) respectively. A preliminary study of chromium speciation in a fresh water standard reference material showed that the conditions necessary for simultaneous determination of the two chromium species was critical, as Cr(VI) was vulnerable to reduction in acidic solutions and Cr(III) was strongly hydrolysed above pH 3.

Key words: Chemiluminescence; Ion exchange chromatography; Chromium speciation; Waters

1. Introduction

The increasing interest in chromium speciation in environmental samples has led to a variety of approaches for differentiating and determining chromium(III) and chromium(VI) species. A number of studies have focused on just one species of particular interest such as chromium(III) in water and foodstuffs by Escobar et al. [1] or chromium(VI) in water by Elleouet et al. [2]. Other investigators have measured one species and obtained the other by difference after total chromium measurement. Mugo and Orians [3] and Beceiro-Gonzalez et al. [4] measured chromium(III) and total chromium, whereas Chakraborty and Mishra [5], Gao [6] and Sperling et al. [7] determined chromium(VI) and total chromium.

The aim of other studies has been to determine both species simultaneously. Essentially, this involves the determination of chromium(III) and chromium(VI) as separate species after elution from a chromatography column. Several workers have reported the use of hyphenated systems linking the chromatography column to atomic spectrometric instruments, such as flame atomic absorption [8,9] or inductively coupled plasmas [10]. Another approach, which is the focus of this

* Corresponding author.

SSDI 0003-2670(94)00111-X

work, involves the use of self-contained ion chromatography systems with standard on-line detectors. The chromatography is not straightforward as the two chromium species are of opposite charge. This can be simplified by converting chromium(III) to a negatively charged complex ion and then separating from chromium(VI) using an anion exchange column [11–14]. However, this usually requires a major disturbance of the sample such as boiling for a short period [15].

Clearly this is not too satisfactory, since to maintain species integrity, particularly as Cr(VI) is not a very stable species, sample treatment should be kept to a minimum. In an attempt to solve this problem Williams et al. [16] developed an ion chromatography method capable of separating Cr(III) and Cr(VI) as their simple ions in an aqueous sample. Very high sensitivities were achieved using a chemiluminescence detector optimised for Cr(III). The Cr(VI) species, which is not chemiluminescence active, was reduced to Cr(III) post column using sulphite. Although good separations were obtained the chromatography was very complex, involving two eluents, two parallel columns and four pumps. Gammelgaard et al. [17] using the same chemiluminescence detection system with sulphite reduction, reported a simpler separation system based on a single column. However, the chromium(VI) eluted very close to the solvent front, which makes it vulnerable to distortion or disturbance depending on the sample composition.

This paper describes the development of a simple single column chromatography system giving clear resolution of the two chromium species from each other and from the solvent front. The quantitative performance is also assessed together with a preliminary study of the stability of the species under varying pH conditions.

2. Experimental

As shown in Fig. 1 the chromatograph set up consisted of a 4000i Dionex Gradient pump (Dionex, Sunnyvale, CA) which was used to deliver the eluent to the column at 1 cm^3 min^{-1}. For the optimised system the column used was a 25-cm

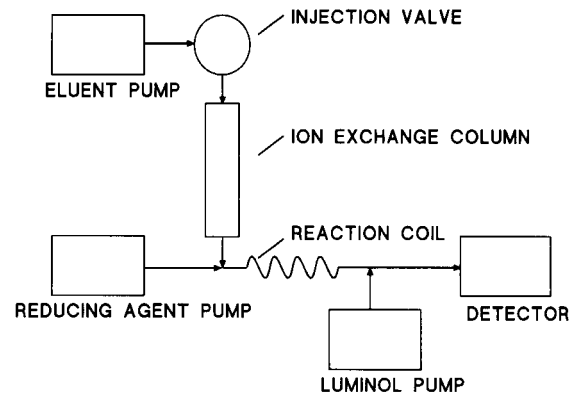

Fig. 1. Schematic diagram of chromatographic system employed.

AS4A anion exchange column (Dionex, Camberely). The solution used to reduce the chromium(VI) to chromium(III) was delivered by a post-column stainless steel pump (Model 64, Knauer, Bad Homburg) at a flow rate of 0.06 cm^3 min^{-1}. The CL reagent was added just prior to the detection coil at 1 cm^3 min^{-1} using an inert plastic pump (Dionex 2000i). The chemiluminescence was monitored with a modified FD-100 fluorescence detector (Spectrovision). The modification involved replacing the fluorescence cell with a flat PTFE coil, volume 30 μl, pressed against the face of the photomultiplier tube.

Sample injection was carried via an inert PEEK Rheodyne injection valve (Model 9010, Cotati, CA) with a PEEK 100-μl sample loop. PTFE connecting tubing was used throughout. All eluents were degassed with helium prior to use and the luminol solution was constantly purged with a slow flow of nitrogen.

Milli Q deionized water (Millipore, Bedford, MA) was used for all solutions. All reagents were AnalaR (BDH, Poole) except luminol (Fluka, Poole) and Aristar potassium hydroxide (BDH). Spectrosol (BDH) 1000 mg l^{-1} chromic nitrate was diluted to make working standards for chromium(III). 2.8289 g AnalaR potassium dichromate was diluted to 1 l to give a 1000 mg l^{-1} chromium(VI) solution, which was diluted to make working standards for chromium(VI). Standards were prepared in 0.01 M nitric acid. The

Certified Reference Material was IAEA/W4, Simulated Fresh Water (SFW). The SFW contained four major elements, 10 mg l^{-1} calcium, 4 mg l^{-1} magnesium and smaller amounts of potassium and sodium, and in addition 20 trace metals at the μg l^{-1} level.

2.1. Eluent

Initially, potassium sulphate concentrations of between 0.0085 M and 0.03 M, pH 2.5, were used. After the preliminary experiments all other studies were carried out with a 0.28 M potassium chloride eluent. The pH of the solution was adjusted to 2.5 by the addition of hydrochloric acid and 0.001 M EDTA was added to the eluent solution to reduce the background CL.

2.2. Post-column reagents

Reducing solution

A 0.015 M sulphur dioxide solution was used to reduce chromium(VI) to chromium(III).

Luminol solution

A solution containing 3.4×10^{-4} M luminol, 0.1 M orthoboric acid and 0.01 M hydrogen peroxide at pH 11.5 was used as the CL reagent. The solution was continuously purged with nitrogen.

3. Results and discussion

3.1. Chromatography

Williams et al. [16] separated the chromium species on two columns run in parallel and used potassium sulphate as the eluent through both columns. The concentrations required for each column differed considerably, 0.085 M potassium sulphate to elute chromium(III) and 0.003 M potassium sulphate to elute chromium(VI). With such differences in concentration it was not possible to use the two columns in series with potassium sulphate as the eluent.

To achieve an efficient and rapid separation of both chromium species on a column, or columns in series, with a single eluent, then the ion exchange capacities of the column must be matched to the eluent strength to take into account the relative distribution coefficients of the two ions. It was soon clear that sulphate was too strong an eluent and it was considered that better compromise separation conditions would be easier to achieve with a weaker eluent.

Table 1
Dimensions and ion exchange capacities of some Dionex columns [18] (N/A = not available)

Dionex column	Column length (cm)	Anion exchange capacity (μeq./column)	Cation exchange capacity (μeq./column)
AS4A	25	20	N/A
AG4A	5	4	N/A
CS5	25	150	70
CG5	5	30	14
CG3	5	N/A	20
CG2	5	N/A	12

When considering the range of columns available the Dionex CG5 column looked promising as it contained a dual function resin with a 70:30 ratio of anion to cation exchange capacity.

This column was used by Gammelgaard et al. [17] in combination with a 0.1 M potassium sulphate eluent, but as stated in the Introduction, the Cr(VI) species eluted very close to the solvent front, which we considered too vulnerable to disturbance. However, studies with a potassium chloride eluent gave too wide a separation even at high concentrations. Next, lower capacity single function columns whose dimensions and capacities are shown in Table 1, were connected in series in various combinations, but with little success.

It is well known that some single function Dionex ion exchange columns, because of the way the substrate is fabricated, actually contain residual amounts of the opposite charge. With this in mind the AS4A anion exchange column was investigated on its own and it was found that increasing the concentration of chloride to approximately 0.3 M gave good separations with short retention times. Surprisingly, the Cr(III) eluted last, which showed that the residual cationic

groups were in sufficient amounts to significantly hold up the positive chromium ion (Fig. 2).

3.2. System performance

During the preliminary studies the calibration curves for both chromium species were non-linear, the response increasing at a faster rate than the concentration. By purging the luminol solution constantly with nitrogen a consistent response was obtained. Fig. 3 shows typical calibrations obtained for this system from mixed chromium standards in acid media. Good correlation was found between the peak area and chromium concentration with correlation coefficients of 0.9988 for chromium(III) and 0.9985 for chromium(VI). Fig. 2 shows a typical chromatogram for chromium(III) and chromium(VI). A chromatogram near the detection limit is shown in Fig. 4. The limits of detection, defined as twice the peak to peak background noise, were 0.05 μg l^{-1} for chromium(III) and 0.1 μg l^{-1} for chromium(VI). The area of the chromium(VI) peaks was found to be less then that of the chromium(III) peaks at a given concentration. It is difficult to explain this finding since it is chromium(III) that catalyses the CL reaction in both cases.

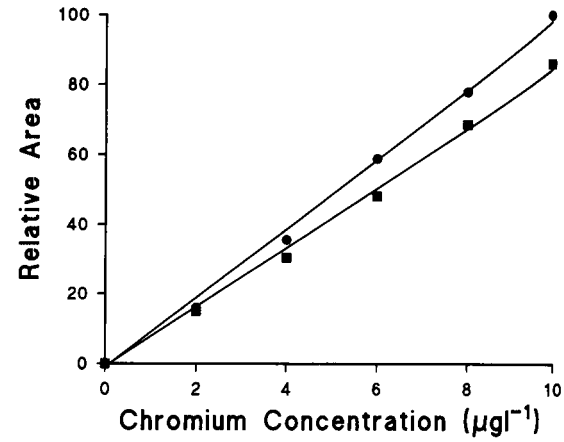

Fig. 3. Calibration curves for chromium(III) and -(VI). (●) chromium(III), (■) chromium(VI). Standard samples containing both chromium species were prepared in 0.01 M nitric acid. Separation conditions as Fig. 2.

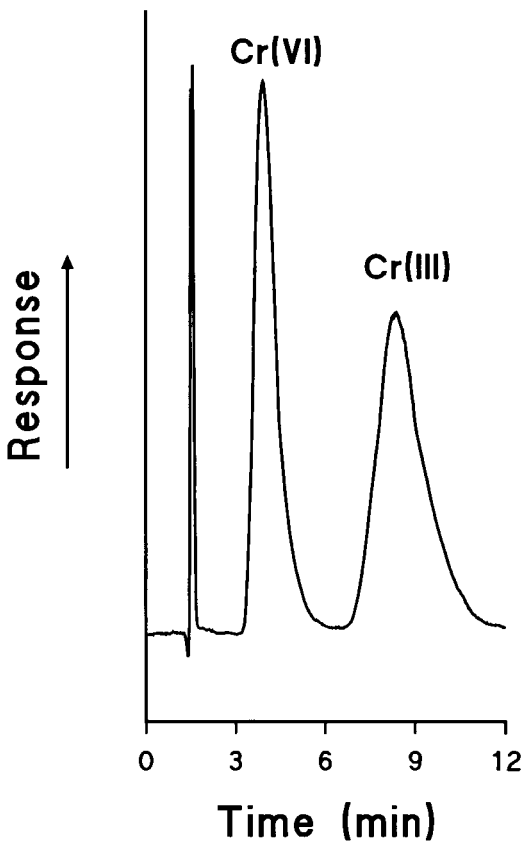

Fig. 2. Typical chromatogram for chromium(III) and chromium(VI). Separation conditions: column, 25 cm Dionex AS4A; eluent, 0.28 M potassium chloride adjusted to pH 2.5; injection volume, 100 μl. Sample a mixture of chromium(III) and chromium(VI) both at a concentration of 10 μg l^{-1} in 0.01 M nitric acid.

3.3. Interferences

A range of common metal ions likely to be present in water samples were studied for interference effects. 10 μg l^{-1} injections of chromium(III) or -(VI) showed no significant interference from the following co-injected cations at concentrations up to 10 mg l^{-1}: Cu(II), Co(II), Zn(II), Ni(II), Mn(II), Mg(II), Ca(II), Al(III) and Fe(III).

3.4. Determination of chromium species in aqueous samples

A study of chromium speciation was carried out using a Certified Reference Material, IAEA/W4, Simulated Fresh Water (SFW). As SFW only contained Cr(III), Cr(VI) was added as a spike. It was soon found that Cr(VI) was not stable in the SFW even though it was stable in pure water standards at the same pH. It was assumed that trace amounts of reducing agents were present, which when coupled with the high acidity of the SFW solution (approx. 1 M HNO_3), made the Cr(VI) very susceptible to attack. The pH of the SFW was increased to 3 to reduce the oxidising power of the Cr(VI), but the species was still destroyed, though at a slower rate. Fig. 5 shows the change in chromatogram with time after the Cr(VI) was added. It would be expected that Cr(VI) would be converted to Cr(III) in acid media. However, although the chromatogram shows an increase in the Cr(III) response, there was also a large increase close to the solvent front. It is known that reduction of Cr(VI) can result in inert inorganic complexes which are unlikely to dissociate during chromatography [19]. Therefore, it is possible that the increase in response near the solvent front could be due to the presence of a complex such as $CrCl_2^+$ formed during reduction.

The pH of the SFW was increased further and it was found that Cr(VI) spikes eventually be-

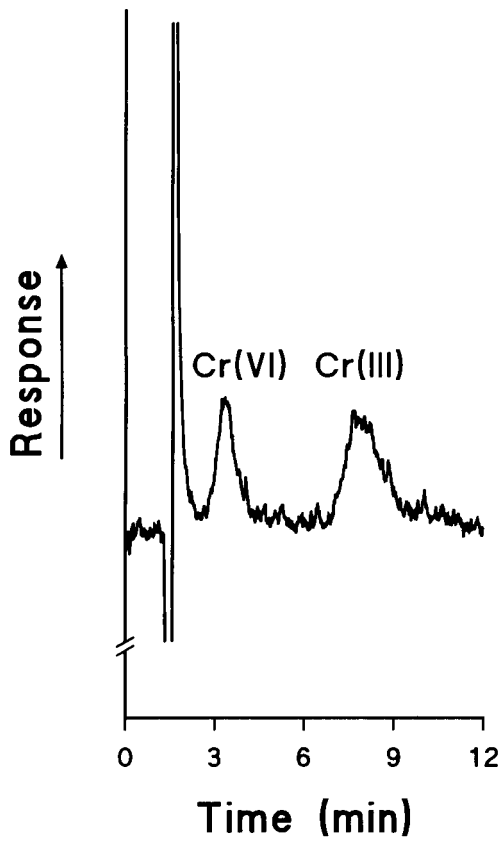

Fig. 4. Typical chromatogram near the detection limit. Conditions as Fig. 2 except chromium concentration 0.25 $\mu g\ l^{-1}$ chromium(III) and chromium(VI).

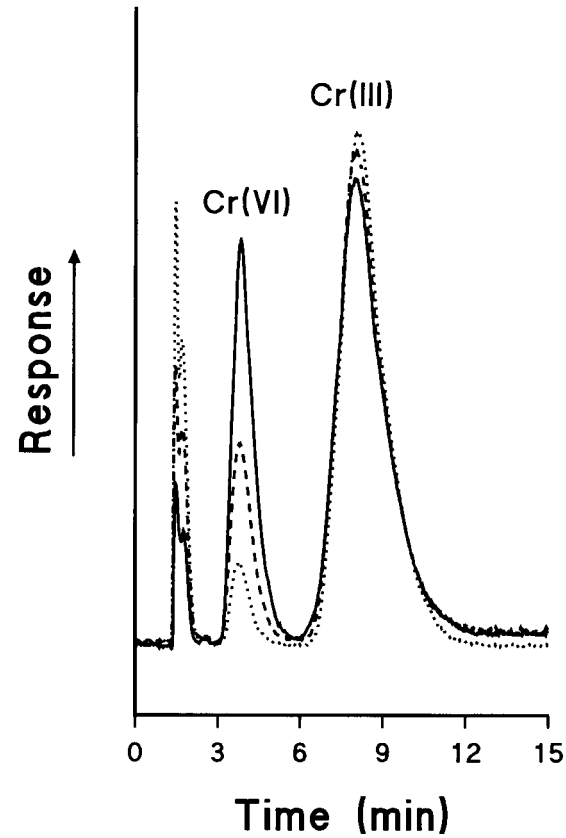

Fig. 5. Decrease in response over time shown by chromium(VI) in acidified SFW. Sample, SFW adjusted to pH 2.98 and spiked with 10 $\mu g\ l^{-1}$ of chromium(VI). Time: 0 min (———), 60 min (– – –), and 120 min (· · ·). Separation conditions as Fig. 2.

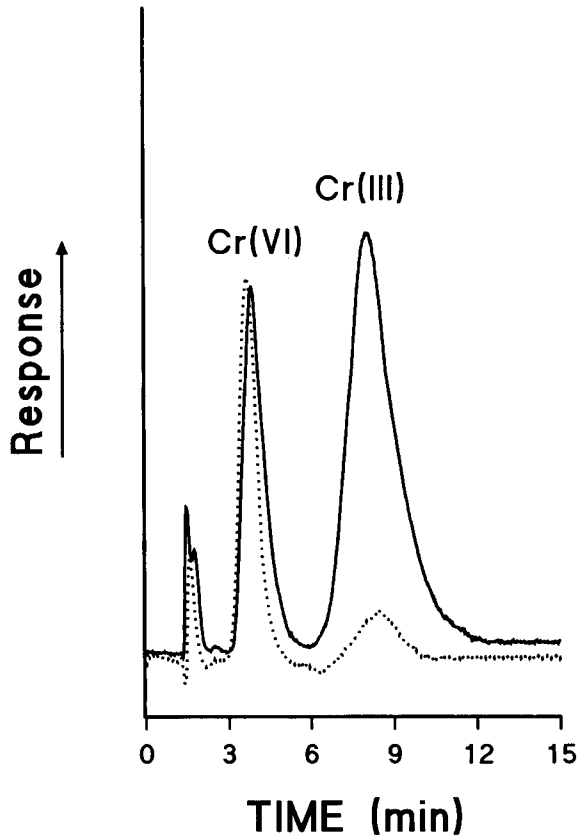

Fig. 6. Effect of pH on the stability of chromium(III) in SFW. Samples, SFW spiked with 10 $\mu g\ l^{-1}$ of chromium(VI) at pH 2.98 (———) and 6.15 (···). Separation conditions as Fig. 2.

came stable at pH 5 or above. This is not surprising as the reduction potential decreases substantially as the pH is raised. However, it can be seen from Fig. 6 that the Cr(III) response has virtually disappeared due to hydrolysis, which becomes significant above pH 3. Because of these findings quantitative investigations of the two species in SFW were carried out at two different pH values, namely, pH 3 for Cr(III) and pH 5 for Cr(VI).

The average value found for Cr(III) in SFW was 10.0 $\mu g\ l^{-1}$, which compares favourably with the certified value of 9.9 $\mu g\ l^{-1}$ (confidence interval 9.0–10.5 $\mu g\ l^{-1}$). The reproducibility was good with a relative standard deviation (R.S.D.) of 4.3% for six replicates. Chromium(VI) was determined in the SFW spiked at 10 $\mu g\ l^{-1}$ and gave a six replicate average of 10.5 $\mu g\ l^{-1}$ with an R.S.D. of 2.7%. Thus good quantitative results were obtained at the low $\mu g\ l^{-1}$ level for both chromium species.

4. Conclusions

The ion chromatography system using an AS4A column and potassium chloride eluent gave a good separation of the two species in a reasonable time, well resolved from the solvent front. Quantitative determinations and recoveries involving the Standard Fresh Water sample were very good with the chemiluminescence detector giving excellent sensitivity at the low $\mu g\ l^{-1}$ level.

The method shows a clear potential for the determination of the chromium species in water with minimal sample pretreatment. However, the simultaneous determination of the two species cannot be carried out if the pH is higher than three due to hydrolysis of the Cr(III) cation. Furthermore, the results of this study show great caution is needed if the sample pH is lowered as this can make the Cr(VI) species more vulnerable to reduction. Finally, it cannot be assumed that simple Cr(III) hydrated cations are produced if any reduction has occurred.

References

[1] R. Escobar, Q. Lin and A. Guiraum, Analyst, 118 (1993) 643.
[2] C. Elleouet, F. Quentel and C. Madec, Anal. Chim. Acta, 257 (1992) 301.
[3] R.K. Mugo and K.J. Orians, Anal. Chim. Acta, 271 (1993) 1.
[4] E. Beceiro-Gonzalez, P. Bermejo-Barrera, A. Bermejo-Barrera, J. Baciela-Garcia and C. Baciela-Alonso, J. Anal. At. Spectrom., 8 (1993) 649.
[5] A. Chakraborty and R. Mishra, Chemical Speciation and Bioavailability, 4 (1992) 131.
[6] R.M. Gao, Talanta, 40 (1993) 637.
[7] M. Sperling, X. Yin and B. Welz, Analyst, 117 (1992) 629.
[8] J. Posta, H. Berndt, S. Luo and G. Schaldach, Anal. Chem., 55 (1993) 2590.
[9] M. Sperling, S. Xu and B. Welz, Anal. Chem., 64 (1992) 3101.
[10] D.T. Gjerde, D.R. Wiederin, F.G. Smith and B.M. Mattson, J. Chromatogr., 640 (1993) 73.

[11] Y. Suzuki and F. Serita, Industrial Health, 23 (1985) 207.
[12] G.L. Ou-Yang and J.F. Jen, Anal. Chim. Acta, 279 (1993) 329.
[13] A. Bond and G. Wallace, Anal. Chem., 54 (1982) 1706.
[14] E. Eijarvi, L. Lajunen and M. Heikka, Finn. Chem. Lett., (1985) 225.
[15] Dionex Technical Note, May 1987, TN24.
[16] T. Williams, P. Jones and L. Ebdon, J. Chromatogr., 482 (1989) 361.
[17] B. Gammelgaard, O. Jøns and B. Nielsen, Analyst, 117 (1992) 637.
[18] Dionex Product Selection Guide, 1991, p. 35.
[19] M. Lederer, The Periodic Table for Chromatographers, Wiley, Chichester, 1992.

ELSEVIER

Analytica Chimica Acta 293 (1994) 245–250

ANALYTICA CHIMICA ACTA

Precolumn derivatization of retinoic acid for liquid chromatography with fluorescence and coulometric detection

S. El Mansouri [a], M. Tod *,[a], M. Leclercq [b], M. Porthault [c], J. Chalom [d]

[a] *Service de Pharmacie, Hôpital Avicenne, 125 Route de Stalingrad, 93009 Bobigny Cédex, France*
[b] *INSERM 331, Institut Pasteur de Lyon, Faculté de Médecine Alexis-Carrel, Rue Guillaume Paradin, 69327 Lyon Cedex, France*
[c] *Laboratoire des Sciences Analytiques, 43 Bd. du 11 Novembre 1918, 69622 Villeurbanne, France*
[d] *Eurobio, 7 Av. de Scandinavie, Les Ulis, France*

(Received December 3rd 1993; revised manuscript received February 28th 1994)

Abstract

Derivatization of the carboxyl function of retinoic acid by fluorescent or electroactive reagents prior to liquid chromatography was studied. Ferrocenylethylamine was synthesized and could be coupled to retinoic acid. The coupling reaction involved activation by diphenylphosphinyl chloride. The reaction was carried out at ambient temperature in 50 min with a yield of ca. 95%. The derivative can be detected by coulometric reduction (+100 mV) after on-line coulometric oxidation (+400 mV). The limit of detection was 1 pmol of derivative on-column, injected in a volume of 10 μl, but the limit of quantification was 10 pmol of retinoic acid.

Key words: Coulometry; Fluorimetry; Liquid chromatography; Retinoic acid

1. Introduction

Retinoic acid (tretinoin) is a metabolite of retinol (vitamin A) and is a mediator of cell differentiation and cell proliferation [1]. Tretinoin is present at very low concentrations (4.3 ± 1.7 pmol ml^{-1}) in normal human plasma [2] and is used to treat acute promyelocytic leukaemia at a dose of 45 mg m^{-2} day^{-1}, resulting in a peak level of 300–1200 pmol ml^{-1} [3].

Chromatographic techniques for assaying retinoids have recently been reviewed [4]. Wyss and Bucheli [5,6] developed the most sensitive liquid chromatographic procedure for the determination of tretinoin in plasma that involves switching columns. Despite its low limit of detection (1.7 pmol ml^{-1}), this method might not be sufficient for studying the decreased plasma retinoic acid concentrations in several populations of patients [7] and lower concentrations in tissues. As retinoic acid is only weakly fluorescent or electroactive (the oxidation potential is ca. 1.2 V vs. Ag/AgCl) [8], only UV detection at 340 nm has been used so far, although this mode of detection is generally less sensitive than fluorescence, chemiluminescence or coulometric detection. One way to improve the detectability of retinoic acid (and related compounds) would be

* Corresponding author.

SSDI 0003-2670(94)00112-Y

to derivatize its carboxyl function with a convenient reagent. Although this approach has been widely and successfully used with other classes of compounds, e.g., prostaglandins and fatty acids, it does not seem to have been applied to retinoids.

Several characteristics of retinoic acid might explain this situation [5]: it is sensitive to light and oxidation, which promote isomerization and degradation, e.g. Motto et al. [9] found that in 90% ethanol, ten isomers of retinoic acid were formed on irradiation with visible light; thermal instability and adsorption on glassware are also potential pitfalls. Hence a convenient derivatization reaction for retinoic acid should be rapid and able to proceed under mild conditions.

The purpose of this study was to devise such a labelling reaction to improve the detectability of retinoic acid. First attempts were made by using fluorescent reagents such as pyrenyldiazomethane [10] and rhodamine–ethanol, following the activation procedure described by Lingeman et al. [11]. Strong quenching of the fluorophores prompted us to study the coupling of retinoic acid to electrophores and finally to develop a new labelling reagent based on the ferrocene nucleus.

2. Experimental

2.1. Apparatus

The LC system consisted of an Shimadzu LC6A pump (Touzart et Matignon, Vitry-sur-Seine), a Rheodyne Model 7125 injector with a 10-μl loop, and either an SPD6A ultraviolet spectrophotometer (Shimadzu), an RF535 fluorescence detector (Shimadzu) or a Coulochem 5100A coulometric detector (Cunow, Osny) with a Model 5020 guard cell and a Model 5011 analytical cell. The columns were either a 5-μm Nucleosil C_{18} (150 × 4.6 mm i.d.) or a 5-μm Nucleosil C_8 (150 × 4.6 mm i.d.) (SFCC, Neuilly-Plaisance). Excitation and emission spectra were recorded on a Perkin-Elmer LS5 spectrofluorimeter.

Tretinoin, isotretinoin, cyclodextrins, diphenylphosphinyl chloride (DPPC), chloromethylpyridinium iodide (CMPI), pyrene, fluorescein (sodium salt), Rhodamine B and nonanoic and lauric acid were obtained from Sigma (l'Isle d'Abeau). Triethylamine (TEA) and unstabilized dichloromethane were purchased from Fluka (Buchs). Rhodamine–ethanol and ferrocenylethylamine were obtained from Eurobio (Les Ulis). Tyramine was purchased from Aldrich (St. Quentin Fallavier).

2.2. Fluorescence quenching measurements

Fluorescence quenching of sodium fluoresceinate and Rhodamine B by retinoic acid was studied as follows. Solutions containing a fixed concentration of the fluorophore (10^{-5} M) and a variable concentration of retinoic acid (0, 0.05, 0.10, 0.20, 0.50 and 1.00 mM) in acetonitrile–0.01 M ammonium acetate (80 + 20, v/v) (fluoresceinate) or acetonitrile–0.01 M ammonium acetate–tetrahydrofuran (65 + 10 + 25, v/v/v) (Rhodamine B) were prepared. Fluorescence intensity was measured at excitation/emission wavelengths of 517/543 nm and 450/576 nm for fluoresceinate and Rhodamine B, respectively. The temperature was 20 ± 1°C. The excitation wavelengths were chosen so as to have a fluorophore absorbance below 0.05 and a negligible absorbance of retinoic acid. Stern–Volmer plots were constructed according to the following equation [12]:

$$I_0/I = 1 + K_q[Q]$$

where I_0 is the fluorescence intensity at zero concentration of the quencher, I is the fluorescence intensity at a given concentration [Q] of the quencher, and K_q is the quenching constant.

2.3. Derivatization conditions

Exposure of the solutions to light was avoided as much as possible in all experiments.

Pyrenyldiazomethane

Fatty acids were labelled with pyrenyldiazomethane according to the procedure described by Nimura et al. [10].

Rhodamine–ethanol

Fatty acids were derivatized with rhodamine–ethanol after activation of the carboxyl function, as described by Lingeman et al. [11].

Tyramine

Tyramine–carboxylic acid derivatives were obtained as described by Lehr and Damm [13].

Ferrocenylthylamine

Derivatization of carboxylic acids with ferrocenylethylamine was carried out in dichloromethane, as described by Lehr and Damm [13]. To 40 μl of a solution of retinoic acid (1–200 nmol) were added 200 μl of 5 mM DPPC solution and 160 μl of 5 mM TEA solution. After vortex mixing for 20 s, 400 μl of 5 mM ferrocenylethylamine solution were added. After 50 min in the dark at ambient temperature, the reaction was complete.

2.4. Chromatographic conditions

Pyrenyl derivatives were separated using the Nucleosil C_{18} column. The mobile phase was acetonitrile–0.01 M ammonium acetate (80 + 20, v/v) at a flow-rate of 1 ml min^{-1}. The UV detection wavelength was 340 nm and the excitation/emission wavelengths were 340/400 nm for fluorescence detection.

Tyramine derivatives were identified using the same chromatographic system, but the UV detection wavelength was 280 or 340 nm.

Ferrocenylethylamine derivatives were evaluated using the Nucleosil C_8 column. The mobile phase was methanol–0.01 M ammonium acetate (70 + 30) at a flow-rate of 1 ml min^{-1} and the coulometric detector was used. The guard cell potential was set at +500 mV and the analytical cell potentials were set at +400 mV (first cell) and +100 mV (second cell).

3. Results and discussion

3.1. Derivatization with pyranyldiazomethane

Derivatization of acetic acid ($k' = 2.46$), isovaleric acid ($k' = 4.40$), nonanoic acid ($k' = 6.80$) and retinoic acid ($k' = 7.00$) was successful, as demonstrated by the emergence of a derivative peak with a concomitant decrease in the pyrenyldiazomethane peak, when using UV detection. However, when using a spectrofluorimeter, the retinoic derivative was undetectable whereas the other derivatives were observed as expected. Hence the retinoic derivative was not fluorescent. This might be explained by three mechanisms: inner filter effect by absorption of the excitation light by retinoic acid, collisional quenching by dipole coupling [14] and static quenching [15]. The last two mechanisms could be prevented by cyclodextrin complex formation with the pyrenyl nucleus or the retinoyl moiety. Cyclodextrins were therefore added to the chromatographic eluent using a postcolumn reactor. β-Cyclodextrin (0.01 M in water) and trimethyl β-cyclodextrin [0.01 M in methanol–water (95 + 5 or 5 + 95, v/v)] solutions were tried, and the UV and fluorescence detectors were connected in series. However, the pyrenylretinoic derivative was not fluorescent so derivatization with pyrenyldiazomethane was abandoned.

3.2. Quenching studies

To avoid fluorescence quenching by retinoic acid, other fluorophores could be used. Two were considered: sodium fluoresceinate and Rhodamine B. Stern–Volmer plots of the quenching of these two fluorophores by retinoic acid yielded straight lines with quenching constants of 415 l mol^{-1} ($r = 0.984$, Rhodamine B) and 3160 l mol^{-1} ($r = 0.995$, fluoresceinate). Hence Rhodamine B is only slightly quenched by retinoic acid, and this nucleus was used as the basis of a labelling reagent for retinoic acid.

3.3. Derivatization with rhodamine–ethanol

Rhodamine–ethanol has been used to form esters with several carboxylic acids after activation by 2-chloro-1-methylpyridinium iodide. Nonanoic and lauric acids were successfully derivatized and were fluorescent, but no derivative could be obtained with retinoic acid.

Derivatization of retinoic acid with a fluores-

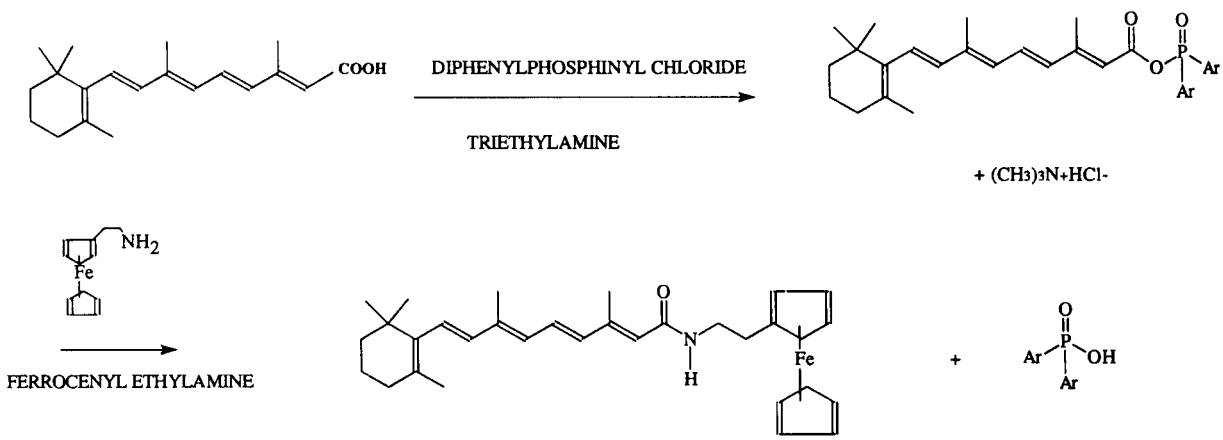

Fig. 1. Scheme of the derivatization reaction using ferrocenylethylamine and diphenylphosphinyl chloride.

cent label was therefore not investigated further and electroactive labels were explored.

3.4. Derivatization with tyramine

Catecholamines were first tried for the derivatization of retinoic acid. Dopamine and noradrenaline were unsuccessful, but retinoic acid could be derivatized with tyramine after activation by DPPC as described by Lehr and Damm [13]. The derivative could be determined with UV detection at 340 nm (retinoic chromophore) and 280 nm (tyramine chromophore). However, double detection by serially connecting the coulometer to the UV detector showed that the derivative was not oxidizable even at +900 mV, whereas the usual oxidation potential for phenols is +600 mV. This inability to be oxidized was attributed to the formation of an ester between the activated carboxylic acid and the phenol function of tyramine, rather than the expected amide.

3.5. Derivatization with ferrocenylethylamine

To overcome these difficulties, ferrocenylethylamine, whose only reactive function is the primary amino group, was used in association with the DPPC activation method (Fig. 1). Ferrocenylretinoylethylamide was prepared and its structure was confirmed by ^{1}H NMR spectrometry in $CDCl_3$: δ 1.02 (6H, s), 1.48 (4H, m), 1.71 (3H, s), 1.99 (3H, s), 2.02 (2H, m), 2.37 (3H, s), 2.60 (2H, t), 3.43 (2H, q), 4.10 (9H, d), 5.62 (1H, s), 6.22 (4H, m), 6.90 (1H, q), 7.26 (1H, s).

The intensity vs. potential curve for the derivative is shown in Fig. 2. The half-wave potential was +300 mV, as usual with ferrocene derivatives. To take advantage of the reversible character of the oxidation of ferrocene derivatives, the coulometer was used in the redox mode: the derivative was oxidized at +400 mV at the first electrode and then reduced at +100 mV at the second electrode, and the difference between the

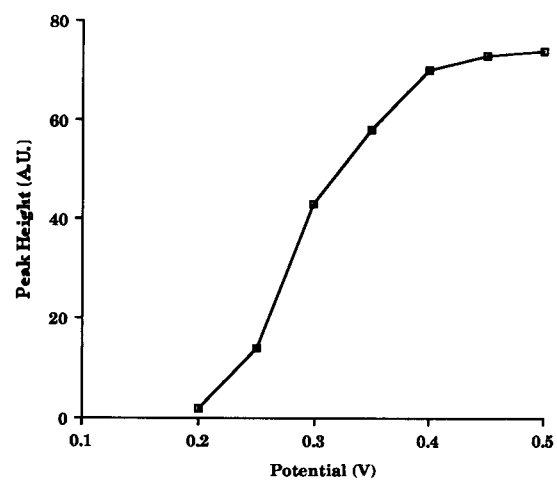

Fig. 2. Hydrodynamic voltammogram of ferrocenylretinoylamide. A.U.: arbitrary units.

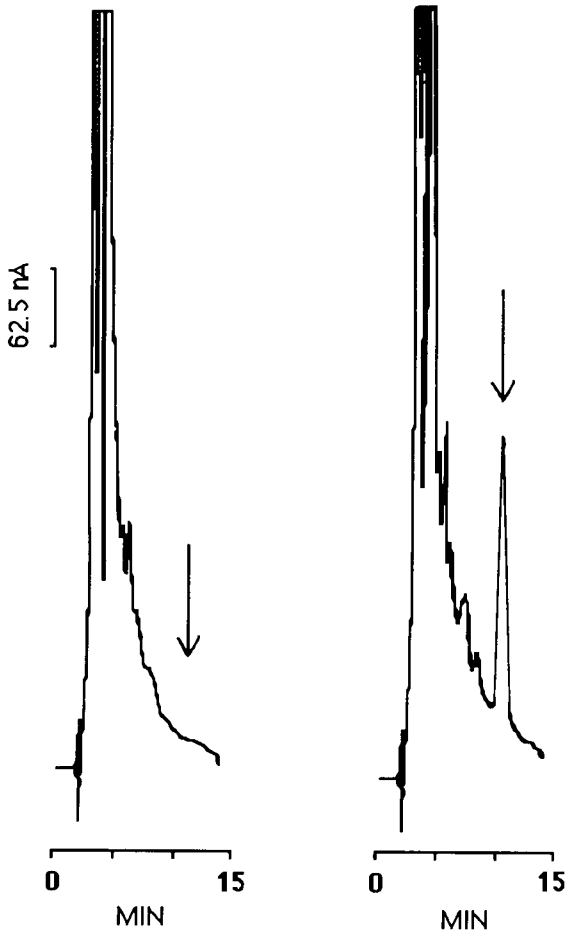

Fig. 3. Chromatogram of a blank (left) and a sample (right) (1.64 pmol injected). The sample was obtained by derivatization of 90 pmol of retinoic acid.

two signals was recorded (Fig. 3). The limit of detection of the derivative, measured at a signal-to-noise ratio of 3, was 1 pmol injected on to the column.

3.6. Optimization of derivatization conditions

To avoid degradation of retinoic acid, no attempts were made to increase the speed of the reaction by heating. Derivatization reaction kinetics were studied over 70 min and showed that the reaction was almost complete after 50 min.

The reaction is base catalysed, as two protons are released for each retinoic acid molecule derivatized. Therefore, the influence of the triethylamine concentration on the reaction yield was studied by varying the triethylamine-to-retinoic acid ratio from 1.5 to 12. The yield was constant for ratios ranging from 2 to 12.

Similarly, the influence of excesses of DPPC and ferrocenylethylamine over retinoic acid was studied, for ratios in the range 1.25–5 and 1.25–10, respectively. The optimum ratios were 5 for DPPC and 10 for ferrocenylethylamine. Under the conditions described, the yield of the derivatization reaction, measured by comparison with a standard of the derivative, was ca. 95%. However, great care must be taken to avoid exposure of retinoic acid and derivative solutions to light, because of the rapid isomerization of all-*trans* to several *cis*-retinoic acid isomers [9]. The peak of the 13-*cis*-retinoic acid derivative, although not baseline resolved from that of the all-*trans* derivative, can also be measured.

Six calibration graphs for retinoic acid (in the range 10–100 pmol) were constructed and the bias and the accuracy of three controls (containing 5, 10 or 15 pmol) were calculated. The limit of quantification, i.e., the smallest amount of retinoic acid that can be measured by derivatization with reasonable accuracy (bias $< 20\%$) and precision (relative standard deviation $< 20\%$) is 10 pmol. However, final determination of this limit and other parameters of validation of the method will have to be determined after extraction of retinoic acid from biological samples and this will be the subject of subsequent work.

4. Conclusions

Determination of retinoic acid by derivatization of its carboxylic acid function using fluorescent probes was unsuccessful because the derivatives did not retain fluorescence. Coulometric detection of a ferrocene derivative seems a promising approach as derivatization can be carried out under mild conditions and the detection conditions (redox mode, low potential) are favourable for obtaining good selectivity and a low detection limit.

References

[1] B.A. Pawson, C.W. Ehmann, L.M. Itri and M.I. Sherman, J. Med. Chem., 25 (1982) 1269.
[2] C. Heckhoff and H. Nau, J. Lipid Res., 31 (1990) 1445.
[3] J. Muindi, S.R. Frankel, W.H. Miller, A. Jakubowski, D.A. Scheinberg, C.W. Young, E. Dmitrovoky and R.P. Warrel, Blood, 78 (1992) 299.
[4] R. Wyss, J. Chromatogr., 531 (1990) 481.
[5] R. Wyss and F. Bucheli, J. Chromatogr., 424 (1988) 303.
[6] R. Wyss and F. Bucheli, J. Pharm. Biomed. Anal., 8 (1990) 1033.
[7] E. Delacoux, T. Estigneef, M. Leclerq, M.C. Rettori, S. Delons, C. Naret and C. Blanchet-Bardon, Clin. Chim. Acta, 137 (1984) 283.
[8] P.D. Bryan and A.C. Capomachia, J. Pharm. Biomed. Anal., 9 (1991) 855.
[9] M.G. Motto, K.L. Facchine, P.J. Hamburg, D.J. Burinsky, R. Dunphy, A.R. Oyler and M.L. Cotter, J. Chromatogr., 481 (1989) 255.
[10] N. Nimura, T. Kinoshita, T. Yoshida, A. Vetake and C. Nakai, Anal. Chem., 60 (1988) 2067.
[11] H. Lingeman, A. Hulshoff, W.J.M. Underberg and F.B.J.M. Offermann, J. Chromatogr., 290 (1984) 215.
[12] C. Ngitto, G. Patonay and I.M. Warner, Trends Anal. Chem. 5 (1986) 37.
[13] K.H. Lehr and P. Damm, J. Chromatogr., 425 (1988) 153.
[14] T. Förster, Ann. Phys., (1948) 55.
[15] G. Patonay, A. Shapira, P. Diamond and I.M. Warner, J. Phys. Chem., 90 (1986) 1964.

ELSEVIER

Analytica Chimica Acta 293 (1994) 251–260

ANALYTICA CHIMICA ACTA

Selective flow injection sorbent extraction for determination of cadmium, copper and lead in biological and environmental samples by graphite furnace atomic absorption spectrometry

Renli Ma, Willy Van Mol, Freddy Adams *

Department of Chemistry, University of Antwerp (UIA), B-2610 Wilrijk, Belgium

(Received 1st December 1993; revised manuscript received 17th February 1994)

Abstract

A flow injection sorbent extraction system was developed for determination of trace and ultratrace cadmium, copper and lead in biological and environmental standard reference materials by graphite furnace atomic absorption spectrometry (GFAAS). Using ammonium diethyldithiophosphate (DDPA) as complexing agent with citrate as masking agent at pH 2, the analytes were selectively preconcentrated with effective removal of the matrixes including the salt matrix in saline water and the other high-content heavy metals in digested biological and geological samples. The two-second eluate containing most of the analyte complexes was collected for the GFAAS measurement. All analytical results obtained were in good agreement with the certified values. Enrichment factors of 12, 13 and 13 compared with 20 μl direct injection of aqueous solution and detection limits (3σ) of 0.003, 0.05 and 0.04 $\mu g\ l^{-1}$ for cadmium, copper and lead respectively, could be obtained with 20-s sample loading at 8.7 ml min^{-1} for sorbent extraction and 20 μl eluate injection for peak area measurement. The relative standard deviation at 0.1 $\mu g\ l^{-1}$ cadmium, 1 $\mu g\ l^{-1}$ copper or 3 $\mu g\ l^{-1}$ lead was around 2%.

Key words: Flow injection; Atomic absorption spectrometry; Ammonium diethyldithiophosphate; Cadmium; Copper; Environmental analysis; Lead

1. Introduction

Manual batch liquid–liquid extraction for matrix separation and analyte preconcentration has been extensively used in combination with flame and graphite furnace (GF) atomic absorption spectrometry (AAS) for trace metal analysis [1–3]. Continuous liquid–liquid extraction for AAS may be automated by using flow injection (FI) techniques with much shorter time periods, lower sample and reagent consumption, higher reproducibility and less risk of contamination and losses [4–9]. FI liquid–solid sorbent extraction with a reversed-phase hydrophobic sorbent packed column further combines the advantage of column operation [10–25]. The development of FI sorbent extraction for AAS has been reviewed [20].

Both FI on-line solvent extraction and sorbent extraction can readily enhance the detection abil-

* Corresponding author.

SSDI 0003-2670(94)00107-W

ity of flame AAS [4–6,10–13] to cover the concentration levels between conventional flame and GFAAS. Nevertheless, in some digested biological and environmental samples cadmium cannot be determined accurately using on-line sorbent extraction combined with flame AAS, because coexisting metals (e.g., iron) are present in much higher concentrations than the element of interest and depress the signal by competing for the complexing agent and the binding sites or by clogging the column during the extraction [12,13]. However, the concentrations of ultratrace heavy metals, e.g., in natural waters and biological samples, may be very low, which require a rather long sample loading time for flame AAS measurement. Combination of FI sorbent extraction with GFAAS can reduce the sample loading time or the extracted metal amount by two to three orders of magnitude thanks to the higher sensitivity of GFAAS detection. GFAAS, however, is a discrete non-flow-through technique with limited sample injection volume and low tolerance to matrix interference, which makes the combination more difficult.

In off-line FI preconcentration procedures for GFAAS [7,26], the extract or eluate is collected and injected into the graphite tube, which is considered to be practical before a fully automated on-line coupling of FI system with the GFAAS detector becomes commercially available. In this manner, the loss of sensitivity could be compensated by multiple injections; the reduction of the sample throughput could be retrieved by determining more elements in one extract or eluate with one or more detectors. Recently several on-line FI procedures for GFAAS have been published [8,9,14–19,21–25,27–30]. Two types of on-line sample introduction techniques are generally involved: thermospray sample deposition and direct sample injection through the autosampler capillary in a volume-based or time-based mode at very low flow rates. In the former technique, larger sample volumes can be introduced, while the cycle time of GFAAS measurement without a drying step is significantly reduced [29,30]. In the latter technique, the autosampler is controlled manually or modified to be controlled automatically.

Three essential points have been considered especially for FI systems with column operation. (1) The reagent solution is purified on-line by passing it through a precolumn packed with the same sorbent material as is used for the analyte extraction, to decrease the blank value. Therefore the sample loading time can be rather long. (2) The extraction column is rinsed with water at a certain acidity before elution in the same or opposite direction of sample loading to remove the remaining interfering matrix so that the measurement can be made without using any matrix modifier. (3) For on-line direct injection the injected volume is made compatible with the capacity of the graphite tube by controlling the eluent volume; by injecting only the central portion of the eluate containing the most concentrated analyte fraction, or injecting the entire eluate very slowly into a preheated graphite tube. With a typical on-line sorbent extraction system developed by Sperling et al. [15] (direct injection of 40 μl of eluate in the time-based mode from 3.0 ml sample), the enrichment factors were 17, 27 and 20, and the detection limits were 0.8, 17 and 6.5 ng l^{-1} for cadmium, copper and lead, respectively.

Dithiocarbamates have been used as complexing agents in all published FI sorbent extraction systems for GFAAS [14–25]; however, the reagents are unstable in acidic medium and unselective among the heavy metals [13]. Some metal–dithiocarbamate complexes are not recommended for GFAAS because of their volatility [5]. The applications of these systems are restricted to the determination of trace and ultratrace heavy metals in water samples or in high-purity alkali and alkaline earth metal salts. Hitherto no report on the application of sorbent extraction to biological and geological samples for GFAAS has been published. In these samples there might be a large concentration of coexisting heavy metals, e.g., iron, which requires a selective extraction system.

In the present work, a FI sorbent extraction procedure has been developed for GFAAS. Ammonium diethyldithiophosphate (DDPA), a selective complexing agent for cadmium, copper and lead in the presence of alkali and alkaline earth metals, aluminum and heavy metals [31], was

used in an acidic medium. The feasibility of the sorbent extraction pretreatment is demonstrated by the application to a few kinds of biological and environmental reference materials from the Community Bureau of Reference (BCR): cod muscle (CRM 422), single cell protein (CRM 274), mussel tissue (CRM 278), plankton (CRM 414), calcareous loam soil (CRM 141), river (CRM 320) and lake (CRM 280) sediments and sea water (CRM 403). The accuracy of the method was also checked by the spike recovery test for a number of natural estuarine and sea water samples. No attempt was made to carry out on-line eluate injection.

Table 1
FIAS-200 programme and the relevant operation

Step No.	Time (s)	Pump 1 (rpm) [a]	Pump 2 (rpm) [a]	Valve	Operation
1	20–180 [b]	100	0	Inject	Sample loading
2 [c]	15	0	120	Inject	Column rinsing
3	1	0	0	Fill	Valve turning
4	1	0	120	Fill	Elution discarding
5	5	0	0	Fill	Collector moving
6	2	0	120	Fill	Elution collecting
7	5	0	0	Fill	Collector moving
8	7	0	120	Fill	Column cleaning

[a] rpm: revolutions per minute.
[b] Sample loading time dependent on the preconcentration factor required.
[c] Only for estuarine and sea water samples.

2. Experimental

2.1. Apparatus

A Perkin-Elmer FIAS-200 flow injection system controlled by an independent computer was set up as shown in Fig. 1 for sorbent extraction with GFAAS. The working programme and the relevant operation is listed in Table 1. Tygon pump tubes were used for the complexing agent (0.76 mm i.d.), the sample (1.52 mm i.d.) and the column rinsing solution (1.14 mm i.d.). A solvent-resistant silicone rubber pump tube (Isoversinic, 1.00 mm i.d.) was used for the organic eluent. The flow rates were 8.7 ml min^{-1} for the sample, 2.2 ml min^{-1} for the complexing agent, 7.4 ml min^{-1} for the column-rinsing solution and 5.7 ml min^{-1} for the eluent. All other tubing was made of PTFE with 0.35 mm i.d. The commercially available conic sorbent extraction column (PE B050-4047, packed with 20 mg octadecyl functional groups bonded silica gel, particle size 40–63 μm) was used for analyte extraction and reagent purification. The precolumns were washed daily with the eluent. The PTFE tube between the conjunction point of the sample with the reagent and the valve was made as short as possible to avoid adsorption loss or memory ef-

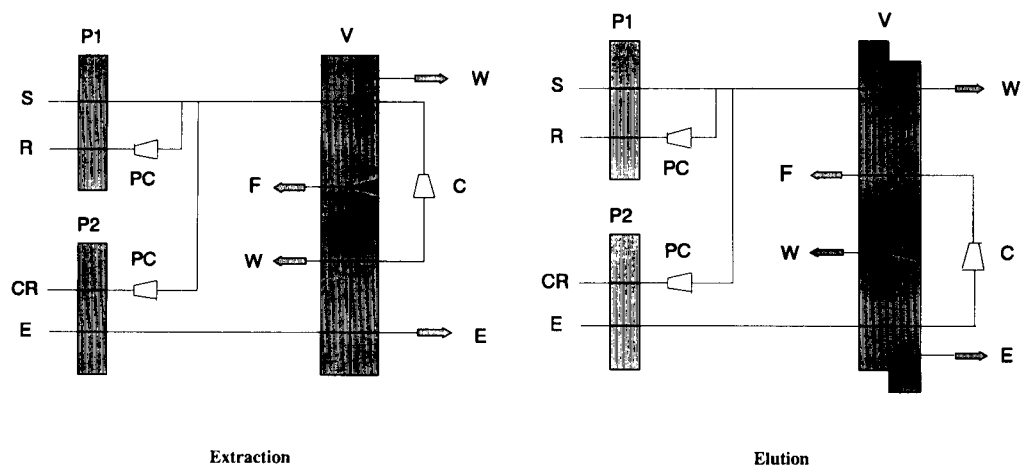

Fig. 1. FI manifold for sorbent extraction and elution. P1, sample pump; P2, eluent pump; S, sample solution; R, reagent solution; CR, column-rinsing solution; E, eluent; PC, precolumn; C, extraction column; W, waste; F, tubing adapter F; V, valve.

fects (5 cm). The PTFE tube after the FIAS valve for elution was also as short as possible (5 cm) to minimize the dispersion of the eluted complexes while tubing adapter F (Pt/Ir capillary, PE B019-3873) was used at the end of it. The middle hole in the 5-hole valve stator was blocked. The eluate was collected in a 0.5 ml micro-test tube with safety lid lock (Eppendorf 0030121.023). All vessels for preparing the standards, samples,reagent solutions and column-rinsing solutions were made of PTFE and were washed daily with 10% (v/v) nitric acid to avoid adsorption loss or contamination.

A Perkin-Elmer Model 3030 atomic absorption spectrophotometer was equipped with a Perkin-Elmer HGA 500 graphite furnace atomizer and an AS-40 furnace autosampler. Hollow cathode lamps were used as light sources at 228.8 nm for cadmium, 324.8 nm for copper and 283.3 nm for lead, respectively, all with 0.7 nm slit. Deuterium arc background correction was used for all three metals. A pyrolytic graphite-coated graphite tube with pyrolytic graphite L'vov platform (Perkin-Elmer) was used. The maximum power heating and internal gas stop were used for atomization. The peak area signal was recorded by a Perkin-Elmer PR-100 printer except that the atomization temperature optimization was based on peak height signals. The injection volumes were 20 μl for cadmium and copper and 40 μl for lead. The graphite furnace time–temperature programme is shown in Table 2. GF detection was carried out while the FI system started extracting the next sample. Every sample solution was extracted and measured three times in sequence.

The FI on-line sorbent extraction flame AAS system, used for the optimization of the sorbent extraction, has been described in our previous report [13].

Table 2
HGA time–temperature programme

Step No.		Temp. (°C)	Ramp (s)	Hold (s)	Int. flow (ml min^{-1})	Read
1		90	1	34	300	
2 [a]	Pb	150	1	14	300	
3	Cd	400	1	19	300	
	Cu	1100	1	19	300	
	Pb	1100	1	19	300	
4	Cd	1500	0	3	0	0
	Cu	2500	0	5	0	0
	Pb	2300	0	3	0	0
5		2650	1	4	300	

[a] Only for lead measurements with 40 μl eluate injection.

2.2. Reagents

All chemical reagents (Merck) were of analytical grade except that Suprapur concentrated nitric acid, perchloric acid and hydrofluoric acid were used for sample digestion and pH adjustment. Ethanol was used as the eluent. DDPA (Aldrich) in 0.1 M citric acid at pH $\approx$ 2 was used as chelating agent at a concentration of 0.01% (m/v) for copper, 0.1% for lead and 0.2% for cadmium in digested samples or 0.5% for cadmium in water samples. A DDPA solution of the same concentration as the chelating agent solution for each element, acidified to pH 2 with nitric acid, acted as the column-rinsing solution. Deionized water from a Milli-Q water system (Millipore) was used throughout. Standard solutions of tested metals were made by stepwise dilution from 1000 mg l^{-1} stock solutions (Merck) with Milli-Q water acidified with nitric acid to pH 2. The chemical modifier used was 5 μg Pd as $Pd(NO_3)_2$ in 5 μl of solution.

2.3. Digestion of solid samples

Biological samples

1.0 ml of HNO_3 was added to 0.1 g of mussel tissue (CRM 278), single cell protein (CRM 274, for cadmium and copper determination) and plankton (CRM 414) or 5.0 ml of HNO_3 to 0.5 g of cod muscle (CRM 422) and 1.0 g of single cell protein (for lead determination only) in the PTFE beaker of a standard digestion bomb. The open bomb, covered by a cap with a small hole to prevent contamination, was heated gently on a hot plate till fuming. After the solution was cooled down, 0.5 ml of $HClO_4$ for 0.1 g samples or 2.5 ml of $HClO_4$ for 0.5 g and 1.0 g samples was added. The bomb was sealed and heated in an oven for 8 h at 150°C. The contents of the bomb

was transferred to a 50 ml flask and diluted with Milli-Q water.

Environmental samples

3.0 ml of conc. HF and 1.0 ml of conc. HNO_3 were added to 0.1 g of calcareous loam soil (CRM 181), river sediment (CRM 320) or lake sediment (CRM 280) in the PTFE beaker of the digestion bomb. The open bomb with the cap was heated gently on a hot plate till fuming. After the solution was cooled down, 0.5 ml of $HClO_4$ was added, the bomb was sealed and heated in the oven for 8 h at 150°C. The contents of the opened bomb was evaporated to dryness on a hot plate. The residue, treated again with the mixture of HF and HNO_3 if necessary, was dissolved in 0.5 ml of HNO_3 and 5 ml of water and diluted to 50 ml.

2.4. Pretreatment of water samples

Natural sea water samples were acidified to pH 1.5 while estuarine water samples were acidified to pH 2.0 and then filtered through a 0.45-μm filter membrane. The salinity was 8 or 16‰ for estuarine water and 35‰ for sea water. No pretreatment was carried out for the standard sea water (CRM 403).

3. Results and discussion

3.1. Sorbent extraction

pH effect and masking effect

The pH effect on the sorbent extraction with 0.1 M acetate–ammonium or citrate–ammonium media for DDPA was tested with flame AAS detection (Fig. 2). Cadmium, copper and lead were extracted quantitatively below pH 8, 9 or 8 from an acetate medium but below pH 3, 5 or 3 from a citrate medium, respectively. Iron was extracted around pH 1 from an acetate medium where the iron(II) signal was about 2/3 that for iron(III); iron was not extracted from a citrate medium. Cobalt, manganese, nickel and zinc were not extracted from either medium. 0.1 M citrate masked iron completely and had a significant influence on copper (pH 6–9), cadmium and lead (pH 4–8). DDPA in 0.1 M citrate at pH 2 was used further to provide high selectivity for the three analytes.

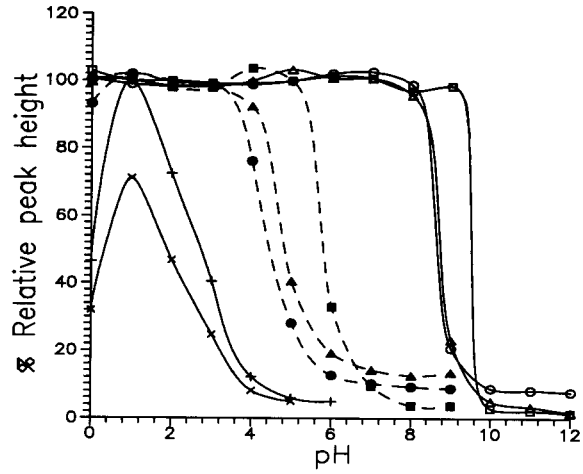

Fig. 2. pH effect on the sorbent extraction. ○ = Cd with acetate; □ = Cu with acetate; △ = Pb with acetate; + = Fe(III) with acetate; × = Fe(II) with acetate; ● = Cd with citrate; ■ = Cu with citrate; ▲ = Pb with citrate.

Interference

The influence of coexisting iron, copper or lead on the sample-loaded volume and the cadmium signal using DDPA in citrate medium with 120-s sample loading for flame detection is illustrated in Fig. 3a. Unextractable iron was tolerable up to 1000 mg l^{-1} without significant interference, while the tolerance to the extractable metals, copper or lead was below 1 or 10 mg l^{-1} with 10% depression, respectively. The tolerance to iron in this case was 1000-fold better than when using diethylammonium diethyldithiocarbamate (DDDC) in acetate medium where the concentration of coexisting heavy metals could not exceed 1 mg l^{-1} even for copper measurement (Fig. 3b). The sample-loaded volumes decreased owing to the decrease of the sample-loading rate; while the decrease of the eluting rate was implied by the broader elution peaks. The decrease of the both rates could be explained by clogging by the high content of coexisting heavy metals retained on the column.

Reagent concentration

Different minimum concentrations of DDPA as complexing agent were found as follows for quantitative extraction of cadmium (0.2%), copper (0.005%) and lead (0.1%) in standard solutions because of the different stabilities and extractabilities of their complexes [13]. The complexation and extraction could be further influenced by the salt matrix or natural organic compounds present in natural waters. According to the spike recovery, a higher DDPA concentration, 0.5%, was required for cadmium determination in water samples with GFAAS detection. DDPA concentrations of 0.01% for copper, 0.1% for lead and 0.2% for cadmium in digest solutions or 0.5% for cadmium in water samples were used. The selectivity to copper and lead could be improved to some extent by controlling the reagent concentration.

Eluent

There was no difference in sensitivity and precision between methanol and ethanol as eluents for sorbent extraction with flame AAS detection [13]. However, considering the influence of eluent evaporation for off-line GFAAS detection, ethanol was selected as eluent. In an open sample cup in the furnace autosampler at room temperature, 1 ml of methanol could be kept only for 5 min within 2% loss of volume while ethanol could be kept for 15 min. However, using 0.5-ml micro-test tubes with a safety lid lock, the ethanolic eluate could be kept closed for considerably longer periods.

3.2. Column rinsing

When the saline water was analysed without rinsing the extraction column before elution, a salt deposit in the graphite tube was observed and the background became too high to be corrected effectively by the deuterium corrector, even after emptying the column by air before elution. Rinsing of the column before elution is effective for removing the salt matrix remaining in the column for this kind of sample. There are two ways to rinse the column: (1) in the opposite direction to that of sample loading, with the sample pump; (2) in the same direction as sample loading with the eluent pump. As is apparent when observing the flame colour with flame detection, and the spike recovery with GFAAS detection for sea water, the column rinsing efficiency in the forward direction is higher than that in the opposite direction. In addition, for column rinsing in the opposite direction, the sample pump pressure must be very high to obtain smooth flows for three pump tubes of different diameters while the sample solution is wasted during the rinsing step. Hence column rinsing in the forward

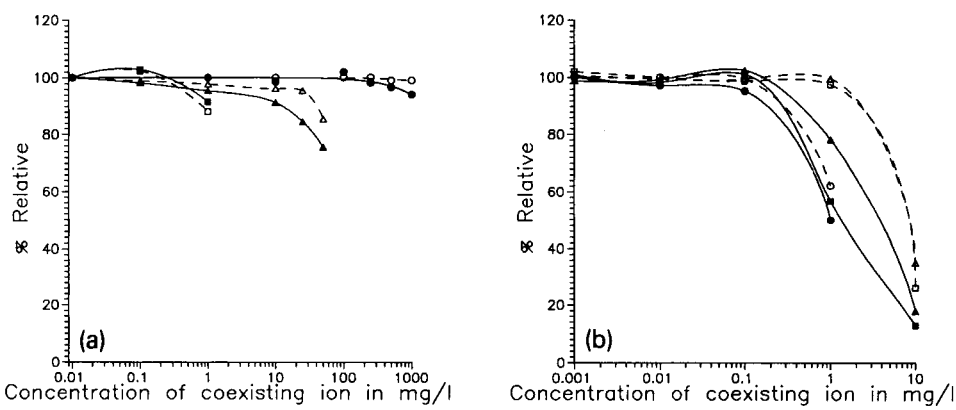

Fig. 3. Interference of coexisting heavy metals on the sample-loaded volume and peak height signal of (a) cadmium with DDPA in citrate medium and (b) copper with DDDC in acetate medium. Key to symbols: (a) sample volume with (○) Fe, (□) Cu, (△) Pb; peak height with (●) Fe; (■) Cu, (▲) Pb; (b) as (a) except □, ■ = Cd.

direction was used for saline water analysis. During this step the eluent was pumped back to the eluent container.

It was found necessary to add DDPA to the column-rinsing solution. The influence of the DDPA concentration in the column rinsing solution is shown in Fig. 4. Cadmium could be rinsed quantitatively with the DDPA concentration above 0.05%. Copper could be rinsed quantitatively with or without DDPA. Lead could be rinsed quantitatively with the DDPA concentration above 0.005%. The same reagent concentration was used for both the complexing agent and the additive in the column rinsing solution for each element.

The first couple of seconds of column rinsing was extremely efficient for removing the salt matrix and thus reducing the background. The background and the corrected signals became stable on prolonging the column rinsing time. A column rinsing step of 15 s was found to be sufficient to obtain a normal background value and good spike recovery of cadmium in sea water for GFAAS.

No difference in the column-rinsing efficiency was observed with the media between 5% (v/v) HNO_3 (pH ≈ 0) and 0.01% HNO_3 (pH ≈ 3) for column rinsing solution according to the cadmium spike recovery test in sea water.

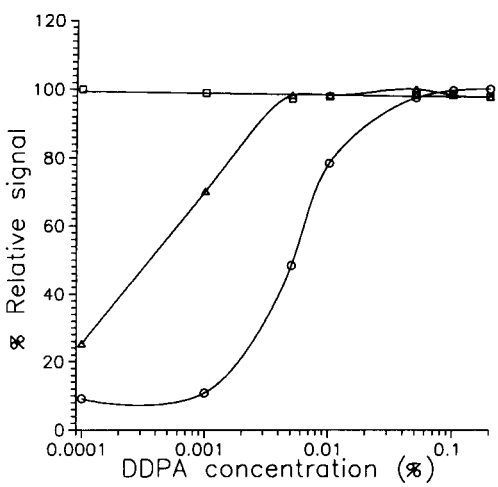

Fig. 4. Influence of the DDPA concentration on column rinsing. ○ = Cd, □ = Cu, △ = Pb.

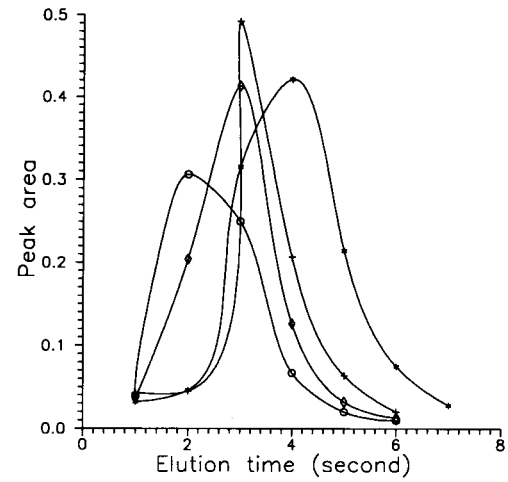

Fig. 5. Effect of the elution time at different elution rates. ○ = 5.7, ◇ = 4.4, + = 3.5, * = 2.5 ml min^{-1}.

3.3. Elution

The influence of the elution time (every second) at different elution rates is illustrated in Fig. 5 for 200 ng l^{-1} cadmium after 20-s sample loading with GFAAS detection. The eluates obtained in the first 1-s elution at all rates, which mainly came from the eluent in the tubing after the column, gave small, nearly stable signals. Most of the complex was eluted in the 2- and 3-s elutions at high elution rates or in the 3- and 4-s elutions at low elution rates. For a 1-s eluate collection, the eluates of the elution during the 2nd second at 5.7 ml min^{-1} or the 3rd second at 3.0–5.3 ml min^{-1} contained around 50% of the complex. For a 2-s collection, the 2- and 3-s eluates at 5.7 ml min^{-1} or 3- and 4-s eluates at 3.5 ml min^{-1} contained over 80% of the complex. The maximum signals increased from elution rates 5.7 to 3.5 ml min^{-1} because of the smaller eluate volume and higher elution efficiency; then they decreased because of the greater dispersion of the eluted complex. Below an elution rate of 5 ml min^{-1} the eluent flow was not very smooth even under the maximum pump pressure with the pump tube for the column rinsing solution. With lower elution rates and shorter eluate collection times, higher sensitivities could be obtained but

the precision was poorer, hence this working condition did not improve the detection limit. In order to minimize the influence of change in eluent flow rate on reproducibility, most of the complex should be collected. In consideration of the possibility of injecting larger volumes or of repeat injections and in order to minimize the influence of eluent evaporation, the collected eluate volume should not be too small. The 2- and 3-s eluate at 5.7 ml min^{-1} was used for further work and provided the best detection limits.

3.4. Chemical modifier

One benefit of the application of extractions to AAS is to remove the sample matrix, so that no matrix modifier must be added in GFAAS measurements. In a preliminary attempt to analyse the BCR standards without any chemical modifier, however, the copper results were too high while the blank value was high and unstable. When only Pd was injected after the analyses, a very high copper signal was found, which decreased gradually with repeated injections of Pd but did not decrease to the baseline. In this case the graphite tube had to be replaced. The reason could be the soaking of the extract into the graphite in which penetration is promoted by the good wetting ability of the organic eluent [2]. The addition of a chemical modifier was necessary to avoid this effect, especially for copper. Using Pd as the modifier, a black film built up gradually on the tip of the injection capillary, but no influence was observed on the sensitivity and precision. A possible reason is that Pd reacts with DDPA [31]. No black deposit was observed with Pt as the modifier, but the cadmium peak shapes changed gradually. Consequently a low concentration of Pd (5 μg in 5 μl), was selected as the modifier.

Table 3
Determination of cadmium in reference materials

Reference material [a]	Certified concentration ($\mu g\ g^{-1}$)	Measured concentration ($\mu g\ g^{-1}$)
Cod Muscle	0.017 ± 0.002	0.016 ± 0.001
Single cell protein	0.030 ± 0.002	0.031 ± 0.002
Mussel tissue	0.34 ± 0.02	0.35 ± 0.01
Plankton	0.383 ± 0.014	0.393 ± 0.036
Calcareous loam soil	0.36 ± 0.10	0.37 ± 0.01
River sediment	0.533 ± 0.026	0.523 ± 0.006
Lake sediment	1.6 ± 0.1	1.68 ± 0.02
Sea water [b]	0.175 ± 0.018	0.161 ± 0.002

[a] The sample loading time was 20 s for the digest solutions.
[b] The sample loading time was 60 s. The concentration is in nmol kg^{-1}.

Table 4
Determination of copper in reference materials

Reference material [a]	Certified concentration ($\mu g\ g^{-1}$)	Measured concentration ($\mu g\ g^{-1}$)
Cod Muscle	1.05 ± 0.07	1.01 ± 0.11
Single cell protein	13.1 ± 0.4	13.9 ± 0.4
Muscle tissue	9.60 ± 0.16	10.02 ± 0.12
Plankton	29.5 ± 1.3	30.9 ± 1.7
Calcareous loam soil	32.6 ± 1.4	32.0 ± 0.5
River sediment	44.1 ± 1.0	45.9 ± 1.4
Lake sediment	70.5 ± 1.5	70.9 ± 0.7
Sea water [b]	3.90 ± 0.37	4.53 ± 0.44

[a] The sample loading time was 20 s for the digest solutions.
[b] The sample loading time was 30 s. The concentration is in nmol kg^{-1}.

3.5. Blank

The blank signal mainly originated from the DDPA reagent which was used as the complexing agent and for column rinsing. The on-line precolumns for the complexing agent solution and the column rinsing solution reduced the blank signal by one third to a half when using 20-s sample loading and 15-s column rinsing. The blank value did not increase linearly with sample loading time, column rinsing time or reagent concentration using the purifying precolumns. It was observed that on increasing the DDPA concentration 20 times from 0.01 to 0.2% with column rinsing, the copper blank was only doubled; increasing the sample loading time 9 times from 20 to 180 s and increasing the injected eluate volume from 20 to 40 μl, the lead blank was tripled. Similar phenomena were reported by Porta et al. [22]. DDPA concentrations as low as possible for every element were used to maintain low blank signals. Under these circumstances the blank signals obtained were around 0.010 A s (absorbance seconds) for cadmium or copper and 0.005 A s

for lead in peak area with 20-s sample loading and 15-s column rinsing for a 20-μl eluate injection, which were similar to the blank signals for 20 μl direct injection of an aqueous solution. Without the column rinsing step the blank values were around half of the above. 0.2% DDPA would be used for determining the three elements in the same eluates without causing too high blanks.

3.6. Precision

In preliminary experiments, the eluate was collected into a sample cup for the furnace autosampler. This resulted in very poor precision (10–20% R.S.D.) even after carefully shaking. The reason was that the eluate was inhomogeneous and could not be mixed well in the sample cup. Precision was improved by collecting the eluate into a 0.5 ml micro-test tube with safety lid lock, closing it and shaking it well before the GFAAS measurement. In this way an R.S.D. of ca. 2% could be achieved at 0.1 $\mu g\ l^{-1}$ cadmium, 1 $\mu g\ l^{-1}$ copper or 3 $\mu g\ l^{-1}$ lead.

In general, the reproducibility of this analytical system was similar to that of conventional GFAAS.

3.7. Determination of cadmium, copper and lead

The developed system was applied to eight kinds of biological and environmental reference materials. The analytical results are listed in Tables 3–5. All results agree very well with the certified values (95% confidence intervals). The measured concentrations are the mean and standard deviation of the determinations of three independent digestions for the solid samples or three independent determinations for the water samples. Some digest solutions were diluted with acidified (HNO_3) deionized water (pH 2) prior to extraction to adjust the concentrations within the linear calibration ranges. In the biological materials, especially the cod muscle and single cell protein, the analyte concentrations are very low, and coexisting iron (3.1 mg l^{-1}) and zinc (0.9 mg l^{-1}) in the single cell protein for lead determination have to be separated effectively. The geological samples with high enough analyte concentrations were used for demonstrating the tolerance of the extraction to the complex matrices. In their diluted solutions for determination, the coexisting iron contents were 2 to 8 mg l^{-1} which was not tolerable by the extraction system with DDDC. For the analysis of digest solutions, the column-rinsing step was not necessary while no phenomena were observed which gave evidence of the column clogging. An advantage of the proposed method is that perchloric acid, which is normally used in the destruction of biological matter and interferes in conventional GFAAS, does not have to be evaporated because the acid is removed efficiently in the extraction procedure. This reduces significantly the digestion time and the

Table 5
Determination of lead in reference materials

Reference material [a]	Certified concentration ($\mu g\ g^{-1}$)	Measured concentration ($\mu g\ g^{-1}$)
Cod Muscle	0.080 ± 0.015	0.081 ± 0.023
Single cell protein	0.044 ± 0.010	0.051 ± 0.019
Mussel tissue	1.91 ± 0.04	1.94 ± 0.04
Plankton	3.97 ± 0.19	4.16 ± 0.27
Calcareous loam soil	29.4 ± 2.6	27.0 ± 0.3
River sediment	42.3 ± 1.6	42.4 ± 0.5
Lake sediment	80.2 ± 2.3	81.3 ± 2.2
Sea water [b]	0.117 ± 0.025	0.117 ± 0.005

[a] The sample loading time was 20 s for the digest solutions.
[b] The sample loading time was 180 s. The concentration is in nmol kg^{-1}.

Table 6
Spike recovery of natural estuarine and sea waters

Water samples	Spike recovery (%)		
	Cadmium [a]	Copper [b]	Lead [c]
Sea water A	89.6 ± 3.0	104.8 ± 6.7	91.8 ± 3.0
Sea water B	90.2 ± 9.5	104.9 ± 5.0	–
Estuarine water A	94.2 ± 9.3	102.7 ± 6.1	106.5 ± 1.4
Estuarine water B	98.8 ± 3.2	106.1 ± 4.7	87.6 ± 0.4

[a] The samples were spiked with 25 ng l^{-1} Cd for sea water samples or 50 ng l^{-1} Cd for estuarine water samples. The sample loading time was 60 s for sea water and 30 s for estuarine water.
[b] The samples were spiked with 0.5 $\mu g\ l^{-1}$ Cu for sea water samples or 1.0 $\mu g\ l^{-1}$ Cu for estuarine water samples. The sample loading time was 30 s for sea water and 20 s for estuarine water.
[c] All samples were spiked with 50 ng l^{-1} Pb. The sample loading time was 180 s.

chance of contamination. In the destruction of sediment and soil samples evaporation with hydrofluoric acid is still necessary to remove silicates completely. For the saline water both analyte preconcentration and salt matrix removal are critical. The spike recoveries of some natural estuarine and sea waters are between 87 and 107% (Table 6).

With 20-s sample loading at 8.7 ml min^{-1}, 20 μl eluate injection and peak area measurement, the enrichment factors were 12, 13 and 13 compared with a 20-μl direct injection of aqueous solution; detection limits (3σ, $n = 10$) were 0.003, 0.05 and 0.04 $\mu g\ l^{-1}$; the calibration graphs are linear up to 0.1, 5.0 (the maximum concentration tested) and 4.0 $\mu g\ l^{-1}$, respectively, for cadmium, copper and lead.

4. Conclusions

FI sorbent extraction with a highly selective complexing agent is an effective analyte preconcentration and matrix removal technique for GFAAS, whose reliability and accuracy were proven by the determination of cadmium, copper and lead at ng l^{-1} to $\mu g\ l^{-1}$ or ng g^{-1} to $\mu g\ g^{-1}$ level in some standard reference materials including saline water, biological materials and geological samples with very complex matrices. The precision and sampling frequency were similar to those for conventional GFAAS with deuterium background correction. The present work was performed in the off-line mode because of technical limitations, but the realization of an on-line automatic direct eluate injection at a stable low rate should further improve the analytical performance.

References

[1] J. Komárek and L. Sommer, Talanta, 29 (1982) 159.
[2] A.B. Volynsky, B.Ya. Spivakov and Yu.A. Zolotov, Talanta, 31 (1984) 449.
[3] Yu.A. Zolotov and N.M. Kuz'min, Preconcentration of Trace Elements, Elsevier, Amsterdam, 1990, p. 223.
[4] B. Karlberg, Anal. Chim. Acta, 214 (1988) 29.
[5] M. Valcárcel and M. Gallego, in J.L. Burguera (Ed.), Flow Injection Atomic Spectroscopy, Marcel Dekker, New York, 1989, p. 177.
[6] V. Carbonell, A. Salvador and M. de la Guardia, Fresenius' J. Anal. Chem., 342 (1992) 529.
[7] M. Bengtsson and G. Johansson, Anal. Chim. Acta, 158 (1984) 147.
[8] K. Bäckström and L.-G. Danielsson, Anal. Chem., 60 (1988) 1354.
[9] K. Bäckström and L.-G. Danielsson, Anal. Chim. Acta, 232 (1990) 301.
[10] J. Ruzicka and A. Arndal, Anal. Chim. Acta, 216 (1989) 243.
[11] Z. Fang, T. Guo and B. Welz, Talanta, 38 (1991) 613.
[12] S. Xu, M. Sperling and B. Welz, Fresenius' J. Anal. Chem., 344 (1992) 535.
[13] R. Ma, W. Van Mol and F. Adams, Anal. Chim. Acta, 285 (1994) 33.
[14] Z. Fang, M. Sperling and B. Welz, J. Anal. At. Spectrom., 5 (1990) 639.
[15] M. Sperling, X. Yin and B. Welz, J. Anal. At. Spectrom., 6 (1991) 295.
[16] M. Sperling, X. Yin and B. Welz, J. Anal. At. Spectrom., 6 (1991) 615.
[17] M. Sperling, X. Yin and B. Welz, Spectrochim. Acta, 46B (1991) 1789.
[18] M. Sperling, X. Yin and B. Welz, Analyst, 117 (1992) 629.
[19] B. Welz, X. Yin and M. Sperling, Anal. Chim. Acta, 261 (1992) 477.
[20] B. Welz, Microchem. J., 45 (1992) 163.
[21] B. Welz, M. Sperling and X. Sun, Fresenius' J. Anal. Chem., 346 (1993) 550.
[22] V. Porta, O. Abolino, E. MenTasti and C. Sarzanini, J. Anal. At. Spectrom., 6 (1991) 119.
[23] R.H. Atallah, G.D. Christian and A.E. Nevissi, Anal. Lett., 24 (1991) 1483.
[24] Z. Liu and S. Huang, Anal. Chim. Acta, 267 (1992) 31.
[25] Z. Liu and S. Huang, Anal. Chim. Acta, 281 (1993) 185.
[26] S. Nakashima, R.E. Sturgeon, S.N. Willlie and S.S. Berman, Fresenius' Z. Anal Chem., 330 (1988) 592.
[27] E. Beinrohr, M. Čakrt, M. Rapta and P. Tarapčí, Fresenius' Z. Anal. Chem., 335 (1989) 1005.
[28] L.C. Azeredo, R.E. Sturgeon and A.J. Curtius, Spectrochim. Acta, 48B (1993) 91.
[29] P.C. Bank, M.T.C. de Loos-Vollebregt and L. de Galan, Spectrochim. Acta, 43B (1988) 983.
[30] P.C. Bank, M.T.C. de Loos-Vollebregt and L. de Galan, Spectrochim. Acta, 44B (1989) 571.
[31] A.K. De, S.M. Khopkar and R.A. Chalmers, Solvent Extraction of Metals, Van Nostrand Reinhold, London, 1970, p. 169.

ELSEVIER

Analytica Chimica Acta 293 (1994) 261–270

ANALYTICA CHIMICA ACTA

Study of the lability of copper(II)–fulvic acid complexes by ion selective electrodes and potentiometric stripping analysis

Helena M.V.M. Soares [1], M. Teresa S.D. Vasconcelos *

Chemistry Department, Faculty of Science, P-4000 Porto, Portugal

(Received 21st December 1993)

Abstract

Two electroanalytical techniques, direct potentiometry with a copper ion selective electrode (ISE) and potentiometric stripping analysis (PSA), were used to evaluate the lability of copper–fulvic acid complexes (Cu–FA) in 0.5 mol/l sodium perchlorate and in synthetic sea water. The determinations were performed at pH 6.5, and for sea water also at pH 7.5. By ISE potentiometry, in 0.5 mol/l sodium perchlorate, the FA total complexation capacity (CC) in the 1–150 mg/l FA concentration range, as well as the 1:1 Cu–FA conditional stability constants for two different types of binding sites (K_1 and K_2) and the respective metal-binding capacities (C_1 and C_2; $C_1 + C_2 = CC$) were obtained. It was found that CC was approximately constant over the FA concentration range studied: 1.81 mmol/g of FA or 5.2 mmol/g of total organic carbon (TOC). For 0.2–18 $|FA|_t/|Cu|_t$ molar ratio range, the values of the complexation parameters were as follows: log $K_1 = 5.77 \pm 0.09$, $C_1 = (4.7 \pm 1.2) \times 10^{-5}$ mol/l and log $K_2 = 4.22 \pm 0.10$, $C_2 = (14.8 \pm 1.7) \times 10^{-5}$ mol/l (95% confidence limits, 20°C). These parameters were also obtained at 25°C. K_1 and K_2 decreased with the decreasing of $|FA|_t/|Cu|_t$. The labile copper fraction was determined by PSA, in a large $|FA|_t/|Cu|_t$ molar ratio range (89–1.6) in 0.5 mol/l sodium perchlorate medium, at −0.5 V vs. SCE and 20°C. The results were compared with the inorganic copper(II) fraction obtained by a computational simulation based on equilibrium considerations. The lowest lability (dissociation of ca. 8% of the Cu–FA complexes) was found for the highest $|FA|_t/|Cu|_t$ ratio, which corresponded to $|Cu\text{–}FA|/TOC = 0.06$ mmol/g. The lability increased up to ca. 61% when $|FA|_t/|Cu|_t$ decreased down to 6 (or $|Cu\text{–}FA|/TOC = 0.8$ mmol/g) and slightly decreased down to ca. 50% for lower $|FA|_t/|Cu|_t$ values (the lowest was 2 mmol/g). In synthetic sea water, the inert copper(II) fraction (i.e., $|Cu|_t/|Cu|_{labile}$ measured by PSA) was not very different from that found for 0.5 mol/l sodium perchlorate for identical $|FA|_t/|Cu|_t$ at pH 6.5. Similar results were obtained at pH 7.5. These results suggest that the PSA kinetic behaviour of FA in sea water may be not very different from that observed for the simpler medium of similar ionic strength.

Key words: Ion selective electrode; Potentiometry; Copper(II)–fulvic acid complexes; Lability; Sea water; Synthetic sea water; Waters

1. Introduction

Copper is an essential micronutrient but it becomes toxic at high levels. In aquatic environ-

* Corresponding author.

[1] Permanent adress: Chemical Engineering Department, Faculty of Engineering, P-4099, Porto Codex, Portugal.

SSDI 0003-2670(94)00092-Z

ment, the metal outcompetes with macronutrients for sorption sites, even at relatively low concentrations, and the copper speciation is largely dependent on the inorganic and organic ligands present in waters. Therefore, in order to understand and predict the interactions of copper with phytoplankton, it is necessary to have a better understanding of the biologically available fraction of the metal.

In biological evaluation studies of the influence of the heavy metals on the mobility and growth of microalgae, these organisms have been grown in synthetic sea water media which may include EDTA as complexing agent (e.g. ESAW) [1]. Although EDTA is one of the strongest chelating agents for transition heavy metals, its concentration in natural sea water, if present at all, is usually too low to compete with inorganic ligands for the metal ions [2]. Fulvic acids (FA) form much weaker complexes than EDTA but they are important components of coastal sea waters (for instance, FA concentrations of ca. 0.1 mg/l were found in coastal sea water at the north of Portugal [3]) and, therefore, the substitution of EDTA by FA in culture media may simulate real sea water better.

The literature describing the properties of FA as a copper complexing ligand is vast but far from straightforward, mainly because fulvic acids have undefined molecular weight, contain multiligand sites and display a wide range of complexing abilities. In addition, the assumption that the metal–FA complexes are inert [4] has been discussed in recent papers [5–7].

In the present paper, the kinetic behaviour of Cu–FA complexes in a large range of metal and ligand concentrations, at pH 6.5 and 7.5, is discussed. Two electroanalytical techniques that give complementary information about complexing equilibria, direct potentiometry with a copper(II) ion-selective electrode (ISE) and potentiometric stripping analysis (PSA), were used.

Table 1
Composition of artificial sea water [1] [a]

Macrocomponents (mmol/l)		Microcomponents (μmol/l)	
NaCl	363	$NaNO_3$	549
$MgCl_2$	47.2	Na_2SiO_3	106
Na_2SO_4	25.0	$NaglyceroPO_4$	21.8
$CaCl_2$	9.14	$Fe(NH_4)_2(SO_4)_2$	5.97
KCl	8.04	$MnSO_4$	2.42
$NaHCO_3$	2.07	$FeCl_3$	5.92×10^{-1}
KBr	7.25×10^{-1}	$ZnSO_4$	2.54×10^{-1}
H_3BO_3	4.34×10^{-1}	$CoSO_4$	5.69×10^{-2}
$SrCl_2$	8.20×10^{-2}	Thiamine–HCl	2.97×10^{-1}
NaF	6.57×10^{-2}	Vitamin B_{12}	1.47×10^{-3}
		Biotin	4.09×10^{-3}

[a] The solution also included PIPES buffer (pH 6.5 and 7.5) and FA (see FA concentrations in Table 2).

2. Experimental

2.1. Reagents and materials

Analytical or equivalent grade reagents were used without further purification. The FA sample was isolated from a Portuguese forest soil collected at Ermesinde (at 12 km from Oporto) by the standard procedure recommended by the IHSS [8]. Although marine and soil FA have some structural differences [3], a soil FA sample was used for extraction. The synthetic sea water solution used in some PSA measurements was prepared as described before [1] but without EDTA (see Table 1). Deionized water with resistivity > 4 MΩ cm was used throughout the experiments.

All material used was cleaned by soaking in 10% nitric acid solution followed by rinsing with water. The sample and standard were stored in polyethylene vessels.

2.2. Apparatus

The ISE measurements were performed with a Sargent-Welch 6050 pH meter which was coupled to a Fischer switch. As working electrodes, a Philips GAH110 glass electrode and a Radiometer 3012 electrode, activated with a Ag_2S/CuS sensor (prepared as reported in [9]), were used. An Orion 90-02-00 (double junction) reference electrode was used with the outer chamber filled with 0.5 mol/l potassium perchlorate. The experiments were performed in a Metrohm EA 880T double wall glass cell.

The PSA experiments were carried out with a Radiometer ISS 820 ion-scanning system, constituted by a REA 120 ion scanning unit, a TTA-IS ion-scanning assembly and a Servograph REC 80 plotter. The electrochemical cell consisted of a polyethylene vessel in which a Radiometer 847-712 mechanical stirrer and the electrodes were inserted. A P1312 platinum wire, a F3500 glassy carbon electrode and a K-4040 saturated calomel electrode (SCE), all Radiometer, were used as the counter, working and reference electrodes, respectively.

Total organic carbon (TOC) was measured with a Ionics 1258 total organic carbon analyzer.

2.3. Analytical procedure

Almost all experiments were performed at pH 6.5 but, for evaluation of the influence of pH on the lability of the complexes in sea water, the PSA experiments were repeated at pH 7.5. For pH adjustment, a piperazine-*N*,*N*-bis(2-ethanesulfonic acid) (PIPES) buffer solution was used. In preliminary experiments, it was verified by ISE that no Cu–PIPES complexes were formed to a significant extent. The lability studies (ISE and PSA) were carried out at 20°C. However, ISE determinations were also performed at 25°C, to allow direct comparison of results with literature data.

ISE measurements were performed in 0.5 mol/l sodium perchlorate solutions with fixed FA concentrations (dilution effect $\leqslant 10\%$, the maximum variation occurring for the lowest FA concentration). A sodium perchlorate background with ionic strength similar to sea water (ca. 0.5 mol/l) was used, because chloride is a severe interferent in the copper ISE. As titrant, 5×10^{-3} mol/l copper(II) nitrate in 0.5 mol/l sodium perchlorate solution was used. The levels of ligand and metal concentrations as well as the remainder experimental conditions are given in Table 2. In each assay, two copper ISEs were used in parallel to test the reproducibility of the potential. The copper ISEs were calibrated before each titration by a similar procedure but in absence of FA. For each titration point, the cell potential was read after stabilization ($\Delta E \leqslant 0.1$ mV/min) had been reached.

For PSA measurements a glassy carbon mercury film electrode was prepared [11] daily by electrolysing a solution containing 2×10^{-5} mol/l of mercury(II) (mercury(II) chloride). For this purpose, electrolysis potential and time were fixed at -0.5 V vs. SCE and 4 min, respectively, and four sequential plating/stripping cycles were performed. The measurements were carried out on 20 ml of working solution, with a constant convection rate of 2550 rpm. The dissolved oxygen was previously removed by bubbling nitrogen through the solution during 10 min and a nitrogen atmosphere was maintained above the solution during the experiments. These were performed in both 0.5 mol/l sodium perchlorate solution and an artificial sea water medium [1], at fixed metal and ligand concentrations (batch pro-

Table 2
Experimental conditions used in the measurements [a]

Medium [b]	pCu_t	pCu_f [c]	FA (mg/l) [d]	EDTA (mol/l)	Electrolysis time (s)
			ISE [e]		
$NaClO_4$	5.3–3.0	6.4–3.1	1.0–150	–	–
			PSA [f]		
$NaClO_4$	6.1–5.2	6.5–5.4	10–150	–	60 or 120
	5.5	< 6.2 [g]	–	4.7×10^{-6}	60
Sea water [h]	4.8–5.7	6.3–5.0	10–150	–	60 or 120
	5.5	< 6.2 [g]	–	1.5×10^{-5}	60

[a] pH 6.5. [b] $I = 0.5$ mol/l. [c] pCu'_f (see text) for PSA experiments, [d] Fixed in each experiment. [e] At both 20 and 25°C. [f] At 20°C and -0.5 V vs. SCE deposition potential. [g] Detection limit of the analytical technique calculated [10] daily from the calibration curve. [h] Also at pH 7.5.

cedure; see concentration ranges in Table 2). A 2 h delay between the preparation of solutions and the measurements guaranteed the establishment of the thermodynamic equilibria. A −0.5 V vs. SCE electrolysis potential was used. This value was chosen sharply to be sufficiently negative to yield a measurable signal for copper under the present experimental conditions in the absence of FA, but was insufficient for direct reduction of the Cu–FA complexes. Depending on the metal-to-ligand ratio of concentrations, an electrolysis time of 60 or 120 s was used (see Table 2). In all experiments, 80 μl of 5×10^{-3} mol/l mercury(II) chloride (oxidising agent) were added at the end of the deposition period (see Discussion bellow). The PSA system was calibrated daily by a similar procedure but in the absence of ligand.

To determine the total organic carbon concentration (TOC) in the FA solution, three independent 40.8 mg/l FA solutions were analyzed with a calibration in the range 1–20 mg/l of TOC. For this purpose, potassium biphthalate standard solutions were used. A value of 0.35($\pm$0.10) g TOC/g FA (standard deviation in parentheses) was found.

2.4. Calculations

The conditional stability constants (K) of the Cu–FA complexes and the mean metal-binding capacities of the two assumed types of active sites ($C1$ and $C2$) from the polymeric ligand were calculated respectively by the Scatchard [12] method and by the method described by Ruzic [13,14]. The methods were applied to experimental data obtained by ISE measurements.

Computational simulations of the chemical equilibrium under conditions similar to those used in the experimental measurements, were performed in the present work for several purposes (see below). The speciation computer program MICROQL [15] was used for this purpose. The calculations were based on the pH, on total copper(II) and ligand concentrations and on stability constants of complexes from the literature [16–18] and/or stability constants obtained in the present work.

3. Results and discussion

3.1. ISE determinations

Fulvic acids have undefined molecular weight, the total equivalent molar concentration being usually estimated by the complexation capacity (CC) [19,20]. From the total ($[Cu]_t$) and free ($[Cu]_f$) copper ion concentrations at each point of each titration curve, the CC of the polymeric ligand was determined from the plot $[Cu]_b = f([Cu]_t)$, where $[Cu]_b$ is the bound copper ion fraction (equal to $[Cu]_t/[Cu]_f$), by a method described in the literature [20]. It is stated that this method provides acceptable results only whether Cu–OH complexes are negligible in all range of copper free concentration used for CC calculation. In the present work, the validity of this condition was evaluated by computational simulation. A maximum error of 6% was estimated for the last points of the titration curve. The CC mean values of five independent determinations performed at each fixed FA concentration and 25°C, are given in Table 3 and Fig. 1. This figure shows that the CC in mol/l varies linearly with the FA concentration (correlation coefficient 0.998, $n = 6$). From the plot, a CC value equal to 1.81 mmol/g FA (5.2 mmol/g TOC), which was given by the slope of the straight line and independent of the FA concentration (in the range 1–150 mg/l FA or 0.35–52 mg/l TOC), was obtained. A similar behaviour was found by Lund et al. [21] for fulvic and humic samples in the range 6–60 mg/l TOC, and indicates that no aggregation or other conformational changes occur to an appreciable extent [6] in the range of FA concentration studied.

The FA mean equivalent molecular weight can be obtained as the inverse of the slope of the plot in Fig. 1. Its order of magnitude, 552 g/mol, is the same as for other soil FA samples from different origins, e.g. [22].

In order to estimate the conditional stability constants (K) of the Cu–FA complexes, the same experimental data were treated by both the Ruzic [13,14], $[Cu]_f/[Cu]_b = f([Cu]_f)$, and Scatchard [12], $[Cu]_b/[Cu]_f = f([Cu]_b)$ plots. These methods are linearizations for the 1:1 complex formation

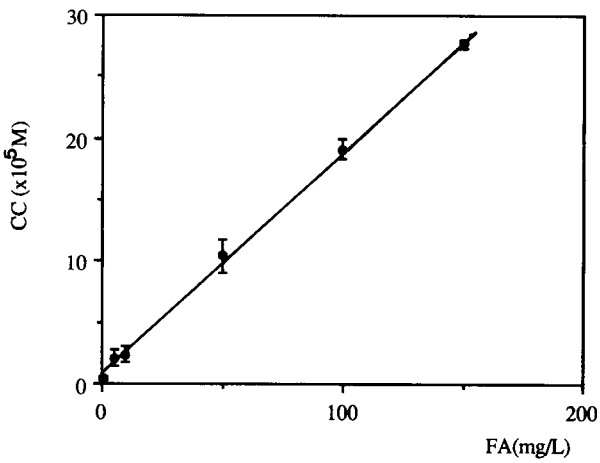

Fig. 1. Mean CC values and respective 95% confidence limits obtained for the different FA concentrations at 25°C. Five independent determinations were performed in each case. Linear regression parameters: $[CC] = (1.81 \pm 0.01) \times 10^{-6}[FA] + (0.84 \pm 0.76) \times 10^{-6}$; $r = 0.998$, $n = 6$.

model but they can provide information about two different types of coordination sites if the respective stability constants are sufficiently different to be distinguished [13]. This was the case for Cu(II)–FA, as illustrated in Fig. 2a and b, where two segments of straight lines with different slopes can be drawn. From the Ruzic plot [13], the mean metal-binding capacities of the two types of active sites (C_1 and C_2) as well as the respective mean conditional stability constants (K_1 and K_2) were obtained. More precise values for K_1 and for K_2 were obtained by the Scatchard plot [12]. For instance, for 50 mg/l FA at 20°C, log $K_1 = 5.78 \pm 0.71$ by Ruzic [13] and 5.54 ± 0.23 by Scatchard [12] plots and log $K_2 = 3.91 \pm 0.10$ by Ruzic [13] and 3.92 ± 0.04 by Scatchard [12] plots.

For the lowest FA concentrations, in the 1–5 mg/l range, a large dispersion of experimental data was observed, due to the low $[Cu]_f$ value measured, near the practical lower limit of linear response of the ISE used. Due to this experimental limitation, the Ruzic [13] or Scatchard [12] methods could not be applied to that FA concentration range. For the remaining FA concentrations the Scatchard method [12] was applied, which provided straight line segments: correlation coefficients of linear regression larger than 0.94 for $n = 25$–39 experimental points were obtained (see typical results in Fig. 2). For the method of Ruzic [13] a similar behaviour was found. The mean values of CC, C_1, C_2, K_1 and K_2 obtained

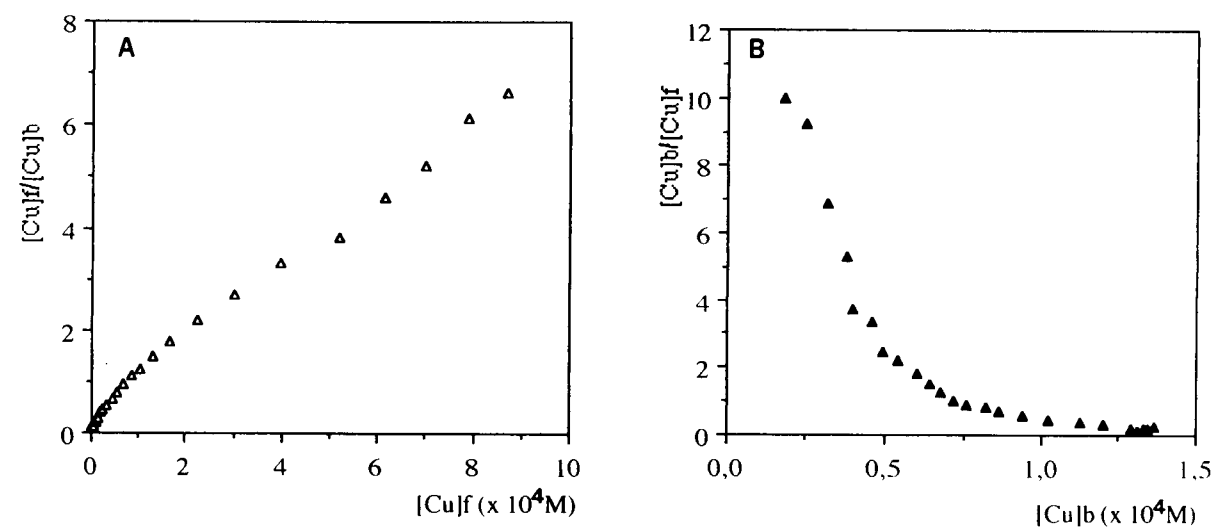

Fig. 2. Typical results obtained by the Ruzic (A) and Scatchard (B) plots for ISE experiments at an FA concentration of 50 mg/l and 20°C.

Table 3
Complexation parameters CC ($\times 10^5$ mol/l) and K of Cu–FA at pH 6.5 [a]

$\|FA\|_t$ mg/l [f]	CC [b,c] (25°C)	C_1 [d] (20°C/25°C)	C_2 [d] (20°C/25°C)	log K_1 [e] (20°C/25°C)	log K_2 [e] (20°C/25°C)
10	2.4	–/–	–/–	4.95/–	3.81/–
(0.018–0.90)	(0.6)			(0.22)	(0.75)
50	10.4	3.4/–	9.0/–	5.54/–	3.92/–
(0.098–4.5)	(1.4)	(1.8)	(3.4)	(0.23)	(0.04)
100	19.1	4.7/4.3	14.8/16.9	5.77/5.52	4.22/4.20
(0.18–18)	(0.8)	(1.2)/(2.9)	(1.7)/(2.6)	(0.09)/(0.21)	(0.10)/(0.10)
150	27.6	–/8.4	–/19.6	–/5.69	–/4.27
(0.27–18)	(0.4)	(3.0)	(2.5)	(0.16)	(0.23)

[a] 95% confidence limits are given in parentheses. [b] Obtained from the $|Cu|_b = f(|Cu|_t)$ curve [20]. [c] For 1 and 5 mg/l $|FA|_t$, the CC values were 0.5 (0.2) and 2.1 (0.6) $\times 10^{-5}$ mol/l, respectively. [d] Obtained by the Ruzic method [13]. [e] Obtained by the Scatchard method [12]. [f] The $|FA|_t/|Cu|_t$ molar ratio range embraced by the titration curve is given in parentheses.

for the 10–150 mg/l FA concentration range are also presented in Table 3. The Table shows that the CC values obtained by both methods ($C_1 + C_2$ = CC) were similar. From titration curves for the 100 mg/l FA concentration, with an $|FA|_t/|Cu|_t$ molar ratio range from 18 to 0.2, the following complexation parameters were obtained: log $K_1 = 5.77 \pm 0.09$, $C_1 = (4.7 \pm 1.2) \times 10^{-5}$ mol/l (or 0.47 ± 0.12 mmol/g FA) and log $K_2 = 4.22 \pm 0.10$, $C_2 = (14.8 \pm 1.7) \times 10^{-5}$ mol/l (or 1.48 ± 0.17 mmol/g FA) (95% confidence limits are given; 20°C); and log $K_1 = 5.52 \pm 0.21$, $C_1 = (4.3 \pm 2.9) \times 10^{-5}$ mol/l (or 0.43 ± 0.29 mmol/g FA) and log $K_2 = 4.20 \pm 0.10$, $C_2 = (16.9 \pm 2.6) \times 10^{-5}$ mol/l (or 1.69 ± 0.26 mmol/g FA) (25°C). The mean values of the conditional stability constants were of similar magnitude to those reported for copper(II) complexes of fulvic acids from soils of different origin, e.g. [21,23].

Table 3 shows that log K_1 and log K_2 increased when the FA concentration was increased. The variation may be due to the different range of $|FA|_t/|Cu|_t$ used for the calculations of the different titration curves: the higher is the $|FA|_t/|Cu|_t$ the higher is the K value. In fact, the polymeric ligand includes a very large number of complexing sites each with a specific microscopic stability constant. The results for FA titrations by a metal ion have shown [24] that the values of the equilibrium constants decrease continuously with the degree of site occupation.

On the other hand, little influence of temperature on log K_1 and log K_2 values was found (Table 3).

3.2. PSA determinations

The combination of ISE and PSA data, at the same ionic strength and pH, allowed us to obtain information about the lability of the FA–copper complexes. PSA measures the inorganic metal concentration plus the reversibly complexed fraction which dissociates at the applied deposition potential [25] during the scale of time of the technique [26]. Therefore, both the ISE and PSA signals depend on the equilibrium constants, but the PSA signal is also influenced by kinetic factors (dissociation rate constant and diffusion coefficient).

In PSA, the metal is electrodeposited on a glassy carbon mercury film (or on an hanging mercury drop) at an imposed negative potential and then chemically oxidised by a suitable oxidising agent (mercury(II) in the present case), the potential being monitored as a function of time. Basically, the PSA technique differs from anodic stripping voltammetry (ASV) in the stripping (chemical vs. electrochemical oxidation) and recording [$E = f(t)$ vs. $i = f(E)$] steps.

Lability of the Cu–FA complexes

To investigate the lability of the Cu–FA complexes, PSA measurements were performed on

solutions with different metal-to-ligand ratios (see Table 4). Determinations were carried out both in 0.5 mol/l sodium perchlorate and in artificial sea water [1] media.

For the sodium perchlorate medium, the inorganic copper(II) fraction ($[Cu]_f$ and ($[CuOH]^+$, $Cu(OH)_2$, $[Cu_2(OH)_2]^{2+}$, $[Cu(OH)_3]^-$ and $[Cu(OH)_4]^{2-}$) were also calculated by a speciation computer program [15], to estimate the copper(II) fraction bound to FA. For this purpose, equilibrium data obtained from the literature [16] for Cu–OH complexes, and by ISE, in the present work, for Cu(II)–FA complexes, were used. In the latter case, the conditional stability constants obtained for the 0.2–18 $|FA|_t/|Cu|_t$ range (titration curve for 100 mg/l FA) were used. The computational equilibrium simulation still involves other approximations: a 1:1 Cu–FA complex formation model with two different types of coordination sites was used; the differences in experimental conditions used in previous studies for the determination of the Cu–OH complexes and in the present work were ignored. Therefore, the $[Cu]_b$ values calculated by equilibrium considerations were approximated values.

The more relevant experimental conditions and the results obtained are presented in Table 4 and in Fig. 3. For the lowest ratios of $[Cu]_b$/g TOC (< 0.06 mmol/g), the lability of the Cu–FA complexes was very low (i.e., the experimental, 90%, and calculated, 98%, percentages of $[Cu]_b$ were similar). This is probably because only the strongest coordination positions of the fulvic acids were occupied, considering that the CC of FA was 89 times higher than the copper(II) concentration in the solution. Indeed, for those experimental conditions, Table 4 shows that almost all $|Cu|_b$ was bound to the stronger binding sites of FA (FA_1, whose metal-binding capacity was C_1): the difference between the total $|Cu|_b$ (stated as

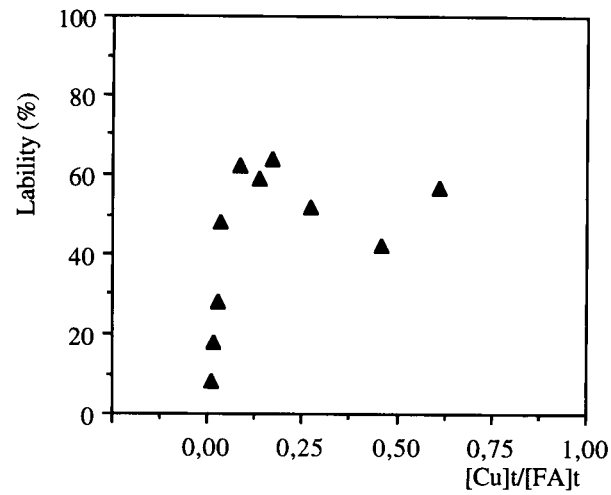

Fig. 3. Variation of the lability of Cu–FA complexes with the $[Cu]_t/[FA]_t$ molar ratio. Measurements were performed by PSA at −0.5 V vs. SCE in 0.5 mol/l $NaClO_4$.

Table 4
Lability of Cu–FA complexes, at 6.5 pH and 20°C

[FA] (mg/l)	$[Cu]_t$ ($\times 10^7$ mol/l)	Molar ratio		0.5 mol/l $NaClO_4$				Sea water
		$\frac{|FA|_t}{|Cu|_t}$	$\frac{|FA|_1}$ [a] $/|Cu|_t$	$[Cu]_b$ [b]/ TOC (mmol/g)	Cal$[Cu]_b$% [b,c,d]	Exp$[Cu]_b$% [c,e]	Lab% [f]	Exp$[Cu]_b$(%) [c,e]
150	31.5	89.0	26.8	0.06	98(92)	90	8	82
100	31.5	61.8	14.8	0.09	96(88)	79	18	75
50	31.5	39.2	10.7	0.17	95(88)	68	28	*g*
10	7.87	29.6	7.5	0.18	77(70)	40	48	65
10	18.9	12.3	3.1	0.41	74(67)	28	62	38
10	31.5	7.4	1.9	0.65	71(63)	29	59	33
10	39.4	5.9	1.5	0.79	69(61)	25	64	32
10	63.0	3.7	0.9	1.2	63(53)	30	52	35
10	110	2.2	0.5	1.7	52(40)	30	42	14
10	142	1.6	0.4	1.9	47(33)	21	57	11

[a] $|FA|_1 = C_1$. [b] $[Cu]_b$ was calculated by a speciation program. [c] Percentage of $[Cu]_t$. [d] $[Cu]_b$ bound only to FA_1, given in parentheses. [e] Mean of 2–4 experiments. [f] Lability = (calculated $[Cu]_b$ − experimental $[Cu]_b$)/calculated $[Cu]_b$. [g] Experiments not performed.

a percentage of $|Cu|_t$ in the solution) and the $|Cu|_b$ bound to C_1 was only 6%. When the excess of ligand decreased progressively, the lability increased up to 62–64%, which occurred in the range 0.4–0.8 mmol $[Cu]_b$/g TOC. A slight decrease of lability was observed for higher $Cu]_b$/TOC ratios, being ca. 50% for 1.9 mmol $[Cu]_b$/g TOC, the highest value analysed.

The kinetic behaviour of the Cu(II)–FA system for $[Cu]_b$/g TOC > 2 mmol$[Cu]_b$/g TOC could not be investigated due to the low sensitivity of the analytical method. In fact, as CC was 5.2 mmol/g TOC and the Cu(II)–FA complexes were relatively weak, to reach $[Cu]_b$/g TOC > 2 mmol/g a large excess of metal in the solution would be required; under these conditions, the analytical signal for the labile metal was practically coincident with the total metal signal (i.e., $[Cu]_b$ was too small to be indirectly detected).

Experimental results describing lability of Cu–FA complexes obtained by electroanalytical techniques are hard to find in the literature. The present results corroborate the opinion of Buffle et al. [24] that the dissociation rate constants of the complexes of polymeric ligand like FA may depend on the metal-to-ligand concentration ratios, as a consequence of the variation of the respective stability constants with the $[Cu]_b$/TOC ratio. Filella et al. [7] have established the limit values of the $[Cu]_b$/TOC ranges where the voltammetric behaviour of Cu–FA complexes, at pH 8, was fully inert, $[Cu]_b$/TOC < 0.3 mmol/g, and fully labile, $[Cu]_b$/TOC > 3 mmol/g. These authors [7] also indicated that, for lower pH values, the lower limit of the range for fully labile complexes might extend to lower $[Cu]_b$/TOC values. The present work provided no limit values for full lability or inertness of Cu–FA complexes. However, in agreement with literature reports [7,24], our results indicate that the inertness of the Cu–FA complexes decreased markedly when the $[Cu]_b$/TOC ratio increased from 0.06 (8% labile) to 0.8 (64% labile). Nevertheless, for $[Cu]_b$/TOC values higher than 0.8 no systematic increase of lability was found. On the contrary, a slight decrease of lability was observed for $[Cu]_b$/TOC > 0.8. Gregor and Powell [5] obtained percentages of labile Cu(II)–FA in the 70–50% range by sampled-d.c. ASV for $|FA|_t/|Cu|_t$ values lower than in the present work (1.2×10^{-7} mol/l $|Cu|_t$ and ca. 1.2 mg FA/l). The authors [5] used FA samples from podzolized soils and peat and the measurements were carried out at pH 4.8.

For artificial sea water, the solution matrix is much more complicated and the stability constants of FA complexes of some other metals present are not known. Therefore, an acceptable estimation of the inorganic copper(II) fraction by computational simulation, based on equilibrium considerations, was not possible. Nevertheless, the $[Cu]_b$ values obtained by experimental measurements were not very different from those obtained in 0.5 mol/l sodium perchlorate medium. These results suggest that the PSA kinetic behaviour of Cu–FA complexes in sea water cannot be very different to that found for the simpler medium of similar ionic strength.

The copper(II) and FA concentration values in sea water can differ more than one order of magnitude from one place to another, as stated in the literature [27]. Therefore, as the lability depends on the $|FA|_t/|Cu|_t$ ratio, it is very difficult to anticipate on any general conclusion about the Cu–FA complexes in sea water, based on the present results. Nevertheless, for particular cases, i.e. coastal sea water at the North of Portugal (near Oporto city), where copper(II) and FA concentrations were measured to be $1–10 \times 10^{-5}$ mmol/l [28] and 0.1 mg/l [3], respectively, the lability may be predicted, if a CC of FA similar to that obtained in the present work (1.8 mmol/g) is admitted. Under these conditions, $|FA|_t/|Cu|_t$ molar ratios between 20 and 2 will be expected and, according to the results presented in Table 3, the Cu(II)–FA complexes will be semi-labile.

Influence of pH

Most experiments in the present study were performed at pH 6.5 (a value lower than for sea water) to minimize the formation of Cu–OH complexes, particularly of insoluble species. This condition seems especially important in ISE determinations, because of the relatively high detection limit of this technique which requires higher $[Cu]_t$ values than for PSA determinations.

To investigate the influence of pH on the

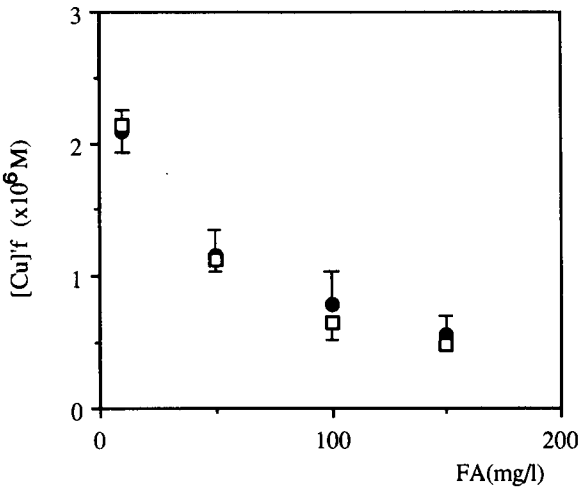

Fig. 4. Influence of pH on $[Cu]_f^Y$ in the artificial sea water medium: ● = pH 6.5; □ = pH 7.5. Mean values of four independent determinations and the respective 95% confidence limits are presented.

labile copper fraction, PSA measurements in artificial sea water were also performed at pH 7.5, a value closer to the pH of sea water. It was verified (see Fig. 4) that the free plus labile copper fractions ($[Cu]_f^Y$) were practically constant in the pH range 6.5–7.5. This result increases the environmental interest of the present study.

Suitability of PSA for speciation studies

PSA has been scarcely used [29] on speciation studies, although potentialities and even advantages of the technique for this purpose have been mentioned in the literature [30]. As far as we know, PSA had never been used before for the investigation of the lability of metal ion complexes. Hence, for comparison purposes, identical procedures to those discussed above were followed for solutions where FA was changed to EDTA (see concentrations in Table 2). For this ligand, computational simulations were done for both sodium perchlorate solution and synthetic sea water, because there are reference data in the literature for the major side equilibria, involving complexation of copper by inorganic ligands (OH^-, CO_3^{2-}, Cl^-, NH_3) and other metal [Mg(II), Ca(II), Fe(III)]–EDTA complexes [16–18]. For both media, the copper fraction determined by PSA was comparable with the sum of the free plus inorganic (or labile) copper fractions. These results indicate that the Cu–EDTA complex is inert in PSA measurements, which corroborate previous results obtained by differential pulse anodic stripping voltammetry (DPASV) [21], and support the suitability of the PSA method for this type of studies.

On the other hand, no FA adsorption interference was observed by PSA. Even for a more complex mixture (a sample of 0.3 mg TOC/l humic acid) no interference was observed by PSA, although important adsorption phenomena were found by DPASV [31]. These results indicate that PSA, due to the characteristics of the stripping step (chemical oxidation), is less sensitive to adsorbed organic matter phenomena than ASV, a technique that has been frequently used for speciation purposes, but for which the problems provoked by adsorbed organic matter are well known, e.g. [32].

Nevertheless, PSA has an important operational drawback for speciation studies when mercury(II) is used as oxidising agent: this metal ion has to be added to the working solution just at the end of the deposition period, because mercury(II) competes for the coordination positions of the chelating agents in solution. This procedure is tedious if the addition of reagents is manual as in the experimental assembly used in the present case.

4. Conclusions

The present work provides experimental evidence for the fact that the lability of Cu–FA complexes depends on the $|Cu|_t/|FA|_t$ molar ratio. For $|Cu|_t/|FA|_t \simeq 89$ almost full inertness was observed for PSA. The lability increased when $|Cu|_t/|FA|_t$ decreased down to 6 but it slightly decreased for lower $|Cu|_t/|FA|_t$ values down to 1.6. The results of measurements performed in synthetic sea water suggest that the PSA behaviour of Cu–FA complexes may be similar to that found in 0.5 mol/l sodium perchlorate medium. From these results it may be expected that for copper(II) and FA levels typical for

coastal sea water at the North of Portugal [$(1-10) \times 10^{-5}$ mmol/l [28] and 2×10^{-4} mmol/l [3], respectively] the Cu–FA complexes are semi-labile at neutral pH.

Acknowledgements

We thank Mr. A.J.T. Sousa for routine work. Financial support from JNICT/ Programa Ciência, Project 1014/CEN/92 (as well as project M-27/9/20) for acquisition of a Christ Alpha 1-4 freeze dryer is gratefully acknowledged. Prof. A.A.S.C. Machado (Chemistry Department, Faculty of Science, University of Oporto, Portugal) is thanked for helpful discussions.

References

[1] P.J. Harrison, R.E. Waters and F.J.R. Taylor, J. Phycol., 16 (1980) 28.
[2] T.M. Florence and G.E. Batley, C.R.C. Crit. Rev. Anal. Chem., 9 (1980) 219.
[3] A.A.S.C. Machado and J.C.G. Esteves da Silva, Chemom. Intell. Lab. Syst., 19 (1993) 155.
[4] G.M.P. Morrisson, G.E. Batley and T.M. Florence, Chem. Br., 25 (1989) 791.
[5] J.E. Gregor and H.K.J. Powell, Anal. Chim. Acta, 211 (1988) 141; and references cited therein.
[6] D.R. Turner, M.S. Varney, M. Whitfield, R.F.C. Mantoura and J.P. Riley, Sci. Total Environ., 60 (1987) 17.
[7] M. Fillela, J. Buffle and H.P. Van Leewen, Anal. Chim. Acta, 232 (1990) 209; and references cited therein.
[8] E.M. Thurman, in F.H. Frimmel and R.F. Christman (Eds.), Humic Substances and their Role in the Environment, Wiley, 1988, p. 31.
[9] J.L.F.C. Lima and A.A.S.C. Machado, in J. Albarges (Ed.). Analytical Techniques in Environmental Chemistry, Vol. 2, Pergamon, Oxford, 1982, p. 419.
[10] J.C. Miller and J.N. Miller, Statistics for Analytical Chemistry, Wiley, New York, 1984, p. 96.
[11] ISS820 Ion Scanning System, Users Handbook, Radiometer, Copenhagen.
[12] J. Buffle, Complexation Reaction in Aquatic Sytems: an Analytical Approach, Ellis Horwood, Chichester, 1988, Chap. 5.
[13] I. Ruzic, Anal. Chim. Acta, 140 (1982) 99.
[14] I. Ruzic, Environ. Sci. Technol., 21 (1987) 1132.
[15] J.C. Westall, MICROQL, A Chemical Equilibrium Program in BASIC, Internal Report, EAWAG, Dübendorf.
[16] W. Stumm and J. Morgan, Aquatic Chemistry, an Introduction Emphasizing Chemical Equilibria in Natural Waters, Wiley, New York, 1981, pp. 242 and 354.
[17] E. Hogfeldt, Stability Constants of Metal Ion Complexes, Part A, Pergamon, Oxford, 1982, p. 217.
[18] A.E. Martell and R.M. Smith, Critical Stability Constants. Vol. 1, Plenum, New York, 1974, p. 204.
[19] J.R. Tuschall and P.L. Brezonik, in R.F. Christman and E.T. Gjessing (Eds.), Aquatic and Terrestrial Humic Materials, Ann Arbor Science Pub., Ann Arbor, MI, 1983, Chap. 13.
[20] T.A. Neubecker and H.E. Allen, Water Res., 17 (1983) 1.
[21] W. Lund, I.A. Helbak and H.M. Seip, Sci. Total Environ., 92 (1990) 269.
[22] J. Buffle, F.L. Greter and W. Haerdi, Anal. Chem., 49 (1977) 216.
[23] G.A. Bhat, R.A. Saar, R.B. Smart and J.H. Weber, Anal. Chem., 53 (1981) 2275.
[24] J. Buffle, J.J. Vuilleumier, M.L. Tercier and N. Parthasarathy, Sci. Total Environ., 60 (1987) 75.
[25] C.M.G. van der Berg, Anal. Chim. Acta, 250 (1991) 265.
[26] W. Davison, J. Electroanal. Chem., 87 (1987) 395.
[27] T.S. West and H.W. Nurnberg (Eds.), The Determination of Trace Metals in Natural Waters, Blackwell, London, 1988, p. 182.
[28] O.M. Lage, A.M., Parente, H.M.V. Soares, M.T. Vasconcelos and R. Salema, Eur. J. Phycol., submitted for publication
[29] S. Mannino and M. Bianco, Analyst, 113 (1988) 87; and references cited therein.
[30] J. Wang, Fresenius' J. Anal. Chem., 337 (1990) 508.
[31] H.M.V.M. Soares and M.T. Vasconcelos, in preparation.
[32] J. Wang, Stripping Analysis – Principles, Instrumentation, and Applications, VCH, Weinheim, 1985, p. 9.

ELSEVIER

Analytica Chimica Acta 293 (1994) 271–276

ANALYTICA CHIMICA ACTA

Biosensors for enantioselective analysis

Thomas Kullick [a], Roland Ulber [a], Hartmut H. Meyer [b], Thomas Scheper [c], Karl Schügerl [a,*]

[a] *Institut für Technische Chemie, Universität Hannover, Callinstrasse 3, 30167 Hannover, Germany*
[b] *Institut für Organische Chemie, Universität Hannover, Schneiderberg 1b, 30167 Hannover, Germany*
[c] *Institut für Biochemie, Wilhelms-Universität Münster, Wilhelm-Klemm-Strasse 2, 48149 Münster, Germany*

(Received 17th January 1994)

Abstract

The development of enantioselective enzyme field effect transistors (EnFETs) for the detection of β-hydroxy acid esters and aromatic amino esters and their application in flow-injection analysis is described. The EnFETs were produced by immobilising the enzyme on the pH-sensitive gate surface of a pH-FET. The characteristics of the sensor signals and their dependence on certain process parameters, such as pH, buffer capacity and flow conditions in the medium being measured, were examined. Due to the short response time, the EnFETs are ideal for application in flow-injection analysis. The use of enantioselective EnFETs in on-line process monitoring is described.

Key words: Biosensors; Flow injection; Aromatic amino esters; Enantioselective analysis; EnFETs; Field effect transistors; β-Hydroxy acid esters

1. Introduction

In the pharmaceutical industry it is very important to produce enantiomerically pure substances, as both antipodes of a chiral bond can have quite different therapeutic results. The methods needed for the determination of enantiomeric conditions are time consuming and expensive when using chiral columns in gas chromatography (GC), liquid chromatography (LC) or various nuclear magnetic resonance (NMR) spectroscopic methods.

Enzyme field effect transistors (EnFETs) can be used for the analysis of the enantiomeric distribution of amino acid and β-hydroxy acid esters.

The measurement concept of EnFETs is based on the detection of pH shifts caused by enzymatic conversion of analytes, which occur in the enzyme membrane covering the pH-sensitive FET gate. The FET serves as a transducer, which means that it converts the measured effect (pH shift) into an electric signal. The magnitude of the pH shift depends on the substrate concentration. Sensors for glucose, maltose and other substances have been developed on this basis [1,2]. EnFETs can be incorporated as detectors in flow-injection analysis (FIA) systems to monitor biological processes. In this way, the contact of the sensor with the medium is minimized. Due to the short re-

* Corresponding author.

SSDI 0003-2670(94)00094-3

sponse time, a high analysis rate is achieved. Depending on the sensor type, it is possible to perform up to 20 analyses per hour.

2. Experimental

2.1. Enzyme–substrate systems

Lipase–esterase and α-chymotrypsin–esterase systems were used for the analysis of *R,S*-3-hydroxy-3-phenylpropanoic acid ethyl ester and *R,S*-phenylalanine methyl ester, respectively. α-Chymotrypsin (bovine pancreas, EC 3.4.21.1, C-4129; Sigma), esterase (porcine liver, EC 3.1.1.1, E-3128; Sigma) and lipase (*Pseudomonas fluorescens* (PS), EC 3.1.1.3; Amano) were used. *R*- and *S*-phenylalanine methyl ester were enantiomerically pure (99%; Sigma). The β-hydroxy acid ester used was produced as racemate at the Institut für Organische Chemie der Universität Hannover. All other chemicals used were commercially available.

Enzyme systems were chosen for the esterase to hydrolyse the substrate unspecifically into the respective acid and alcohol, while the other enzyme produced a high enantiomeric specificity: (a) α-chymotrypsin only hydrolysed *S*-phenylalanine methyl ester [3–5], and (b) lipase only hydrolysed *S*-3-hydroxy-3-phenylpropanoic acid ethyl ester [6].

All acids released in the enzymatic conversion dissociate within the membrane at pH 7–8, yielding the anion and the proton [7]. Esterase-FETs were used to determine the ester concentration in the medium, while the enantiomer-specific FET determined the amount of *S*-antipodes.

The pH-sensitive FETs used were purchased from abc (Puchheim/Munich). The slope was 53 to 55 mV per pH decade.

2.2. Immobilisation of enzymes

Co-crosslinking [8] with glutardialdehyde, using human serum albumin (HSA) as coimmobiliser, was applied to immobilize the enzyme. The suspended enzyme [esterase, 20 μl; α-chymotrypsin, 5 mg into 20 ml buffer (5 mM K_2HPO_4 with 0.5 M KCl, pH 8); lipase (PS) 5 mg into 20 ml buffer] was mixed with HSA [esterase, 2 μl; α-chymotrypsin, 0.5 μl; lipase (PS) 1 μl] and glutardialdehyde (1 μl). The mixture was immediately applied to the pH-sensitive gate surface under a stereo-microscope, using a defined volume. Within 30 to 90 s a membrane formed; the enzyme was thus immobilized.

The EnFETs, produced in this manner, were washed with distilled water and were immediately ready for use. They were stored in buffer solution at 6°C.

The membrane thickness was measured using a surface profiler (Dektak 3030, VEECO).

2.3. Experimental set-up

The sensor and a Ag^+/Ag reference electrode (Ingold, Type 373-M3, 3 mm) were integrated in a fed batch reactor to characterize the sensor and to obtain calibration graphs. An eight-channel controller circuit was used to record the data on an *x,t* plotter and a multipoint data recorder (Philips PM 8237 A). During the measuring process, the solution was stirred by means of a magnetic stirrer.

The sensors used consisted of eight pH-FETs mounted together in a fiberglass reinforced synthetic holder. Seven of these pH-FETs were coated with enzymes, while one uncoated pH-FET was used to monitor the pH of the sample. By taking the difference in the signals from the EnFETs and the pH-FET, fluctuations in pH were compensated for. Calibration curves were obtained by adding substrate in the increments.

2.4. Integration of enantiomeric selective EnFET sensors in an FIA system

The developed biosensors were used in commercially available FIA systems (EVA/Eppendorf) [9–11] (Fig. 1). The sensor and the reference electrode were integrated into a flow-through measuring chamber (Fig. 2).

CAFCA (computer assisted FIA control and analysis), developed at the Institut für Technische Chemie der Universität Hannover, was used to record the collected data.

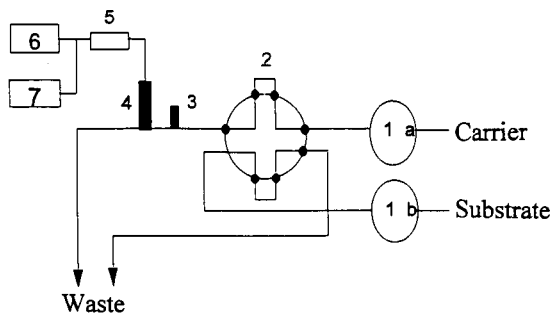

Fig. 1. Experimental set-up for on-line analysis. 1a and 1b = Pump; 2 = injector; 3 = bubble trap; 4 = flow through measuring chamber; 5 = eight channel system; 6 = x,t-plotter; 7 = CAFCA system.

The carrier buffer was pumped through the measuring chamber at a flow rate of 2 ml/min.

2.5. *On-line analysis during enzymatic hydrolysis using EnFET–FIA systems*

Using the FIA system, the enzymatic conversion of *S*-phenylalanine methyl ester to phenylalanine by α-chymotrypsin and the enzymatic hydrolysis of *S*-3-hydroxy-3-phenyl-propanoic acid ethyl ester by lipase (PS) were analysed in an on-line process [12].

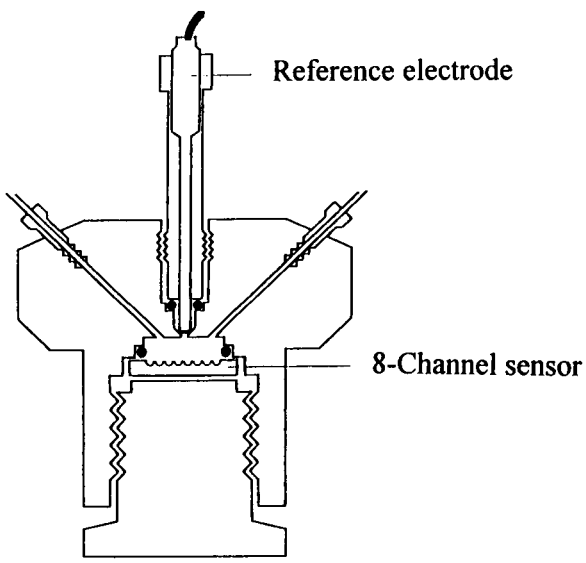

Fig. 2. Flow through measuring chamber.

Before the sensors were used in the FIA system, they were calibrated using various injection times and substrate concentrations.

3. Results and discussion

Figs. 3 and 4 show typical calibration curves for the sensors. The measuring range of the EnFETs is clearly divided into two sections. (1) The dynamic section, in which the calibration curve is almost linear (small changes in concentration cause large signal changes). (2) The saturation section, which is characteristic for higher concentrations.

The dynamic section of the lipase (PS) sensor has a turning point, which probably depends on the quality of β-hydroxy acid ester emulsion. Measuring ranges in the linear sections of the esterase-FET are up to 2 g/l for *R,S*-phenylalanine methyl ester and up to 1 g/l for *R,S*-3-hydroxy-3-phenylpropanoic acid ethyl ester. Values for the α-chymotrypsin-FET are up to 2 g/l for *S*-phenylalanine methyl ester and up to 5 g/l for *S*-3-hydroxy-3-phenylpropanoic acid ethyl ester.

The sensor signal has good reproducibility. Sensor life time was longer than 40 days (Fig. 5). The initial signal decline can be explained by the loss of enzyme not immobilized into the membrane. The enantioselectivity of the enzymes was maintained in the immobilised state (Fig. 6).

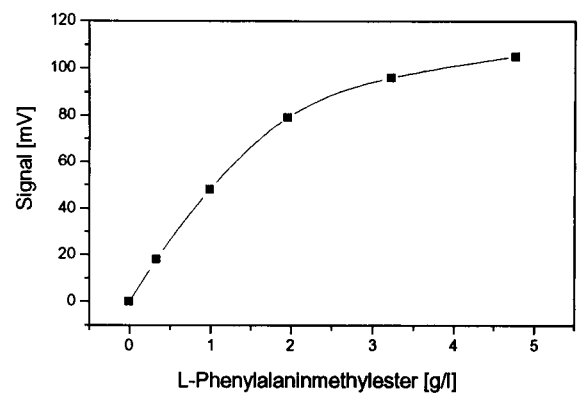

Fig. 3. Calibration curve of the esterase-FET.

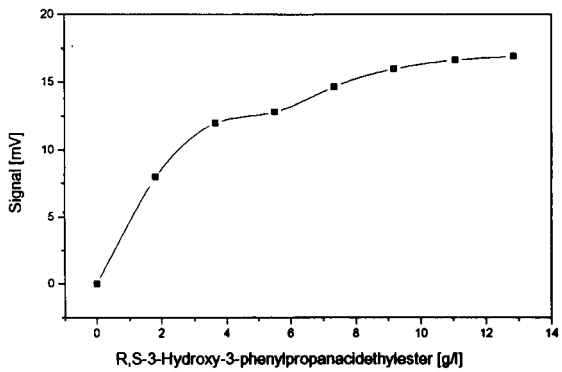

Fig. 4. Calibration curve of the lipase (PS)-FET.

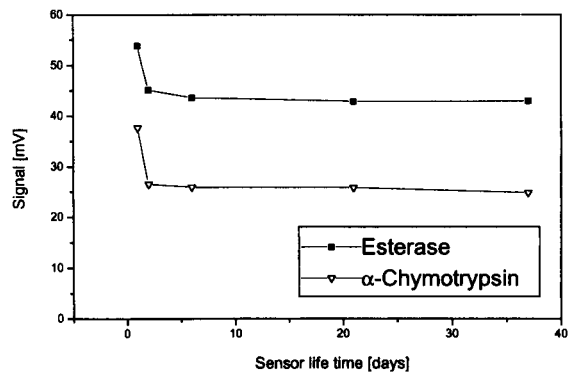

Fig. 5. Sensor life time of esterase- and α-chymotrypsin-FET.

3.1. Influence of various parameters on the sensor signals

The influence of pH, buffer ion concentration and flow conditions on the signal intensity and membrane thickness affecting the response time is shown in Figs. 7–9 for the lipase (PS) sensor. Corresponding characteristics were found for the esterase and α-chymotrypsin sensors.

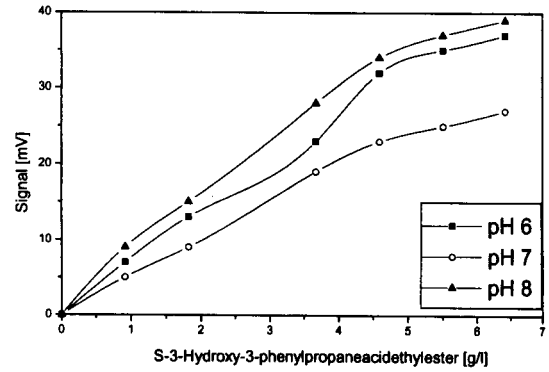

Fig. 7. Influence of pH [lipase (PS)-FET].

The maximum signal, as seen in Fig. 7, was obtained at a pH of 8; this is also the pH optimum for lipase [4]. A lower activity was found at pH 7. This is the result of the buffer system used, which has its greatest capacity at this specific pH (pK_S for $H_2PO_4^- = 7.21$ [7]). The pH has a complex influence on the sensor, as both the enzyme activity and buffer capacity are affected by pH changes.

Buffer ion concentration has a major influence. Solutions with a low buffer capacity allow greater sensitivity than those with a high buffer ion concentration (Fig. 8).

Signals for measurements at high flow rate are small compared to those taken at low flow rate

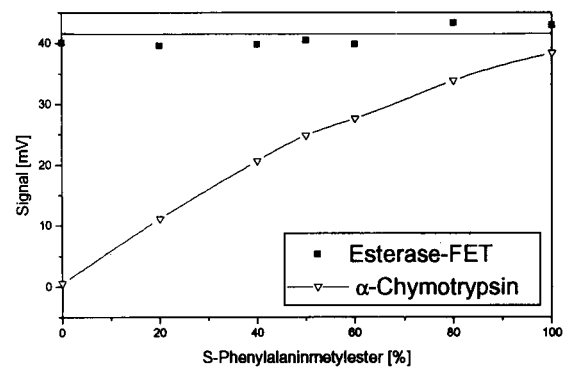

Fig. 6. Enantioselectivity of EnFETs.

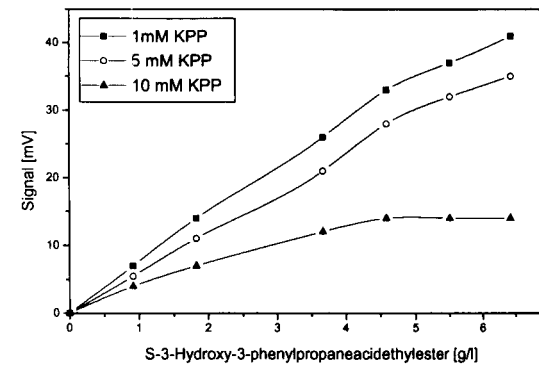

Fig. 8. Influence of buffer ion concentration [lipase (PS)-FET].

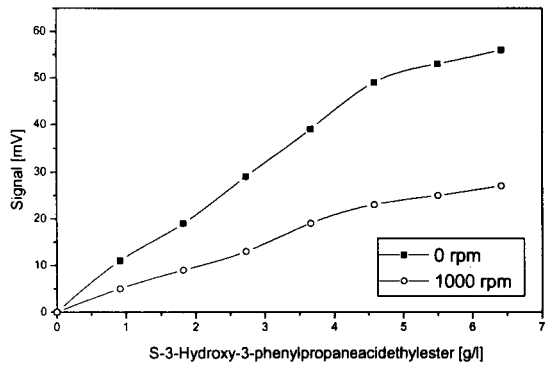

Fig. 9. Influence of flow conditions [lipase (PS)-FET].

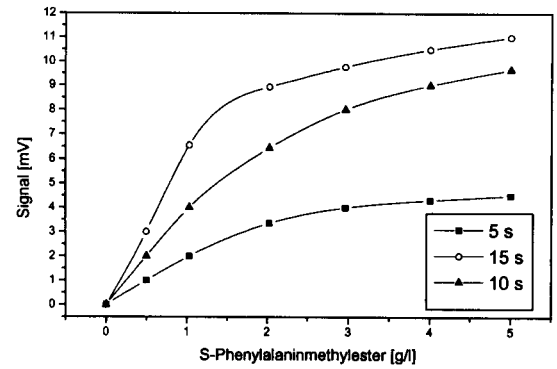

Fig. 11. Dependence of the esterase-FET signal on the active injection time.

(Fig. 9). The proton concentration at the membrane decreases with increasing stirring speed.

The response time of the lipase (PS)-FET increases linearly with increasing membrane thickness.

3.2. Applications of enantioselective EnFETs in an FIA system

Since no acceptable results could be obtained for lipase (PS)-FETs using active injections, a passive injection method was used. The flow of substrate through the measuring chamber was stopped for a fixed period of time. Figs. 10 and 11 show the dependence of the sensor signal of esterase- and lipase-FETs on the injection time. The short response times of α-chymotrypsin- and esterase-FETs allows an analysis frequency of 20 samples h^{-1}. Lipase (PS)-FETs achieve 12 analysis h^{-1}.

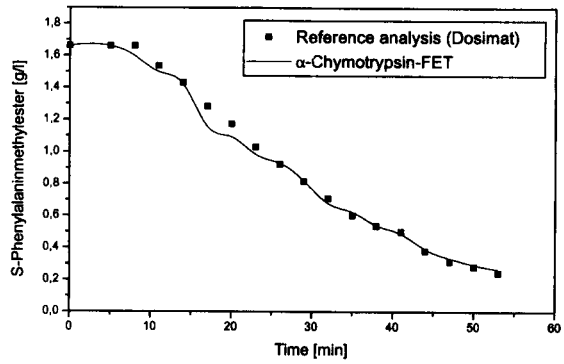

Fig. 12. Enantioselective on-line analysis of enzymatic hydrolysis of *S*-phenylalanine methyl ester (α-chymotrypsin-FET).

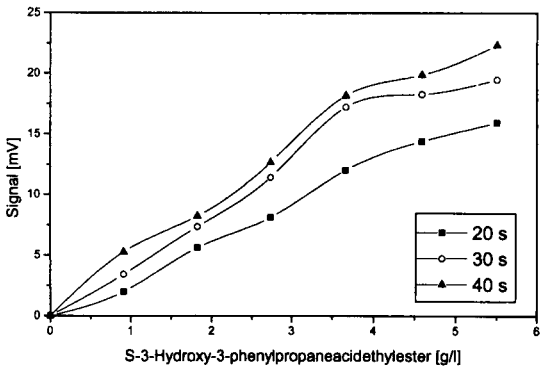

Fig. 10. Dependence of the lipase (PS)-FET signal on the passive injection time.

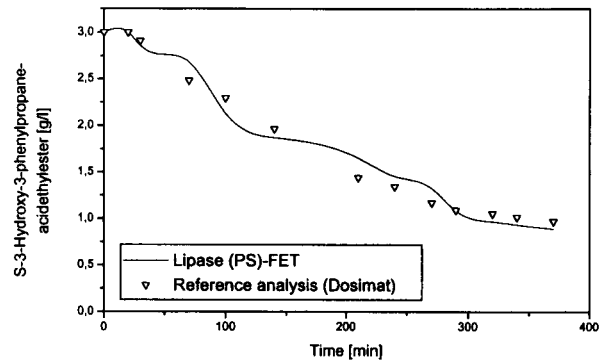

Fig. 13. Enantioselective on-line analysis of enzymatic hydrolysis of *S*-3-hydroxy-3-phenylpropanoic acid ethyl ester [lipase (PS)-FET].

The results of the enantioselective on-line analysis of the enzymatic hydrolysis of *S*-phenylalanine methyl ester and *S*-3-hydroxy-3-phenylpropanoic acid ester are shown in Figs. 12 and 13. Both correspond to the reference analysis made using a Dosimat 665 (Metrohm). This system registered the freed protons of hydrolysis by neutralisation. The ester concentration was calculated using the amount of base used.

4. Conclusions

Enantiospecific EnFETs make quick and reliable analysis of enantiomeric conditions of aromatic amino acid esters and various β-hydroxy acid esters possible. Application of these sensors in FIA enabled us to monitor on-line the concentration of these substances with a high analysis frequency. This cannot be done by conventional methods of analysis. The sensor can be integrated in the reactor for continuous monitoring of the production process. Changes in and production of undesirable antipodes can be registered on-line by this method.

References

[1] T. Kullick, Entwicklung eines Glucosesensors auf der Basis eines Glucosedehydrogenase-FETs, Diplomarbeit Universität Hannover, 1990.
[2] U. Brand, Biosensoren auf der Basis von pH-sensitiven Feldeffekttransistoren für den Einsatz in der biotechnologischen Prozeßkontrolle, Dissertation Universität Hannover, 1990.
[3] P.B. Boyer, The Enzymes, Vol. V, Academic Press, New York, 3rd edn. 1975, p. 71.
[4] T.E. Barmann, Enzyme Handbook, Vol. III, Springer Verlag, Berlin, 1969.
[5] D. Schomberg and M. Salzmann, Enzyme Handbook, Vol. V, Springer Verlag, Berlin, 1991.
[6] E. Voss, Diplomarbeit Universität Hannover, 1990.
[7] R. Altmann and G. Brandes, Chemisch-technische Stoffwerte - eine Datensammlung, VEB Deutscher Verlag für Grundstoffindustrie, Leipzig, 1984.
[8] W. Hartmeier, Immobilisierte Biokatalysatoren, Springer Verlag, Berlin, 1986.
[9] J. Möller, Flow Injection Analysis, Analytiker Taschenbuch, Springer Verlag, Berlin, 1988, p. 7.
[10] J. Ruzicka and E.H. Hansen, Flow Injection Analysis 2, Wiley, New York, 1987.
[11] U. Brand, B. Reinhardt, F. Rüther, T. Scheper and K. Schügerl, Anal. Chim. Acta, 238 (1990) 201.
[12] K. Schügerl, A. Lübbert and T. Scheper, Chem. Ing. Tech., 59 (1987) 701.

ELSEVIER

Analytica Chimica Acta 293 (1994) 277–293

ANALYTICA CHIMICA ACTA

Multiple standard addition with latent variables (MSALV): Application to the determination of copper in wine by using differential-pulse anodic stripping voltammetry

Ana Herrero [a], M. Cruz Ortiz [a,*], Julia Arcos [a], Jesús López-Palacios [a], Luis Sarabia [b]

[a] *Department of Analytical Chemistry, Colegio Universitario, Apdo 231, E-09080 Burgos, Spain*
[b] *Department of Mathematical Analysis, Colegio Universitario, Apdo 231, E-09080 Burgos, Spain*

(Received 2nd November 1993; revised manuscript received 28th February 1994)

Abstract

MSALV, multiple standard addition with latent variables, is a new method designed to overcome the difficulties presented by the determination of an analyte in a complex sample in which equilibria exist whose displacement may alter the response of the sensors when the analyte is added in a multiple addition. MSALV has been used to quantify the Cu content in samples of wine using differential-pulse anodic stripping voltammetry (DPASV) with a mercury electrode and ethylenediaminetetraacetic acid (EDTA) and KCl as complexing agents. The existence of the EDTA–Cu(II) complex and Cu(I)–chloride complex intermediate leads to a change in the sensibility of the sensors when Cu(II) is added, which must be born in mind during construction of the multiple addition model. The use of latent variables calculated by partial least squares (PLS) provides a solution which is both quantitatively adequate and chemically interpretable. The results of four repeated determinations of Cu in samples of red wine are shown. In each case the latent variables were calculated from the intensities recorded at fifteen potentials in eight voltammograms corresponding to the successive additions of wine and/or copper.

Key words: Anodic stripping voltammetry; Differential pulse voltammetry; Multivariate calibration; Copper; Partial least squares; Standard addition; Trace metals; Wine

1. Introduction

The determination of traces of metals in wine is currently of great importance. Elements such as Cu, Fe, Zn, Ni and Cr may be present in small quantities in wines, whether they originate from the grape, from the use of phytosanitaries in the vines or from processes of secondary contamination. The determination of these elements is extremely important, in some cases because they are toxic, and in others because some aspects of the quality of a wine are intimately related to the metals they contain.

The quantities of copper normally found in young wines must range between 0.1 and 0.3 mg

* Corresponding author.

SSDI 0003-2670(94)00102-R

l^{-1}. However, when the vineyard is treated with copper dust larger quantities may get into the musts. In some cases the Cu content is increased through contact with contaminating machinery during the technological process. During fermentation the yeasts fix the majority of the copper contained in the must. Quantities of approximately 0.2–0.4 mg l^{-1} of metal can cause a clouding of wine which is known as copper cracking ("casse cuivrese").

Traditionally, the determination of Cu traces in wine has been carried out by spectrophotometric techniques [1]. However, electrochemical techniques are an important alternative, among which stripping voltammetry (SV) stands out because of its high sensibility and the low detection limits it can reach [2].

The study of the viability of SV for the determination of the Cu in wine led to the design of the multiple standard addition with latent variables (MSALV) procedure. This procedure has a general application in the quantitative determination of analytes in complex matrices in the presence of chemical equilibria in which the analyte itself participates, such that the latent structure of the signals recorded must be used as an "indirect observation" of the content of the analyte to be determined. Put in another way, MSALV does not require the matrix of the sample problem to remain chemically inactive upon addition of the analytes.

MSALV is a synthesis of the generalized standard addition method GSAM and of partial least squares (PLS). GSAM is essential even when one is dealing with a single analyte because of the need to use several latent variables. PLS is needed to look for the latent variables related to the quantity of analyte added. Furthermore, MSALV incorporates an initial experimental step to obtain a "reference sample" similar to those obtained in the multiple addition process. In this way, off-line problems are avoided.

The results of four repeated determinations of Cu in samples of red wine are shown. In each case the latent variables were calculated from the intensities recorded at fifteen potentials in eight voltammograms corresponding to the successive additions of wine and/or copper.

2. Materials and equipment

Analytical-reagent grade chemicals were used without further purification. All the solutions were prepared with deionised water obtained with a Barnstead NANO Pure II system. Nitrogen (99.99%) was used to remove dissolved oxygen.

Cu(II) standard solutions were prepared by dissolving copper powder p.a. (Merck) in a minimum volume of HNO_3 and by diluting with water to give the desired Cu concentration. The complexing agent, ethylenediaminetetraacetic acid (EDTA), and KCl were used in each case as supporting electrolytes.

Differential pulse voltammetric (DPV) measurements were carried out using a Metrohm 646 VA processor with a 647 VA stand in conjunction with a Metrohm multimode electrode (MME) used in the hanging mercury drop electrode (HMDE) mode. The three-electrode system was completed by means of a platinum auxiliary electrode and an Ag/AgCl/KCl (3 M) reference electrode.

The additions were done with a Metrohm 665 Dosimat.

Analysis of the data was done with PARVUS [3]. All calculations were done on a Tandon 486/33 computer.

3. Experimental procedure

Differential pulse voltammetric measurements were carried out by the following procedure. The solution was placed in the voltammetric cell and purged with nitrogen for 10 min. Once the solution had been deoxygenated a deposition potential, $E_{dep} = -1.228$ V, was applied to the working electrode during a time, $t_{dep} = 605$ s. At the end of this accumulation period the stirrer was switched off and, after 20 s had elapsed, an anodic potential scan was initiated from E_{dep} to 0.1 V. The following values were taken for the rest of the instrumental settings: scan rate, 10 mV s^{-1}; modulation pulse amplitude, 50 mV; pulse time, 40 ms; pulse repetition time, 0.6 s; stirring rate in the accumulation period, 1290 rev min^{-1}; mercury drop size, 0.40 mm^2.

4. Results and discussion

In a previous work [4] the determination of Cu by differential-pulse anodic stripping voltammetry was used and optimized in aqueous samples in the presence of EDTA as complexing agent. However, when this process is applied to samples of wine the voltammetric peak is displaced towards more positive potentials and is concealed by the oxidation of the electrode itself.

In order to avoid this problem, KCl was added to the sample of wine. In fact, in this medium a well-defined peak is obtained at a potential of −130 mV due to the oxidation of Cu in the presence of EDTA and a new peak is also observed due to the stabilisation of Cu(I) due to the formation of the Cu(I)–chloride complexes [5,6] at a potential close to −450 mV. Fig. 1a shows a Cu voltammogram in an aqueous sample. Fig. 1b is a Cu voltammogram in a sample of wine without the addition of KCl while the voltammogram in Fig. 1c was obtained after the addition of KCl to the wine.

4.1. Multiple standard addition

The method of standard additions, SAM, is a tool well known to electrochemists and spectroscopists. A detailed description of its principles and a bibliography on its applications can be found in Refs. 7 and 8. SAM is described briefly below with the aim of introducing the notation and of high-lighting the problems found in its application to the oxidation peak Cu(0)/Cu(II)–EDTA.

For a pre-determined potential, E, the current recorded, i, is proportional [9] to the concentration of Cu(II) in the sample

$$i = k_E[\mathrm{Cu}] = k_E \frac{n}{v} \qquad (1)$$

where n is the number of moles of Cu(II), v the volume of the solution and k_E the sensibility corresponding to the sensor (potential E).

Eq. 1 is valid both for the sample of wine, $h = 0$, and for the successive samples obtained upon addition of Cu(II) to the wine, $h = 1, \ldots, a$

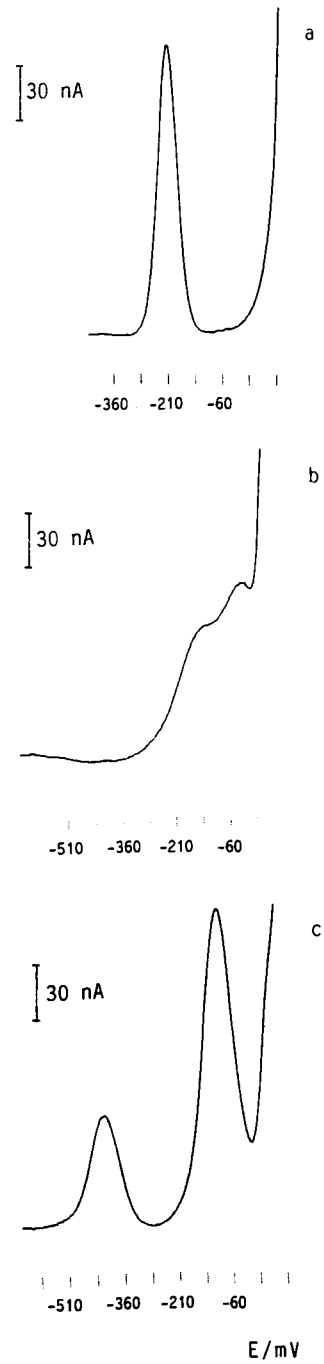

Fig. 1. Differential pulse voltammogram of copper in 5.84×10^{-3} M EDTA. For experimental conditions see text. (a) In aqueous sample, $C_{Cu} = 10^{-6}$ M; (b) in a sample of wine; (c) in a sample of wine with 0.38 M KCl.

Table 1
Experimental data of the volume-corrected current for the potentials indicated and the successive additions of ΔN moles of Cu

Addition	ΔN ($\times 10^8$)	Potential (mV)																
		−550	−520	−490	−460	−430	−400	−370	−340	−310	−280	−250	−220	−190	−160	−130	−100	−70
0	0.00	0.351	0.576	1.164	1.887	1.786	0.927	0.354	0.196	0.188	0.262	0.442	0.818	1.547	2.676	3.319	2.659	1.825
1	0.11	0.357	0.603	1.232	1.958	1.853	0.951	0.356	0.198	0.196	0.275	0.480	0.886	1.695	2.953	3.666	2.874	1.878
2	0.22	0.356	0.603	1.230	1.960	1.810	0.919	0.347	0.197	0.198	0.286	0.498	0.920	1.761	3.061	3.758	2.914	1.872
3	0.33	0.357	0.607	1.229	1.939	1.769	0.851	0.334	0.195	0.199	0.292	0.509	0.946	1.826	3.174	3.905	2.990	1.880
4	0.44	0.346	0.593	1.198	1.879	1.708	0.857	0.326	0.196	0.204	0.298	0.516	0.961	1.862	3.253	4.003	3.053	1.882
5	0.55	0.360	0.615	1.233	1.910	1.706	0.847	0.324	0.195	0.208	0.311	0.544	1.016	1.990	3.498	4.312	3.258	1.938
6	0.66	0.375	0.636	1.275	1.958	1.728	0.853	0.328	0.204	0.217	0.321	0.568	1.065	2.105	3.720	4.587	3.450	2.016
7	0.77	0.376	0.644	1.287	1.936	1.717	0.839	0.320	0.196	0.212	0.327	0.581	1.098	2.180	3.878	4.753	3.550	2.033
8	0.88	0.377	0.647	1.293	1.960	1.707	0.833	0.317	0.198	0.217	0.331	0.593	1.126	2.259	4.061	5.013	3.755	2.105

$$i_h v_h = k_E n_h \text{ with } h = 0,1,\ldots,a \quad (2)$$

The first part of Eq. 2 is the volume-corrected current which will be denoted as q_h for each $h = 0, 1,\ldots, a$. In Eq. 2 k_E is unknown as is n_h, the number of moles of Cu after h additions, since n_0 is also unknown. But if one subtracts from each of the equations that part corresponding to the sample problem indexed by $h = 0$ one finds that the increase in volume-corrected signal is proportional to the increase in moles of Cu(II)

$$\Delta q_h = q_h - q_0 = k_E(n_h - n_0)$$
$$= k_E \Delta n_h \text{ with } h = 1,\ldots,a \quad (3)$$

After a additions have been carried out, a pairs $(\Delta q,\Delta n)$ are obtained through which the value of k_E is estimated by least squares. Substituting this k_E value in Eq. 2 when $h = 0$ gives the value of n_0 which are the moles of Cu in the wine. It should be noted that the variables in Eq. 3 are increases in intensity and increases in moles while those in Eq. 2 are intensities and moles. As the additions were made to the sample of wine, matrix effects that would cause k_E to be different from solutions, with analyte added to the sample, are not a problem. SAM can also be used for a multicomponent mixture with several analytes of interest, in which case the analytical method should be fully selective in Kaiser's terms [10]. Each response must be a function of a single analyte.

Eq. 3 can be used only under certain conditions. It requires the response to be zeroed, the functional relationship to be linear and interferences from other components in the sample to be absent.

From the experimental series carried out on various wines, the result of a multiple addition representative of the problems encountered will be shown. It consists of eight standard additions of 1.1×10^{-9} mol of Cu(II) to a sample of wine. Each voltammogram was digitalized taking currents at 17 equally spaced potentials from −550 mV to −70 mV.

In order to apply SAM one only needs the volume-corrected currents at the potential $E_{max} = -130$ mV, despite which the values of the other potentials have been given in Table 1 as they will be used in the following section.

Table 2
Results of the regression done with the eight pairs of values Δq and Δn corresponding to $E_{max} = -130$ mV

$\Delta n \times 10^8$	0.110	0.220	0.330	0.440	0.550	0.660	0.770	0.880
Δq	0.347	0.439	0.586	0.684	0.993	1.268	1.434	1.694

Regression model $\Delta q \times 10^8 = k\ \Delta n + b$

	Estimated value	Standard deviation	Significance level	Confidence interval (95%)
k	1.813740	0.120035	0.00001	(1.51994, 2.10755)
b	0.032821	0.066676	0.64003	(−0.13038, 0.19602)

$\rho = 0.9871$ $R^2 = 97.41\%$ R^2adj. $= 97.01\%$
Standard error of estimation = 0.0855705

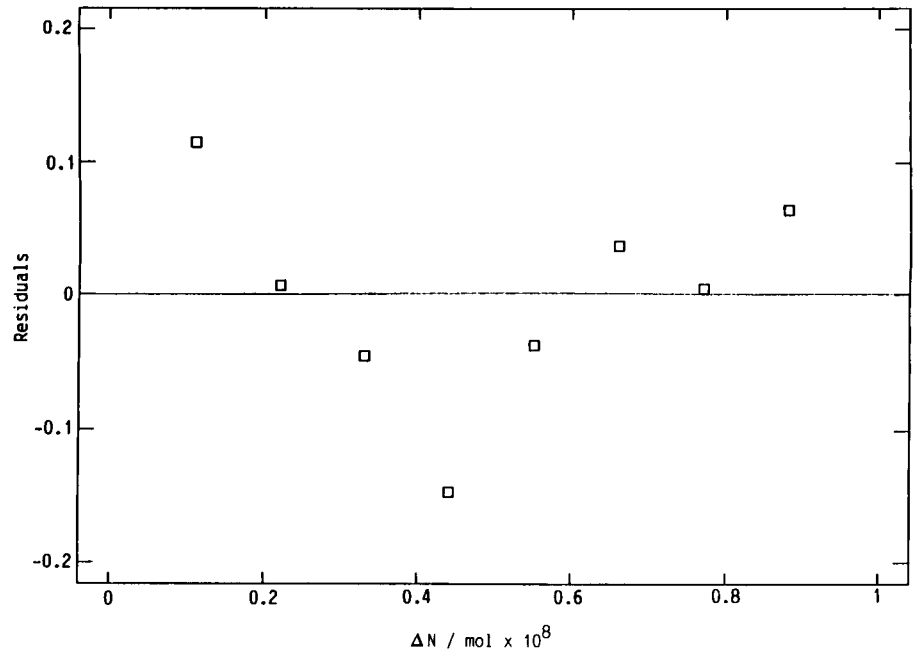

Fig. 2. Residuals of data in Table 2 plotted against the independent variable ΔN (mol $\times 10^8$), increases in moles of Cu in the SAM procedure.

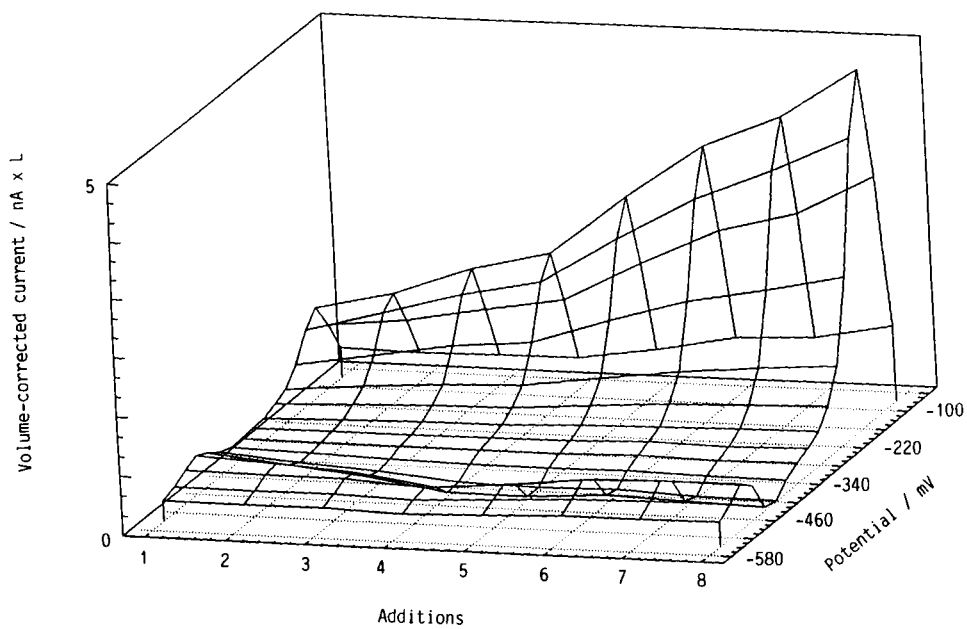

Fig. 3. Volume-corrected current against the different potentials and successive additions of copper (data from Table 1).

The increases Δq and Δn corresponding to E_{max} and each of the eight additions have been given in Table 2. In the same table, the results of the linear regression Δq over Δn are shown. The intercept is significantly null at the level 0.64. The correlation coefficient is not very high as one is dealing with a calibration line. The most notable feature is the non-random aspect of the residuals of the regression which indicates an inadequacy of the linear model as can be seen in Fig. 2. A different pattern can be seen for the first four residuals with regard to the last four. The greatest standardized residuals, in absolute value, are those corresponding to the first and fourth increases in moles; their magnitude, on the order of 2.5, is too great to be attributed to random reasons.

It should be recalled that Eq. 3 is valid for any potential, such that the regression can be done with the currents of any other column in Table 1. In general these regressions explain less variance and the residuals show the same pattern which is accentuated in a regular fashion when the potential is changed towards more negative values.

The changes are foreseeable, there being no need to consult the numerical results of the regression, by observing Fig. 3, which represents the volume-corrected currents in Table 1 for each addition and each of the 17 potentials. To make it clearer, it is preferable to represent the q_h values rather than the Δq_h ones. It is obvious that the relative growth in q_h is different in the first four additions than in the last four. For the peak potentials of Cu(II) there is always growth, while the situation changes at more negative potentials and even at the peak potentials of Cu(I), q_h decreases in the first four additions. The regularity observed in the behaviour found in many of the experimental series leads one to consider the univariate linear regression model, Eq. 3, inadequate for the determination of the quantity of Cu in wine.

It would seem logical to bear in mind the existence in the model of the two voltammetric peaks resulting from the presence of the Cu(I) chloride and Cu(II)–EDTA complexes, which makes it necessary to consider at least two sensors (potentials) to explain the variation of the corrected current as a function of the number of moles of Cu(II) added to the medium. In this case GSAM, designed [11,12] for the simultaneous determination of various analytes even when the sensors are not completely selective [13], would have to be used. A detailed explanation for sensors with a linear response and an analysis of the effect of the non-specificity of the sensors can be seen in Ref. 8.

The intrinsic characteristics of the experimental technique used, DPASV, make it impossible to independently vary the contents of Cu(I) and Cu(II) in order to apply GSAM. In the deposition step prior to the stripping, both the Cu(I) and the Cu(II) which would have been added to the sample to make up a single amalgam Cu(Hg) and the oxidation peaks observed in the stripping stage do not allow the increases in the signal to be directly related with the quantities of Cu(I) and Cu(II) added. Furthermore, the currents corresponding to the oxidation of Cu(0)/Cu(I) respond directly to the increase in both Cl^- and Cu(II) in solution. As a result one cannot expect a response of each sensor with the same sensibility for the successive additions; that the sensibilities be maintained constant is an essential condition for the GSAM method or any other method which is based on a regression on the volume-corrected currents.

4.2. Model with the latent structure

The above can be read in another way: the internal relationships between the concentration of Cl^-, EDTA and Cu are reflected in the behaviour of the volume-corrected currents at the different potentials. It will be necessary to examine in what way the latent structure of Δq_h is related to the increase in moles of Cu to demonstrate the viability of a linear multivariate model.

The problem is formally posed in the following way: the matrix **F** of currents recorded at p potentials is obtained experimentally. Its first row, $h = 0$, corresponds to the sample of wine with volume v_0 and n_0 moles of Cu. The next rows, $h = 1, \ldots, a$, correspond to the samples of volume

v_h and $n_0 + hn_1$ moles of Cu which are obtained after h additions of n_1 moles of Cu to the wine.

$$\mathbf{F} = (i_{hj}) = \begin{bmatrix} i_{01} & i_{02} & \dots & i_{0p} \\ i_{11} & i_{12} & \dots & i_{1p} \\ \vdots & \vdots & & \vdots \\ i_{h1} & i_{h2} & \dots & i_{hp} \\ \vdots & \vdots & & \vdots \\ i_{a1} & i_{a2} & \dots & i_{ap} \end{bmatrix} \quad (4)$$

The matrix of the volume-corrected currents are obtained by

$$\mathbf{Q} = \mathbf{VF} \text{ with } \mathbf{V} = \begin{bmatrix} v_0 & 0 & \dots & 0 & \dots & 0 \\ 0 & v_1 & \dots & 0 & \dots & 0 \\ \vdots & \vdots & & \vdots & & \vdots \\ 0 & 0 & \dots & v_h & \dots & 0 \\ \vdots & \vdots & & \vdots & & \vdots \\ 0 & 0 & \dots & 0 & \dots & v_a \end{bmatrix} \quad (5)$$

Finally, the matrix of increases in volume-corrected current with regard to the sample of wine is obtained by subtracting from each row of **Q** the first one.

$$\Delta\mathbf{Q}_{ap} = (q_{hj} - q_{0j}) = (\Delta q_{hj}),\ h = 1, \dots, a;$$
$$j = 1, \dots, p \quad (6)$$

The increases in moles of Cu in the successive additions are written as

$$\Delta\mathbf{N}_{a1} = \begin{bmatrix} 1n_1 \\ \vdots \\ hn_1 \\ \vdots \\ an_1 \end{bmatrix} \quad (7)$$

The aim is to find a linear combination of the columns of $\Delta\mathbf{Q}$ that explains the variable response $\Delta\mathbf{N}_{a1}$.

In order to choose the mathematical method with which to build the model it is good to bear in mind that a multivariate linear regression by least squares, MLR, would consist of calculating **K** in Eq. 8.

$$\Delta\mathbf{N}_{a1} = \Delta\mathbf{Q} \begin{bmatrix} k_1 \\ \vdots \\ k_h \\ \vdots \\ k_p \end{bmatrix} = \Delta\mathbf{Q}_{ap}\mathbf{K}_{p1} \quad (8)$$

MLR estimates **K** in such a way that the correlation between the predictor variables and the response is greatest, which is why on many occasions MLR includes excessive noise producing an overfit. One must add to this the high correlations, even collinearities, among the predictor variables which lead to unstable models with great variance in the estimated response and hence making them of little value for quantification of analytes [14,15].

On the other hand, the principal component regression can eliminate collinearities and remove noise from data in $\Delta\mathbf{Q}$ without removing useful information. This model-building procedure has two steps:

(i) Extraction of e significant components of $\Delta\mathbf{Q}$, namely the e directions of greatest variance

$$\Delta\mathbf{Q}_{ap} = \mathbf{S}_{ae}\mathbf{L}_{ep} + \mathbf{E}_{ap} \quad (9)$$

(ii) Use of MLR to regress the matrix $\Delta\mathbf{N}$ onto the scores matrix, **S**,

$$\Delta\mathbf{N}_{a1} = \mathbf{S}_{ae}\mathbf{K}_{e1} \quad (10)$$

Matrix **K** has the same meaning in Eqs. 8 and 10: in the first it is formed by the sensitivity of each of the p sensors while in the second it is the sensibility of each of the e principal components used in the model.

However, the independence between the procedure for obtaining the principal components, Eq. 9, and the variable response may produce an underfit because the information useful for explaining the copper content is not necessarily related to the principal components which explain more variance [14].

As a result of this problem the PLS method [14,15] has been developed. This is commonly used with spectroscopic methods [16] and is be-

ginning to be used with electrochemical methods [17,18]. A good tutorial account of PLS [19,20] and a historical perspective [21] may be found elsewhere.

PLS combines the best properties of both the afore-mentioned methods: in the space of the variable predictors it searches the directions with maximum variance avoiding those not correlated with the response. This characteristic is especially desirable in the problem posed. The presence of chloride ions and EDTA in the medium means that one does not always obtain the same linear relation independent of the copper added as the competitive reduction between Cu(II)–organic species and a Cu(I)–chloro complex intermediate must be born in mind.

With regard to the MLR, PLS introduces a bias in the estimation of the coefficients of the model in order to achieve a more stable prediction of the variable response. This is not a problem, as the model is going to be used to predict the quantity of copper in a sample of wine and the value of the coefficients of the variables in itself lacks interest. As a result, it is advantageous to use PLS in the analysis of the latent structure which is related to the copper content.

A detailed exposure of PLS can be found in Refs. 14 and 15 and its connection with other methods and recent advances in Refs. 22 and 23. The construction and evaluation of the PLS method applied to our problem is the following [15,20]:

(i) Latent structure of the predictor variables

$$\mathbf{\Delta Q}_{ap} = \mathbf{T}_{ae}\mathbf{B}_{ep} + \mathbf{E\Delta Q}_{ap} \quad (11)$$

(ii) Latent structure of the response

$$\mathbf{\Delta N}_{a1} = \mathbf{U}_{ae}\mathbf{C}_{e1} + \mathbf{E\Delta N}_{a1} \quad (12)$$

(iii) Internal relationship between the latent structures

$$\mathbf{U}_{ae} = \mathbf{T}_{ae}\mathbf{D}_{ee} + \mathbf{EU}_{ae} \quad (13)$$

PLS builds the matrices of the scores **T** and **U** that are those which explain the greatest possible variability of **ΔQ** and **ΔN** subject to the linear restrictions of (iii). The residual matrices **EΔQ** and **EΔN** allow one to evaluate the variability of the predictor variables or that of the response not explained by the model while the **EU** points to possible deviations in the proportionality which is theoretically postulated between **T** and **U**.

A critical aspect of the PLS model is the number of latent variables, namely the number of rows of matrix **B** in Eq. 11. In its determination one must bear in mind the explained variance not only of the predictor variables but also of the response. It is possible that increasing the number of latent variables only models the variability of **ΔQ** not related with the variability of the quantity of copper **ΔN**.

A great deal of attention must be paid to the prediction ability of the model built. It is evaluated by means of the variance in prediction. In order to calculate this a full crossvalidation was used: three training sets formed by 5, 5 and 6 of the rows which make up **ΔQ** and **ΔN** were calculated from Table 1, such that each of the rows remains outside the training set once in the complete process. The advantages of performing a full crossvalidation with regard to a stepwise crossvalidation, Wold's original method [24,25], can be consulted in Ref. 26. With each of these groups a PLS model was constructed and the crossvalidated variance was evaluated as a function of the number of latent variables. The more similar it is to that of the model built with all the data, the more stable the model will be. While, by definition, the explained variance increases when the number of latent variables e is increased, the crossvalidated variance may decrease which indicates that these components depend too much on concrete values (additions and/or currents) and

Table 3
Results of the PLS model obtained with the experimental data from Table 1

	% Explained variance		
	With one latent variable	With two latent variables	With three latent variables
Response **ΔN**			
Explained variance	97.95	99.63	99.64
Crossvalidated variance	97.90	99.40	96.59
Predictor **ΔQ**			
Explained variance	73.20	91.68	98.49

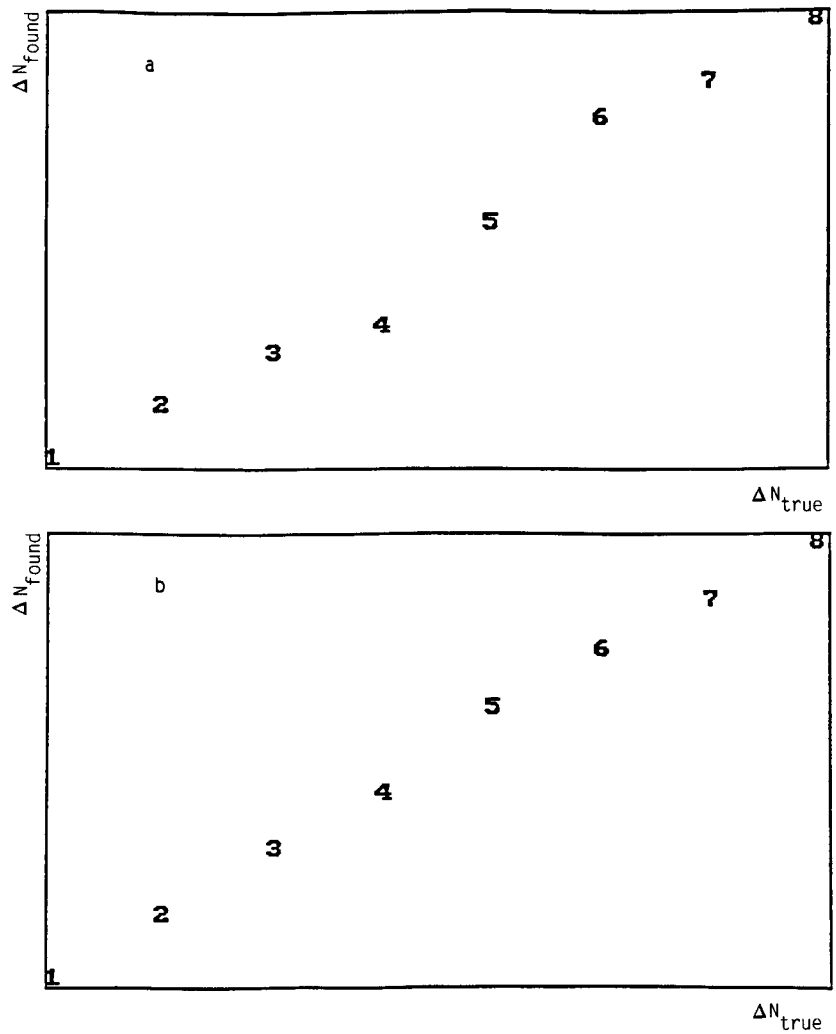

Fig. 4. Increase in moles calculated with PLS model. (a) Model with one latent variable; (b) Model with two latent variables. 1,...,8 represent successive additions of copper to the sample of wine.

should not form part of the model. A standardization common to all the data is not used in the crossvalidation process, but rather the average and standard deviation corresponding to each training set group are calculated. The importance of this aspect can be consulted in Ref. 27.

Table 3 summarizes the percentage of explained variance and crossvalidated variance ac-

Table 4
Difference between the true increases in moles of Cu and those calculated with the PLS model (data from Table 1)

$\Delta N\ (\times 10^8)$	0.110	0.220	0.330	0.440	0.550	0.660	0.770	0.880
$\lvert \Delta N_{true} - \Delta N_{found} \rvert$	0.005	0.002	0.002	0.014	0.024	0.019	0.005	0.019

cording to the components considered in the model. Applying the criteria previously cited, the model must consist of two latent variables which explain 99.63% of the response, **ΔN**, and 91.68% of the predictor variables, **ΔQ**. The inclusion of the third component only increases significantly the explained variance of the predictor variables, indicating that this third source of variability in the currents of the voltammograms is not related to the copper content added. The crossvalidated variance is very similar to the explained variance in the first two components and decreases with the addition of another component, which confirms the existence of two latent variables.

The variance explained by the PLS model, 99.63%, is greater than the 97.44% obtained in the univariate regression with the maximum peak current at −130 mV, Table 2.

The need for the second component can be visualized by means of the representation of the values calculated with one and two components as compared with the real increase in moles of Cu added, Fig. 4. The second latent variable models a different relation for the first four additions compared with the last four.

Table 5
Modelling power of the latent variables of the PLS model data from Table 1

	With one latent variable	With two latent variables	With three latent variables
E_{-550}	0.44	0.82	0.82
E_{-520}	0.58	0.82	0.88
E_{-490}	0.41	0.79	0.90
E_{-460}	0.00	0.69	0.91
E_{-430}	0.33	0.83	0.96
E_{-400}	0.49	0.88	0.93
E_{-370}	0.46	0.88	0.87
E_{-340}	0.00	0.12	0.81
E_{-310}	0.72	0.70	0.89
E_{-280}	0.88	0.92	0.91
E_{-250}	0.95	0.95	0.95
E_{-220}	0.95	0.94	0.96
E_{-190}	0.95	0.95	0.98
E_{-160}	0.92	0.92	0.95
E_{-130}	0.91	0.91	0.92
E_{-100}	0.86	0.87	0.88
E_{-70}	0.69	0.80	0.80

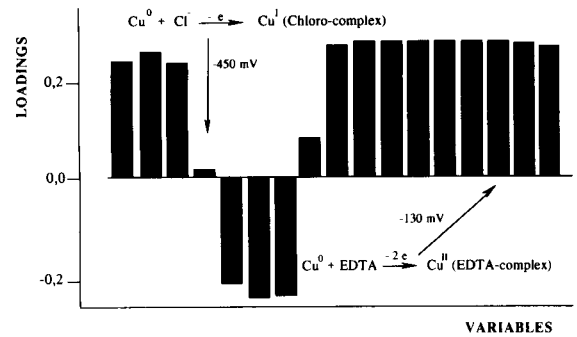

Fig. 5. Coefficients of the variables (loadings) in the first latent variable of PLS model (data from Table 1).

Table 4 shows the differences between the real concentration of copper and that calculated, the relative error being always less than 4%

4.3. Analysis of the latent structure

In general, models on latent variables are of great interest when the chemical interpretation of its components is possible, whilst some authors affirm that this is an essential condition for the correct use of these models in chemistry: "No predictor without interpretation and no interpretation without the capacity to predict" [14].

According to the values in Table 5, the currents corresponding to the potentials from −310 mV to −70 mV, the range within which one finds the maximum current for the wave Cu(0)/Cu(II)–EDTA, contribute with great modelling power (percentage of variance of the variable explained by this component) to the formation of the first latent variable. All these currents contribute with a loading, the first row of matrix **B** in Eq. 11, approximately equal and positive, Fig. 5. At the same time, the currents corresponding to potentials from −550 mV to −340 mV contribute with a significantly lower modelling power and their loadings are positive for the potentials lower than the oxidation peak of the Cu(0)/Cu(I)–chloride (−450 mV) and negative for the immediately higher potentials, such that the global contribution of the currents of this second

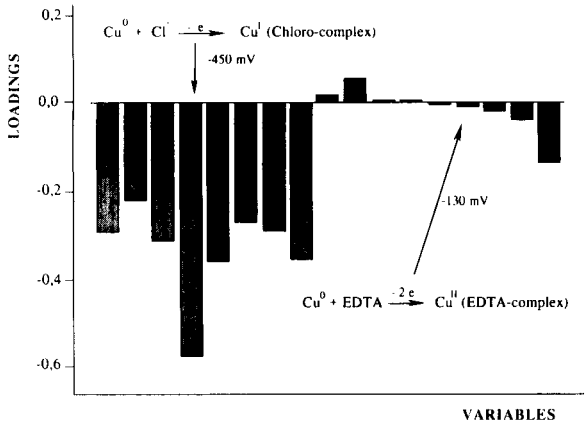

Fig. 6. Coefficients of the variables (loadings) in the second latent variable of PLS model (data from Table 1).

peak to the first component is practically null. In summary, the first latent variable explains the most significant fraction, 97.95%, of the variance of $\Delta \mathbf{N}$ through the $\Delta \mathbf{Q}_j$ corresponding to the oxidation Cu(0)/Cu(II)–EDTA.

For the second latent variable, the increases in the currents corresponding to the wave Cu(0)/Cu(II)–EDTA, lack modelling power. Only those corresponding to the wave Cu(0)/Cu(I)–chloride have modelling power. The loadings of this second latent variable, the second row of **B**, are shown in Fig. 6. They are all negative for the potentials around the peak maximum, while the loadings corresponding to the other peak are all practically zero. In other words, this component models a fraction of the variance of $\Delta \mathbf{N}$, 1.68%, independently of that explained by the previous latent variable and related to the formation of the Cu(I)–chloro complex intermediate. Representing the additions by their scores, matrix **T** of Eq. 11, in the plane formed by the first two latent variables gives Fig. 7, which shows a triangular disposition, characteristic of the existence of an interrelation between the two reactions.

The construction of a model to relate the Cu content to the voltammograms has to be analysed in the same way as the previous one, since, depending on the relationship which exists between the concentrations of copper, EDTA and chloride in the wine, the second component combined with the Cu(I)–chloride intermediate complex could possibly be irrelevant with regard to the background noise, in which case analysis of the latent variables and explained and crossvalidated variances must demonstrate the need for only one component. This fact was observed in several of the wines analysed, without this leading to models with worse predicting qualities; four of these cases were chosen to demonstrate the

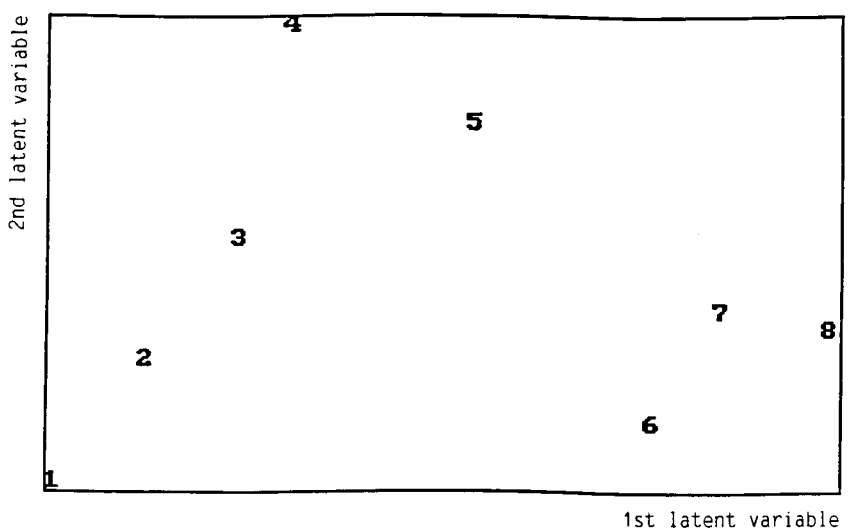

Fig. 7. Scores over the first two latent variables. 1,...,8 represent successive additions of copper to the sample of wine.

MSALV procedure which is proposed for the determination of Cu in wine. The application of this type of analysis avoids the need to explicitly establish the effect of the concentrations of EDTA and of chloride in the quantification of Cu in the sample by means of an adequate experimental design.

4.4. Multiple standard addition with latent variables, MSALV

Once it has been shown that the PLS regression determines a latent structure which can be chemically interpreted, this model must be applied to the currents recorded for the sample of wine in order to determine its Cu content. It is important to remember that the model built can only be applied to samples similar to those used to build it. There are therefore two immediate objections: (i) The currents for the samples of wine are not subtracted from the same reference as the samples used in the model; because the currents corresponding to the additions were subtracted from those of the wine, Eq. 6, but those of the wine $(q_{01},\ldots,q_{0p})$ are absolute which implies that if there is background noise in the currents this will give us an overestimation of the quantity of copper as these base currents make up part of the recordings for the problem sample of wine. In the case of the stripping technique used there is always a background current. (ii) The sample of wine may not contain Cu, at least theoretically, so that one would again apply an inadequate model since the samples used to make the addition did contain copper.

Both problems were eliminated by adding an initial step to the experimental process consisting of: (i) Recording a reference voltammogram on a solution made up of the original sample of wine to which a quantity of Cu, KCl and EDTA was added. The total volume is written as v_r and its total content in moles of Cu as n_r. (ii) Adding a known volume of wine giving a solution of volume v_0, with $n_r + n_0$ moles of Cu. The quantity n_0 is the moles from this second addition of wine. (iii) Additions of Cu, of n_1 moles each, are then made.

The matrices **G**, **W** and **M** formalize these experimental data, and are analogous to the matrices **F**, **V** and **N** used in the analysis of the latent structure, while differing from them in the meaning of the first two rows which include the scheme of additions explained in the previous paragraph.

$$\mathbf{G} = (i_{hj}) = \begin{bmatrix} i_{r1} & i_{r2} & \ldots & i_{rp} \\ i_{01} & i_{02} & \ldots & i_{0p} \\ i_{11} & i_{12} & \ldots & i_{1p} \\ \vdots & \vdots & & \vdots \\ i_{h1} & i_{h2} & \ldots & i_{hp} \\ \vdots & \vdots & & \vdots \\ i_{a1} & i_{a2} & \ldots & i_{ap} \end{bmatrix} \tag{14}$$

$$\mathbf{W} = \begin{bmatrix} v_r & 0 & 0 & \ldots & 0 & \ldots & 0 \\ 0 & v_0 & 0 & \ldots & 0 & \ldots & 0 \\ 0 & 0 & v_1 & \ldots & 0 & \ldots & 0 \\ \vdots & \vdots & \vdots & & \vdots & & \vdots \\ 0 & 0 & 0 & \ldots & v_h & \ldots & 0 \\ \vdots & \vdots & \vdots & & \vdots & & \vdots \\ 0 & 0 & 0 & \ldots & 0 & \ldots & v_a \end{bmatrix} \tag{15}$$

$$\mathbf{M} = \begin{bmatrix} n_r \\ n_r + n_0 \\ n_r + n_0 + 1n_1 \\ \vdots \\ n_r + n_0 + hn_1 \\ \vdots \\ n_r + n_0 + an_1 \end{bmatrix} \tag{16}$$

The matrix of the volume-corrected currents is

$$\mathbf{Z} = (z_{hj}) = \mathbf{GW} \tag{17}$$

Subtracting from each row of **Z** the first one gives

$$\mathbf{Q} = (q_{hj}) = (z_{hj} - z_{rj}),\ h = 0, 1,\ldots,a;$$

$$j = 1, 2,\ldots,p \tag{18}$$

which corresponds to the matrix of moles of Cu added

$$\mathbf{N} = \begin{bmatrix} n_0 \\ n_0 + 1n_1 \\ \vdots \\ n_0 + hn_1 \\ n_0 + an_1 \end{bmatrix} \quad (19)$$

Finally the PLS model is built starting from

$$\mathbf{\Delta Q} = (q_{hj} - q_{0j}),\ h = 1, \ldots, a;\ j = 1, 2, \ldots, p \quad (20)$$

such that it explains the increase in moles of Cu

$$\mathbf{\Delta N} = \begin{bmatrix} 1n_a \\ \vdots \\ hn_a \\ \vdots \\ an_a \end{bmatrix} \quad (21)$$

by means of a function of the variables column of $\mathbf{\Delta Q}$ which are the increases in volume-corrected currents with regard to the line of reference. With a compact notation $\Delta N = F(\Delta Q_1, \ldots, \Delta Q_p)$ the model will be built.

The quantity of moles n_0 present in the sample of wine will be determined by $F(q_{01}, \ldots, q_0 p)$ since $(q_{01}, \ldots, q_{0p})$ represent the increase in the volume-corrected currents with regard to the line of reference corresponding to the moles of Cu added to those of the wine. The closed formula of the PLS model proposed in Ref. 28 was used for this calculation.

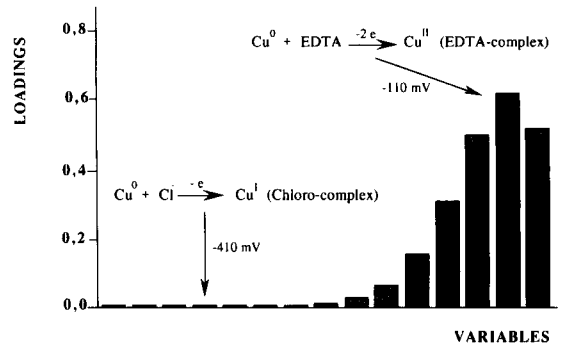

Fig. 8. Loadings in the first latent variable of PLS model (data from Table 6).

4.5. Application of MSALV

Methodology. The MSALV was applied to several samples of wine. Table 6 shows the matrices of the volume-corrected currents **Z**, Eq. 17, obtained at 15 potentials equally spaced between −500 mV and −80 mV. In this case the procedure consists of six additions of 0.03 μmoles of Cu which each forms part of the matrix **M**, Eq. 16, associated with this experiment and recorded in Table 6. The PLS regression on matrix $\mathbf{\Delta Q}$ deduced from this table was done without prior standardization.

With the first latent variable there is a 99.408% explained variance and a 99.362% crossvalidated

Table 6
Experimental data of the volume-corrected current for the potentials indicated and the successive additions of Cu, in moles, following the MSALV procedure

Addition	ΔN ($\times 10^6$)	Potential (mV)														
		−500	−470	−440	−410	−380	−350	−320	−290	−260	−230	−200	−170	−140	−110	−80
r	–	0.416	0.393	0.453	0.553	0.437	0.265	0.268	0.335	0.497	0.867	1.642	3.223	5.580	6.516	4.772
0	n_0	0.860	0.830	1.026	1.149	0.925	0.575	0.584	0.723	0.999	1.701	3.056	5.559	8.684	10.062	8.376
1	0.03	0.902	0.884	0.989	1.149	0.882	0.573	0.568	0.742	1.145	1.981	3.859	6.951	11.019	13.098	10.417
2	0.06	0.918	0.939	1.057	1.189	0.937	0.604	0.639	0.827	1.327	2.241	4.252	8.132	13.033	15.236	12.354
3	0.09	0.911	0.906	1.071	1.207	0.968	0.630	0.656	0.941	1.352	2.446	4.777	9.124	14.609	17.306	13.889
4	0.12	0.941	0.908	1.044	1.237	0.982	0.620	0.645	0.874	1.410	2.642	5.243	10.221	16.260	19.902	16.334
5	0.15	0.933	0.954	1.091	1.253	0.988	0.662	0.716	0.917	1.490	2.910	6.015	11.311	17.761	21.538	18.135
6	0.18	0.958	0.661	1.117	1.261	1.031	0.675	0.704	0.982	1.635	3.188	6.387	12.245	19.712	23.662	20.408

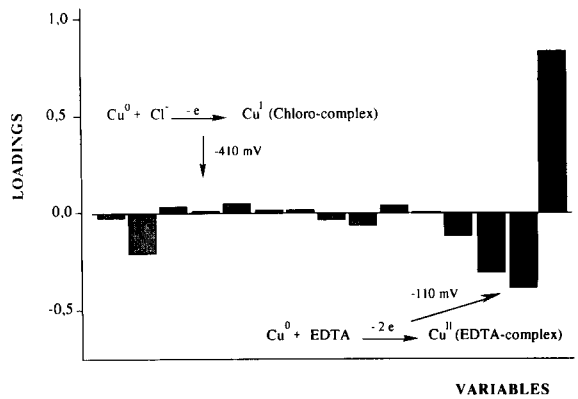

Fig. 9. Loadings in the second latent variable of PLS model (data from Table 6).

variance, while with the second component the variance reaches 99.752% and 99.446%, respectively. It is clear that the 0.084% increase shown by the crossvalidated variance is sufficiently small so as not to include this second component; only a blind numerical consideration would lead to its automatic acceptance. The examination of the loadings corresponding to both latent variables, shown in Figs. 8 and 9, confirms that the first latent variable is related exclusively to the potentials associated with the wave Cu(0)/Cu(II)–EDTA, while the second latent variable presents no relation with the peak potentials corresponding to the oxidation Cu(0)/Cu(I)–chloride and should not be included in the model. The most important loading in this second variable is that corresponding to potential −80 mV whose current is the only variable which shows a high modelling power as can be deduced from Table 7. In fact this latent variable explains the effect due to the displacement of the peak towards the oxidation barrier of the electrode itself, which reaffirms its exclusion from the model. One must conclude that the oxidation of the Cu(0)/Cu(I)–chloride did not occur to a significant degree in relation to the increase in moles of Cu in the addition.

The PLS model for the increase in Cu, expressed in μmole, at the 50 different potentials of Table 6 is

$$\Delta N = 3.57\times10^{-5}\ \Delta Q_1 + 2.49\times10^{-5}\ \Delta Q_2 + 4.06\times10^{-5}\ \Delta Q_3 + 2.88\times10^{-5}\ \Delta Q_4 + 3.22\times10^{-5}\ \Delta Q_5 + 4.33\times10^{-5}\ \Delta Q_6 + 9.02\times10^{-5}\ \Delta Q_7 + 2.20\times10^{-4}\ \Delta Q_8 + 5.02\times10^{-4}\ \Delta Q_9 + 1.17\times10^{-3}\ \Delta Q_{10} + 2.36\times10^{-3}\ \Delta Q_{11} + 3.84\times10^{-3}\ \Delta Q_{12} + 4.80\times10^{-3}\ \Delta Q_{14} + 4.40\times10^{-3}\ \Delta Q_{15}$$

Applying this expression to the vector $(q_{01},\ldots,q_{0p})$, the difference between the second and first row of Table 6, gives 0.0513 μmole. Given that the volume of the sample is 0.02 l this gives a concentration of 2.57×10^{-6} mol dm^{-3}.

Table 7
Modelling power of the latent variables of the PLS model (data from Table 6)

	With one latent variable	With two latent variables
E_{-500}	0.79	0.82
E_{-470}	0.00	0.22
E_{-440}	0.46	0.48
E_{-410}	0.84	0.84
E_{-380}	0.50	0.58
E_{-350}	0.76	0.77
E_{-320}	0.70	0.67
E_{-290}	0.75	0.75
E_{-260}	0.88	0.88
E_{-230}	0.96	0.96
E_{-200}	0.95	0.95
E_{-170}	0.98	0.98
E_{-140}	0.98	0.98
E_{-110}	0.98	0.98
E_{-80}	0.95	0.95

Table 8
Statistical parameters of the values ΔN^a obtained with the PLS model for several samples

ΔN_{true}	ΔN_{found}				
	Mean	Median	Sample size	Standard deviation	C.V. (%)
0.01	9.99×10^{-3}	0.010	5	1.01×10^{-3}	10.08
0.02	0.020	0.020	4	5.56×10^{-4}	2.77
0.03	0.029	0.030	14	3.09×10^{-3}	10.47
0.04	0.039	0.039	5	1.39×10^{-3}	3.55
0.05	0.050	0.050	5	5.31×10^{-4}	1.06
0.06	0.059	0.058	13	3.20×10^{-3}	5.41
0.07	0.070	0.070	5	8.63×10^{-4}	1.22
0.09	0.090	0.091	9	3.28×10^{-3}	3.63
0.12	0.120	0.120	9	3.19×10^{-3}	2.66
0.15	0.147	0.148	9	2.89×10^{-3}	1.96
0.18	0.178	0.179	8	4.47×10^{-3}	2.51
0.21	0.210	0.210	7	3.87×10^{-3}	1.84

a Expressed in μmoles.

Accuracy. Table 8 shows the true increases, ΔN_{true}, in μmoles and those obtained with PLS in several runs of MSALV. It can be seen that the variation coefficients, which include variability as a result of different days and different analysts, are acceptable.

Precision. Table 9 shows the results of applying MSALV to four different wines, A, B, C and D. In each case two replicate determinations were made to get an indication of whether the results obtained can be reproduced. In the eight PLS models constructed the concentration was determined with a single latent variable because in all of them the analysis of the loadings and of the modelling power of the variables leads to results similar to those obtained in the preceding discussion. However, the explained and crossvalidated variances with one and with two latent variables were noted as the only data of the characteristics of the model.

It is possible to calculate an interval for the prediction with the data of each regression. In

Table 9
Confidence intervals and Cu content of wine calculated with the MSALV procedure for various red wines

	Sample A			
	Replicate 1		Replicate 2	
	Explained variance	Crossvalidated variance	Explained variance	Crossvalidated variance
With one latent variable	99.553	99.601	99.807	99.771
With two latent variables	99.881	99.819	99.834	99.675
$C_{Cu(II)}$ calculated with MSALV (M)	1.700×10^{-6}		1.740×10^{-6}	
Confidence interval calculated with Eq. 22	$\pm 0.406 \times 10^{-6}$		$\pm 0.305 \times 10^{-6}$	
	Sample B			
	Replicate 1		Replicate 2	
	Explained variance	Crossvalidated variance	Explained variance	Crossvalidated variance
With one latent variable	99.408	99.362	99.826	99.813
With two latent variables	99.752	99.446	99.793	99.769
$C_{Cu(II)}$ calculated with MSALV (M)	2.570×10^{-6}		2.460×10^{-6}	
Confidence interval calculated with Eq. 22	$\pm 0.485 \times 10^{-6}$		$\pm 0.357 \times 10^{-6}$	
	Sample C			
	Replicate 1		Replicate 2	
	Explained variance	Crossvalidated variance	Explained variance	Crossvalidated variance
With one latent variable	99.837	99.836	99.867	99.776
With two latent variables	99.866	99.739	99.875	99.737
$C_{Cu(II)}$ calculated with MSALV (M)	1.555×10^{-6}		1.550×10^{-6}	
Confidence interval calculated with Eq. 22	$\pm 0.448 \times 10^{-6}$		$\pm 0.514 \times 10^{-6}$	
	Sample D			
	Replicate 1		Replicate 2	
	Explained variance	Crossvalidated variance	Explained variance	Crossvalidated variance
With one latent variable	98.629	98.049	98.948	98.379
With two latent variables	98.595	97.201	99.064	98.184
$C_{Cu(II)}$ calculated with MSALV (M)	1.355×10^{-6}		1.355×10^{-6}	
Confidence interval calculated with Eq. 22	$\pm 0.270 \times 10^{-6}$		$\pm 0.267 \times 10^{-6}$	

Ref. 29 an empirical formula is suggested, based on the weighting of the various sources of variability: (i) Variance of the residuals in prediction. (ii) Non-explained variance of the predictor variables for the signal of the sample problem in relation with the non-explained variance of the samples of addition. (iii) Position of the sample problem in the multidimensional space formed by the signals of the samples of addition.

An adaptation to the case under study is to consider the crossvalidated variance, s_{cv}^2, (see Ref. 27) as a residual variance in prediction, since we do not have a set of data big enough to separate it into a set of evaluation and prediction. The formula used is

$$\frac{s_{cv}}{\sqrt{2}}\sqrt{\frac{RV(q_{01},\ldots,q_{0p})}{RV(\mathbf{E\Delta Q})}+\mathrm{Lev}(q_{01},\ldots,q_{0p})+\frac{1}{a}} \tag{22}$$

In this, $RV(q_{01},\ldots,q_{0p})$ is the residual variance obtained by applying Eq. 11 to the vector $(q_{01},\ldots,q_{0p})$ of the signal increases associated with the sample of wine. $RV(\mathbf{E\Delta Q})$ is the residual variance not explained by the model for the signals of the samples of addition, Eq. 11. The quotient of both variances is a measure of the similarity between the vector $(q_{01},\ldots,q_{0p})$ and the rows of $\mathbf{\Delta Q}$.

The leverage of vector $(q_{01},\ldots,q_{0p})$ denoted by $\mathrm{Lev}(q_{01},\ldots,q_{0p})$ in Eq. 22 is a measure of the grade of influence which the vector has over the regression. It is evaluated by the relative weight:

$$\mathrm{Lev}(q_{01},\ldots,q_{0p})=\sum_{j=1}^{e}\frac{tq_j^2}{\sum_{i=1}^{a}t_{ij}^2} \tag{23}$$

tq_j being the scores of the vector $(q_{01},\ldots,q_{0p})$ according to the model of Eq. 11 and t_{ij} those corresponding to the additions used in the calibration, in this present case remembering that $e=1$.

Finally a, the last term of Eq. 22, is the number of rows of $\mathbf{\Delta Q}$, in other words, the number of additions of Cu made.

In this way the intervals calculated using the PLS model are obtained, shown in Table 9 for each determination. An acceptable regularity can be seen both among the replicates and among the different wines. It is also clear that Eq. 22 produces an overestimation of the expected variability in prediction as can be seen when the values obtained for the concentration of Cu in the replicate analyses are revised.

With the routine application of the proposed process in mind, our team is currently working on the optimization of the estimated precision by: the adequate weighting of the parameters in Eq. 22, the design of the calibration and the comparison of experimental measurements between different commercially available instruments.

5. Conclusions

Some of the frequent problems in the use of highly sensitive electroanalytical techniques can be eliminated by means of the PLS regression together with an adequate experimental strategy. Thus, the non-existence of a defined base line in a complex matrix and the variation in sensitivity at a given potential due to the modification of chemical equilibria when the analyte is added in the calibration process, can be treated using the MSALV process proposed in this work.

Acknowledgment

The authors thank the Interministerial Commission for Science and Technology for the finance received for this work (Project ALI 91-0441).

References

[1] Recueil des Méthodes Internationales d'Analyse des Vins, Office International de la Vigne et du Vin, Paris, 1971.
[2] J. Wang, Stripping Analysis: Principles, Instrumentation and Applications, VCH, Derfield Beach, FL, 1985.
[3] M. Forina, R. Leardi, C. Armanino and S. Lanteri, PARVUS: An Extendable Package of Programs for Data

Exploration, Classification and Correlation, Release 1.2, provisionally available from the authors.
[4] A. Herrero, M.C. Ortiz, J. Arcos and J. López-Palacios, Analyst, in press.
[5] G. Scarano, E. Morelli, A. Seritti and A. Zirino, Anal. Chem., 62 (1990) 943.
[6] S. Daniele, M.A. Baldo, P. Ugo and G.A. Mazzocchin, Anal. Chim. Acta, 219 (1989) 9.
[7] C. Liteanu and I. Rica, Statistical Theory and Methodology of Trace Analysis, Ellis Horwood, Chichester, 1980.
[8] M.A. Sharaf, D.L. Illman and B.R. Kowalski, Chemometrics, Wiley, New York, 1986.
[9] J.J. Lingane, Electroanalytical Chemistry, Interscience, New York, 2nd. edn., 1958.
[10] H. Kaiser, Pure Appl. Chem., 34 (1973) 35.
[11] B.E.H. Saxberg and B.R. Kowalski, Anal. Chem., 51 (1979) 1031.
[12] C. Jochum, P. Jochum and B.R. Kowalski, Anal. Chem., 53 (1981) 85.
[13] R.W. Gerlach and B.R. Kowalski, Anal. Chim. Acta, 134 (1982) 119.
[14] H. Martens and T. Naes, Multivariate Calibration, Wiley, New York, 1989.
[15] M. Forina, I. Frank and S. Lanteri, Regressione, Progetto COMETT per la Chemiometria, Università di Genova, 1991.
[16] J. Swerts, P. Van Espen and P. Geladi, Anal. Chem., 65 (1993) 1181.
[17] A. Henrion, R. Henrion, G. Henrion and F. Scholz, Electroanalysis, 2 (1990) 309.
[18] J.J. Berzas and J. Rodríguez, Fresenius J. Anal. Chem., 342 (1992) 273.
[19] P. Geladi and B.R. Kowalski, Anal. Chim. Acta, 185 (1986) 1.
[20] K.R. Beebe and B.R. Kowalski, Anal. Chem., 59 (1987) 1007.
[21] P. Geladi, J. Chemom., 2 (1988) 231.
[22] B.M. Wise and N.L. Ricker, J. Chemom., 7 (1993) 1.
[23] F. Lindgren, P. Geladi and S. Wold, J. Chemom., 7 (1993) 45.
[24] S. Wold, Technometrics, 20 (1978) 397.
[25] S. Wold, C. Albano, W.J. Dunn, K. Esbensen, S. Hellberg, E. Johansson and M. Sjöström, in H. Martens and H. Russwurm (Eds.), Food Research and Data Analysis, Applied Science, London, 1983, p. 147.
[26] I.N. Wakeling and Y.J. Morris, J. Chemom., 7 (1993) 291.
[27] S. Lanteri, Chemom. Intell. Lab. Syst., 15 (1992) 159.
[28] E. Marengo and R. Todeschini, Chemom. Intell. Lab. Syst., 12 (1991) 117.
[29] Unscrambler II (v 4.0), User's Guide, Camo A/S, Norway, 1992.

ELSEVIER

Analytica Chimica Acta 293 (1994) 295–300

ANALYTICA CHIMICA ACTA

Chemometric studies on minor and trace elements in cow's milk

L. Favretto [a,*], D. Vojnovic [b], B. Campisi [a]

[a] *Dipartimento di Economia e Merceologia delle Risorse Naturali e della Produzione, Università di Trieste, Trieste, Italy*
[b] *Dipartimento di Scienze Farmaceutiche, Università di Trieste, Trieste, Italy*

(Received 20th January 1994)

Abstract

In raw milk nine minor and trace elements (Cr, Mn, Fe, Ni, Cu, Zn, Mo, Cd and Pb) were determined in the dissolved ash by means of atomic absorption spectrometry and electrothermal atomization in a graphite furnace. The application of linear principal component analysis to the data matrix has permitted the reduction of the number of variables to four principal components accounting for 74% of the total variability. The two-dimensional plot of the scores (the milk samples) for the first principal components has pointed out a differentiation according to the two kinds of cow's feeding. Successively, the technique of linear discriminant analysis has fully confirmed the separation between the two types of milk.

Key words: Atomic absorption spectrometry; Principal component analysis; Linear discriminant analysis; Milk; Trace metals; Graphite furnace

1. Introduction

Linear principal component analysis (LPCA) and linear discriminant analysis (LDA) are statistical techniques that have turned out to be very helpful for interpretation and utilization of multivariate data in several fields of research, and therefore also in food research.

The method of principal components applied to a group of data, consisting of n measurements on p elements, permits in fact the description of the multivariate structure of the data by obtaining linear transformations of the correlated variables **x** (vectors of observations on the original variables), which, once transformed, become uncorrelated. In this way, it becomes possible for researchers to both evaluate the interdependences among the various variables and reduce the original data set to a small number of q principal components accounting for most of the variability [1].

The multivariate procedure of linear discriminant analysis is instead a supervised pattern recognition method employed for the differentiation between two or more classes of objects. The linear transformation of the multivariate observations into univariate observations, according to Fisher's method [2], permits in fact the separation of the populations to which the observations belong as good as possible.

* Corresponding author.

SSDI 0003-2670(94)00109-Y

In recent years, these methods of investigation have been widely applied to chemometric differentiation of foods and food products [3]. By means of chemometric procedures trace elements in milk and dairy products were studied in order to group element clusters according to their origin [4] or perform an exploratory evaluation of the differences in milk produced in two Italian regions [5].

In this paper we will employ both these statistical procedures to analyze the structure of a data matrix consisting of 49 measurements on 9 minor and trace elements in raw milk. The purpose is to determine whether the concentrations of the trace elements in the analyzed milk samples can be distinguished according to the feeding of cows. Therefore, we will use LPCA as an exploratory method and LDA as a confirming chemometric procedure.

2. Experimental

2.1. Sampling, apparatus and reagents

The milking was performed directly into plastic laboratory flasks in an Istrian farm (Verteneglio, Croatia). The sampling was carried out with an irregular frequency between March 12 and November 15, 1986. All the elements were independently determined twice in each sample, considering the mean as final value. The preparation of samples for electrothermal graphite furnace atomic absorption spectrometry (carried out with a Perkin-Elmer HGA 500 graphite furnace electrothermal atomizer coupled to a 1100 atomic absorption spectrometer with an AS-40 autosampler) and the employed analytical methodology are reported in the literature [6].

2.2. Statistical data processing

All the statistical analyses have been performed by means of the SPSS released 5.0 – Professional Statistics, run on an IBM-compatible hardware.

The starting data matrix **X** is formed by $n = 49$ cases (the series of cow's milk samples) and $p = 9$ variables (the concentration of the minor and trace elements). In this paper the whole sample n has been divided into two subsamples according to the sampling period (n_1: March 12–April 15 and n_2: April 26–November 15, 1986). The grouping of the samples has been made on the basis of the different feeding given to the cows in a continuous way during the mentioned periods: the former ($n_1 = 15$) an artificial mixture of grains (barley and maize), the latter ($n_2 = 34$) natural pastures and hay. To perform the principal component analysis, the original variables are being scaled such that each data z_{jk} is in standard units with zero mean and unit standard deviation. Hence, the dispersion matrix employed to obtain the characteristic vectors is a correlation matrix.

The sample correlation matrix **R** has been worked out from the **Z** matrix as follows: $\mathbf{R} = 1/(n-1)\mathbf{Z}'\mathbf{Z}$, where $\mathbf{Z}'$ is the transposed **Z** matrix. Among the criteria used in deciding the number ($q < p$) of principal components (pc's) to be retained we have considered as pc's the characteristic roots (eigenvalues) larger than one (the aver-

Table 1
Range of the concentration (c, $\mu g\ g^{-1}$) of the elements in milk from two sampling periods and basic statistics

Sampling period	C	Cr	Mn	Fe	Ni	Cu	Zn	Mo	Cd	Pb
Class 1	Min	2.06	12.3	196	2.80	3.18	375	7.50	0.26	1.13
(March 12–	Max	9.10	26.0	726	16.70	39.7	1,962	27.2	3.46	28.0
April 15, 1986)	$\bar{c}$	3.59	16.7	419	7.97	11.3	963	14.5	1.32	8.06
($n_1 = 15$)	s^2	3.75	21.5	30,276	13.6	155	295,690	33.3	0.93	64.6
Class 2	Min	1.88	7.25	81	1.77	4.60	2,005	6.05	0.07	1.30
(April 26–	Max	6.25	32.2	536	28.2	123	5,192	61.0	1.58	29.2
November 15,	$\bar{c}$	3.44	14.7	234	7.64	49.4	3,277	26.2	0.60	9.02
1986) ($n_2 = 34$)	s^2	1.16	39.8	11,200	44.1	906	870,520	169	0.134	29.8

Table 2
Correlation matrix between the pairs of elements ($n = 49$)

	Cr	Mn	Fe	Ni	Cu	Zn	Mo	Cd	Pb
Cr	1.00								
Mn	−0.06	1.00							
Fe	0.09	0.49	1.00						
Ni	−0.04	0.15	0.06	1.00					
Cu	−0.12	0.23	−0.22	0.48	1.00				
Zn	0.04	−0.22	−0.49	−0.33	0.42	1.00			
Mo	−0.09	0.59	0.12	0.12	0.47	0.26	1.00		
Cd	−0.00	0.15	0.23	−0.02	−0.29	−0.39	−0.17	1.00	
Pb	−0.08	−0.10	−0.35	0.07	0.07	0.09	−0.06	0.25	1.00

age root when PCA starts with a correlation matrix) [1]. The correlations between each variable and the first four principal components have been computed. The $\mathbf{Y} = \mathbf{ZV}$ matrix ($n \times p$) of pc-scores has been estimated from the eigenvector matrix **V**. Then a matrix transformation has been obtained with an orthogonal rotation (Normal Varimax) in order to improve the examination of the structure of the data set [7].

Linear discriminant analysis has been used as a confirmatory method [2].

3. Results and discussion

3.1. Basic statistics

Table 1 contains the concentration range of the elements analyzed in milk from the two sampling periods, along with the corresponding sample means and variances. One-way analysis of the variance (one-way ANOVA) has been exploratory applied to the pairs of vectors of the same variable and are further considered.

3.2. Linear principal component analysis

The method of principal components applied to the data matrix has permitted the differentiation between the two groups of milk samples.

The correlation matrix **R** (9 variables and 49 observations) is displayed in Table 2. No strong correlations are observed between the pairs of variables. In this data matrix the highest positive correlations are pointed out for molybdenum–manganese (0.59), copper–nickel (0.48), copper–molybdenum (0.47) and zinc–copper (0.42), while the largest negative correlation regards the variables zinc–iron (−0.49).

The eigenvalues obtained from this matrix are the following: 2.26, 2.08, 1.34, 1.01, 0.94, 0.49, 0.35, 0.29 and 0.24. By choosing only higher-than-

Table 3
Principal component matrix and rotation matrix, along with the communality of variables (h^2)

Variables	Principal component				h^2	Rotated component			
	1	2	3	4		1	2	3	4
Cr	−0.15	−0.07	−0.35	0.58	0.48	0.04	−0.36	−0.55	0.23
Mn	0.07	0.88	0.07	−0.19	0.82	0.34	0.83	−0.08	0.15
Fe	−0.49	0.72	−0.19	0.10	0.80	0.66	0.37	−0.47	−0.01
Ni	0.36	0.33	0.38	0.68	0.84	0.06	0.07	0.01	0.91
Cu	0.83	0.25	0.16	0.19	0.82	−0.50	0.41	0.12	0.62
Zn	0.73	−0.36	−0.19	−0.12	0.72	−0.84	0.03	0.10	0.04
Mo	0.56	0.61	−0.08	−0.32	0.80	−0.25	0.85	−0.01	0.11
Cd	−0.55	0.16	0.59	−0.05	0.69	0.73	−0.07	0.40	0.01
Pb	0.12	−0.30	0.78	−0.09	0.72	0.03	−0.18	0.81	0.20

one eigenvalues, nine variables have been reduced to four principal components accounting for 74.3% of the total variability. All the eigenvalues appear positive and even if the fourth one is very close to unity, it has been considered here as a principal component since it accounts for an additional 11.2% of the variance.

The correlation between each pc and each original variable is given in Table 3. Most of the coefficients corresponding to the first pc are positive. In particular, copper is highly correlated with it and the same holds for zinc, and also for molybdenum though with a lower correlation. A nearly zero correlation is found for manganese, whereas both cadmium and iron show a low negative correlation. Manganese, iron and, slightly, molybdenum are positively correlated with the second pc. A weak negative correlation appears for zinc. With the third pc only lead and, more slightly, cadmium are positively correlated, while a lower correlation appears for nickel. Chromium, on the contrary, appears negatively correlated with this pc. The last pc considered here is positively correlated with nickel and chromium with medium values, whereas a very low negative value is observed for molybdenum.

The scores for the first two pc's are plotted as a scatter diagram in Fig. 1. When all the data are considered, the pattern of the projected scores shows a quite evident v-shaped form. Although in this exploratory plot the distance between the two score groups is small, at least for these samples, a separation is quite evident. From Table 3 one can infer that the separation of the scores along the first eigenvector is probably due to copper and zinc, whereas manganese and iron tend to determine the pc-scores along the second eigenvector.

In order to improve the differentiation between the two groups, a Varimax rotation has been performed. After an orthogonal transformation the rotated matrix looks similar in structure to the unrotated pc-matrix, although some modifications are clearly evident, such as the fourth rotated component with a high/medium correlation with the nickel and copper variables. However, it can be said that the separation of the two groups of scores has really been improved by the

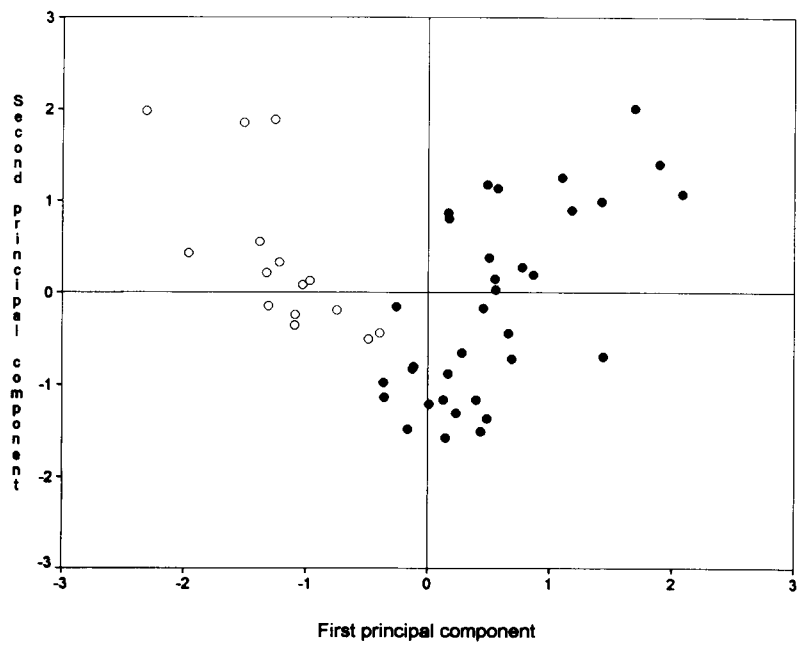

Fig. 1. Projection of the first two principal components of the scores for the 49 milk samples separated in two classes: (○) $n_1 = 15$, (●) $n_2 = 34$.

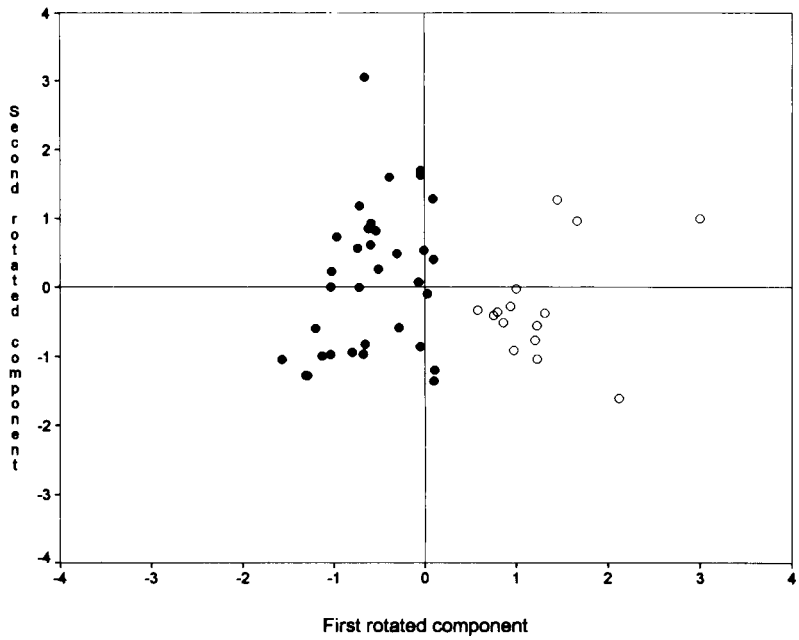

Fig. 2. Projection of the first two rotated components of the scores for the data used in Fig. 1.

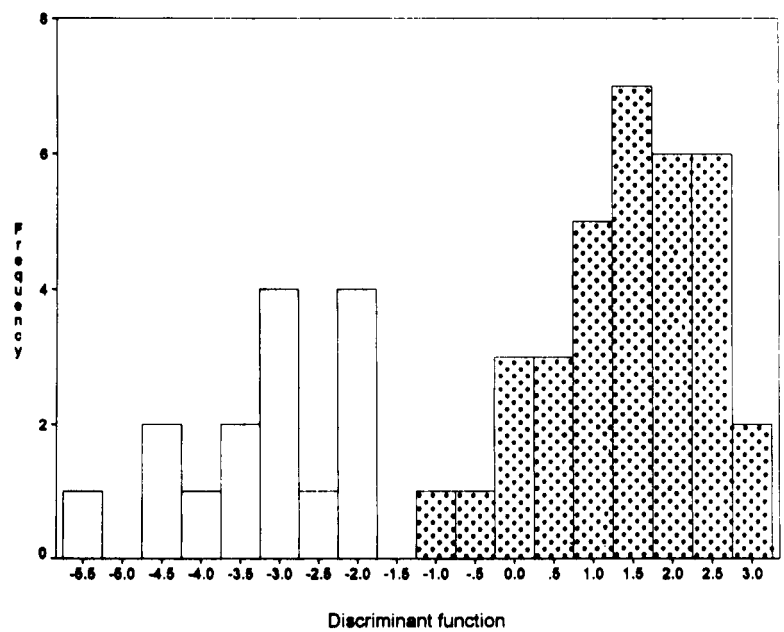

Fig. 3. Distribution of data expressed as discriminant scores along the discriminant axis: white histogram: $n_1 = 15$ (centroid -3.22); dotted histogram: $n_2 = 34$ (centroid 1.42).

adopted rotation procedure, as shown in Fig. 2. In fact, in the rotated plot the two types of scores are visually divided by a plane parallel to that formed by eigenvector 2 and eigenvector 3.

3.3. Linear discriminant analysis

An indicative one-way ANOVA for testing the equality of group means for each variable is given by the following F_{obs} values, which have to be compared to a critical F value for $k-1(=1)$ and $n-k(=47)$ degrees of freedom (the significance level is given in parenthesis): Zn 79.7 (0.0000), Cu 22.2 (0.0000), Fe 21.2 (0.0000), Cd 14.7 (0.0004), Mo 11.0 (0.002), Mn 1.2 (0.28), Pb 0.24 (0.62), Cr 0.12 (0.73), Ni 0.03 (0.86). The discriminating power reaches a maximum for zinc, while it is significant for copper, iron, cadmium and molybdenum. For the remaining trace elements the hypothesis is that both groups tend to have equal means.

The data are displayed as discriminant scores in Fig. 3. This plot on the standardized discriminant axes shows that the scores for each group are well separated from each other. Using the discriminant function there has not been any misclassified case. In fact, the classification between the two groups has turned out to be 100% correct, at least for the sample considered here.

4. Conclusions

We can say that classical methods of multivariate statistical analysis appear useful tools for the differentiation of milk products owing to the sensitivity of LPCA and LDA procedures. Moreover, further exploration of these methods may improve our study by the determination of the composition of the different feeding given to the cows involved in this research.

References

[1] J. Edward Jackson, A User's Guide to Principal Components, Wiley, New York, 1991.
[2] R.A. Johnson and D.W. Wichern, Applied Multivariate Statistical Analysis, Prentice-Hall, Englewood Cliffs, NJ, 1982.
[3] H. Martens and H. Russwurm Jr., Food Research and Data Analysis, Applied Science Publishers, New York, 1983.
[4] L. Favretto, L. Gabrielli Favretto, G. Pertoldi Marletta and M. Saitta, Anal. Chim. Acta, 201 (1987) 253.
[5] L. Gabrielli Favretto, G. Pertoldi Marletta, P. Bogoni and L. Favretto, Z. Lebensm. Unters. Forsch., 189 (1989) 123.
[6] D. Vojnovic, G. Procida and L. Gabrielli Favretto, Food Addit. Contam., 8 (1991) 343.
[7] M. Forina, C. Armanino, S. Lanteri and R. Leardi, J. Chemom., 3 (1988) 115.

ELSEVIER

Analytica Chimica Acta 293 (1994) 301–309

ANALYTICA CHIMICA ACTA

H-FLUO: an expert system connected to a hypertext to guide experimenters in basic applied fluorescence

Philippe B. Pingand [a,*], Dan A. Lerner [b]

[a] *CJN, Dept. of Artificial Intelligence, 40 Av. Diacon, 34090 Montpellier, France*
[b] *LCPI, ENSCM, 8 Rue de l'Ecole Normale, 34053 Montpellier Cédex 1, France*

(Received 3rd November 1993)

Abstract

H-FLUO is a software dedicated to solving various queries issued by end-users of spectrofluorimeters when they come across a problem in the course of an experiment. The main goal is to provide a diagnostic for the non-pertinent use of a spectrofluorimeter. Many artifacts may get the operator into trouble and except for experts, the simple manipulation of the controls of a fluorimeter results in effects not always fully appreciated. The solution obtained is an association between a powerful hypermedia tool and an expert system. A straight expert system imposes many moves between the spectrofluorimeter and the diagnostic tool. In our hypermedia tool, knowledge can be displayed by the means of visual concepts through which one can browse and navigate. The user perceives at all times his problem as a whole. We will demonstrate typical situations in which an event will trigger a chain reasoning leading to the debugging of the problem. The system is not only meant to help a beginner but can also conform itself to guide a well-trained experimenter. We think that its functionalities and user-friendly interface are very attractive and open new vistas in the way future users may be trained, whether they work in research labs or industrial settings, as it could diminish the time spent on their training. With these latest considerations in mind, we put the emphasis on fluorescence and limited the exposition of the computing aspects/hypermedia and expert system inner workings to a minimum.

Key words: Fluorimetry; Raman spectrometry; Artifacts; Expert systems; Sample contamination; Scattering; Training

1. Introduction

Presently, most software incorporated into fluorimeters allow the acquisition and manipulation of spectral data. Even if they happen to be very useful and sophisticated in their computational and representation offering, they generally rely on parameters defined by the user. Unlike these software, the main object of the program H-FLUO presented here is to help an experimenter who meets with problems while working on a fluorimeter. The program guides him to regain control over his experiment by setting all parameters right. Every suggested setting is done in correspondence with the underlying physics and

* Corresponding author.

SSDI 0003-2670(94)00108-X

provides information to highlight its fundamental and practical aspects. The user is free to browse, to go from one piece of information to another, to come back to any previous step if he feels interested. This is done independently of the nature of the problem, of the type of the instrument and of the level of knowledge of the user in the field of fluorescence. This paper focuses more on the benefit of using the program to carry out measurements in fluorescence but a short description of the structure and function of the program is given.

2. Scope and start-up of the program

Any technology based on detection of fluorescence, or luminescence in its broadest meaning, requires the determination of the excitation wavelength or of the emission wavelength (or of both) for the sample under study. The experimental acquisition of these data, especially by a beginner, is not an easy task due to the many interfering parameters which must be set. With a complex matrix or some biological samples, many artifacts may bring the operator into trouble [1–3]. This is true even if the latter must only carry out a known procedure such as concentration measurements of an analyte under predefined conditions, since manipulation of the controls of the fluorimeter results in effects not always fully appreciated.

In this artificial intelligence (AI)-based program, the visual and interactive presentation of the different operational modules associated with the functional sub-systems of a fluorimeter or spectrofluorimeter allows the user to inform the program about his problem. The program then uses this information to initiate the search for a guided and documented solution. The latter is usually reached after a number of such information exchanges and suggested moves.

Let us describe a typical experiment which in its progress would induce the user to call upon this program. An average or beginning user works on a dilute aqueous solution of a compound for which the only available data is the wavelength of maximum absorption, let say 340 nm.

Exciting the sample at this wavelength, he obtains a broad spectrum centred at 410 nm which

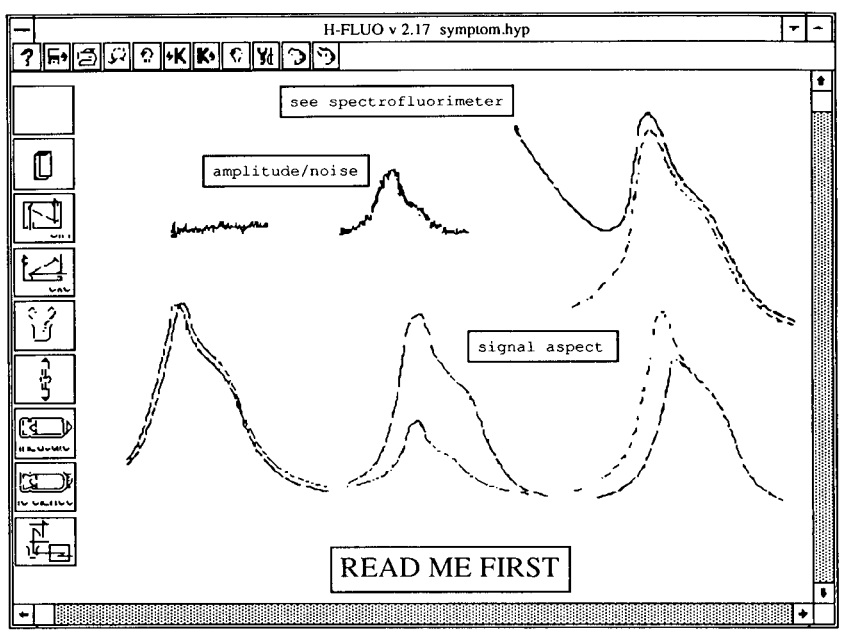

Fig. 1. By mouse interaction, the user may define the characteristics of his problem.

displays a shoulder or "local defect" at about 383 nm. He tries then a slightly more dilute sample for which he notices that this effect is still more pronounced. He thinks of an impurity, but is not sure and decides to put the program to use.

Presentation screens are displayed (for an example, see Fig. 1) which may give several types of information. It may be put into words which describe for instance all the possible classes of problems a user may come across. It may also be visual: graphs or spectra exhibiting the characteristic features associated with the problems. These graphs are intended to help the user point to his problem by clicking the mouse. Once this is done, the program loads another screen according to the choices made.

3. Software implementation

H-FLUO is destined to a wide population of experimenters in the field of fluorescence. It is the result of extensive research and combines a great reasoning power with a highly ergonomic user interface.

3.1. Expert system

Expert systems' application fields are nowadays well-known. They are within the domain of artificial intelligence, and have been applied in analytical chemistry [4–7]. The chosen domain is well-adapted to data processing by an expert system from a theoretical point of view. Indeed manipulations on a spectrofluorimeter as well as the underlying physics may be managed in a deductive way; knowledge may be hierarchical, and organized in a logical way into different modules. These modules may be relatively independent from each other.

Conversely, it is difficult to issue any diagnostic by debugging an experiment by means of a straight expert system: a quite strong and continuous interaction should be allowed between the end-user and the system. The end-user elaborates progressively the diagnostic.

In most cases it is impossible to give all the data from the very beginning of the session. And even if this were possible, this solution would appear fastidious in normal use. Finally, one should keep in mind that the non-expert user may be obliged to switch between the computer and the fluorimeter several times, to check such and such point as stated by the expert system.

3.2. Hypermedia – access to information

The development of hyper-text and -media tools introduces a deep mutation in the way one has access to information. Access is not sequential any more, the user now "navigates" through the information system which includes texts, figures, graphs and pictures, and he browses according to his thought or reasoning. In a hypertext, information is stored into information units named nodes. Nodes are linked together by links. When nodes contain texts, graphs or pictures, data in general, one speaks of hypermedia.

It is important to notice that the user's point of view is considerably broadened by means of a hypermedia tool, for he may access data in whatever order he wants. He may even reverse his browsing process and come back to any point he focused on before.

3.3. Hypermedia – a complementary tool to existing software

These tools do not substitute to other existing tools, but should be considered as excellent complements to installed data processing systems (databases, expert systems, etc.). They are particularly used as front-end software. Though hypermedia are good information presenters, they are a priori not well-adapted to manage information dynamically. Their potential application field seems extremely wide: dedicated tools as well as training tools can be created.

3.4. The solution adopted

The solution is based on a mixed architecture expert system/hypermedia [8]. It involves powerful links between both tools. Data are stored in the hypermedia and in the expert system, but only the former is accessible to the end-user.

Knowledge is dynamically managed by the expert system, and both tools are driving each other by sending orders during the work session.

Two modes are available: the conception mode, in which the software is created and updated, and the end-user mode.

Transferring information from the hypertext to the expert system

The developed hypermedia includes classical hypertext features, allowing one to browse along the links of a semantic network. Redirections towards any other node of any network in the application are possible. Furthermore, nodes contain a collection of slots – or attributes – which are defined by the designer (in conception mode only). Nodes may contain texts, graphs, pictures, numeric values or facts (for the expert system use). Browsing by anchor mechanism is available, by mouse action on sensitive areas on text and picture slots of any node, and also on the background screen.

During a user session, two fundamental processes may occur: knowledge transfer from and to the user. The latter takes place when the end-user is not an expert in fluorimetry, and/or when he wants information about the way in which experiments are conducted. Knowledge transfer towards the computer is the means by which experimental symptoms are described by the user.

These processes are not concurrent, and the first one is downplayed as the user gains experience [9] in experimental fluorimetry.

The description of an experiment is simply done by selection of facts on precise nodes of the current semantic network. The end-user activates a node, opens it, and selects the item which best fits his concern. In the next figure (Fig. 2) we present the different kinds of cells which may be used.

A value is preselected for each node at the beginning of the user session. In most cases it is "not specified".

Whenever the user enters information, he does so in a context. Expert or beginner, he may use any piece of information presented by the hypermedia interface. By doing so he perceives the problem in its whole.

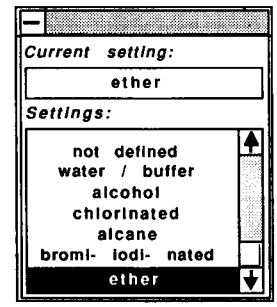

Fig. 2. Data selection from a node: the solvent used.

As soon as a datum is entered, it is transmitted to the knowledge processor – the expert system – which computes it with the other data previously entered. The facts database is updated, and a coherence control is processed.

Transferring information from the expert system to the hypermedia

When the expert system receives a new datum from the user interface, a deductive inference process starts. It generally leads to a partial/final conclusion. Most of the time this process is not completed: some piece of information still lacks and it is not possible to go on further. This induces a question to the end-user, via the hypermedia tool which constitutes the user interface. This demand may be sent along with information messages. This is an automated process, which manages the output of another semantic network on the hypermedia screen, if needed.

Let us take an example:

Let us suppose that the user is working at a wavelength of 230 nm, and that he uses a glass cell. This material is opaque, thus the diagnostic "flat spectrum" is immediate. During the session, he has entered:

```
null signal
working wavelength=230 nm
```

The expert system computes the inference process, followed by three actions:

- it asks the question ``what is the cell made of? ''
- it loads the semantic network concerned: `cell`
- it opens the ``cell material '' node of the network, and thus prepares the fol-

lowing input, namely the material of the cell. The screen is then as presented in Fig. 3.

Thus the system progressively computes an on-line diagnostic. It is quite difficult to render the quality of interaction, which is far more sophisticated than a straight expert system dialogue. Intermediate solutions consist in links with external applications during interaction [10].

The conception mode. In the previous sections we have described the behaviour of the H-FLUO system during a user session. It is the run-time mode of the program. The conception mode allows the specialist to build the application itself. It is presented in this section. Information is located in two environments: inside the expert system, where it takes place as classical production rules, and at the hypermedia level, where data may be textual information, graphs, pictures, numerical values, etc.

Hypermedia. Knowledge is presented to the end-user as a set of semantic networks, each one corresponding to a screen. A network is a priori specific for a definite sub-domain.

Thus the end-user will start a session with a welcome network-screen, which allows him to put in the main parameters of his manipulation. He then will be guided toward other screens, dedicated for instance to a spectrofluorimeter part: the excitation monochromator, the light source, the power supply, etc.

Each network contains a set of nodes which each stands for a definite semantic entity for the specialist. A node generally contains a textual information, allowing the user to check his knowledge and to situate himself at any time.

The hypermedia level may very well be thought of as a lecture on manipulation in fluorimetry, and also on the underlying physics to a certain extent... In such a user context, it is possible to do experimental simulations, thus saving fluorimeter time, and costly errors.

Expert system. The expert system level is designed to manage the instantaneous knowledge of the end-user according to the diagnostic progress of the experiment. The system computes the possible deductions from the available data, that is to say from data generally put in by the user. (This is not always the case, for data may remain known by the system from one session to the next one, such as the physical characteristics of the fluorimeter.) A database is thus progressively constituted by the user.

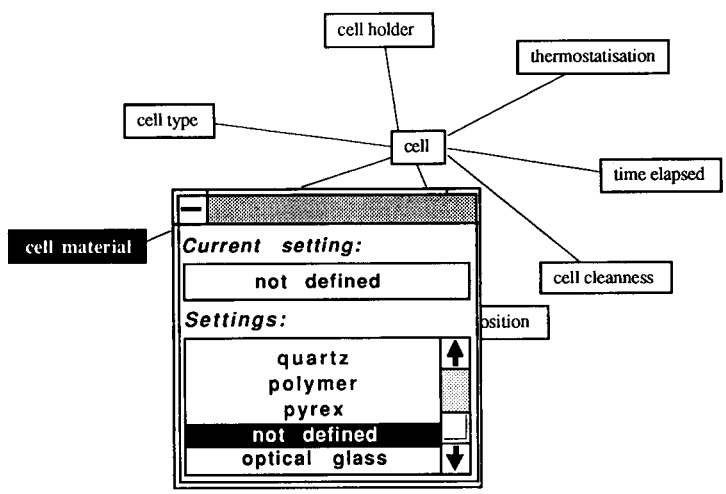

Fig. 3. Any input is made while viewing the context.

In the previous example the expert system activates the following production rule:

```
IF  Fact(Signal_profile, flat) AND
    Value(excitation_wavelength,
    @Exc_w),
    @Exc_w<310 AND
    UNKNOWN Fact(cell_material,*)
THEN
    OPEN( ``CELL.HYP '', ``cell mate-
    rial '') AND
     MESSAGE  ``What is the cell
    made of? '';
```

Both conclusions of this rule are piloting actions of the hypermedia tool, which we have described before.

Knowledge is organized into specialized modules. These correspond to the underlying physics of a fluorimeter; they are quite closely matching the different "stages" of the instrument. Thus we find a setting module: wavelength, width and height of slits, gain. Another module manages emission and excitation filters. Several modules are specialized in an experimental problem: flat spectrum, low amplitude signal, etc.

3.5. State of the art

Designing the current version of H-FLUO has involved specialists in spectrofluorimetry and specialists in knowledge transfer. These tasks have to be performed by separate persons, in order to avoid artifacts in implementation: "trivialities" may suffer lack of explanation for the non-specialist, "habits" may very well pollute the exposé.

The system has been achieved over a period of about one year. It has been tested in several sites of different sizes, contexts, and aims. It uses Windows® and runs on any 386 or 486 personal computer with 4 M RAM.

The current version counts 14 semantic networks, thus 14 screens to be presented to the end-user by the hypermedia interface. The expert system counts slightly more than 300 production rules. The disk space for the whole system is about 5 Mbytes. The main part of this space is dedicated to pictures to illustrate the different parts of the instrument and technical discussions (spectra, schemes, etc.)

End-user limitations

The run-time mode does not allow the end-user to redesign the semantic networks. Thus it is not possible to create new nodes, or to extend existing nodes.

However, the end-user may fill any node to describe his own context, and/or run simulations on any virtual spectrofluorimeter use: he does not alter the information structure.

Conceptor mode

The expert system generator includes some features which ensure global coherence and check of the knowledge database when the designer is working. For instance statistics may be issued whenever the conceptor needs them to check the use of such particular rule, or module of knowledge.

The current version has achieved a "critical mass" which ensures strong stability and coherence, and further extensions should be thought of as secondary modules, with limited scopes.

4. What does the system manage?

4.1. Level / skills of the end-user

Our system is not only aimed at the beginner; it can also help a trained user. The beginner is completely guided by the system: he is invited to describe his problem, and he is asked questions step by step.

The trained user may – from the very beginning – give pieces of information which seems necessary to him to complete the diagnostic. To do so, he may use short-cuts, with which he instantiates the corresponding facts to certain nodes, without waiting for the normal deduction process questions. For instance, if the main symptom is a flat spectrum, and if the user thinks his sample is photostable, then this fact may be put in from the start. Thus the expert system will not explore the direction "sample stability" the same way.

4.2. The field of knowledge taken into account

The scope of the program was voluntarily limited to the experimental science of manipulation

in the case of fluorescent or phosphorescent compounds in solution. Nevertheless the studies by time-dependent techniques such as lifetime determination are not considered. It is planned to encompass later all these aspects of molecular luminescence, including the analysis of luminophores on a solid support

4.3. Commercial and home-made instruments

In the previous section we indicated that the knowledge scope was voluntarily focused to "the experimental science of manipulation". It is a practical knowledge by essence, strongly linked to the constituents of the fluorimeter being used.

The software is not limited to a single type of instrument. Conversely we wanted any commercial fluorimeter or spectrofluorimeter to be manageable by the system. Our approach was the following: we did work first on research fluorimeters, built in our laboratory. These spectrofluorimeters have the advantage of being totally flexible to any desired configuration. Thus they represent virtually any variety of commercialized fluorimeters.

The embarked knowledge allows one to manage diagnostic on such a sophisticated apparatus. Thus any sub-set of knowledge necessary for a commercial fluorimeter from brand X, Y or Z is available.

4.4. Customization of the user site

Most of the time a definite user uses the same spectrofluorimeter. We wanted our system – in a maximal end-user comfort concern – to keep permanently the data concerning the fluorimeter characteristics. Thus if it does not include a cell thermostat, then this fact is definitively acquired.

All these spectrofluorimeter's data are contained in a special database which is added at the beginning of session. Thus several questions are avoided. This way of reasoning is only optional, thus a multiple fluorimeter site user would not be in trouble.

4.5. Time evolution of some elements

If the instrument customization has been chosen by the user, then certain physical characteristics linked to aging may be managed.

Indeed, a spectrofluorimeter possesses elements whose lifetime is limited, such as the light source – the lamp. In current use, the lifetime may be estimated according to the level of use of the fluorimeter. The lamp's age is entered during the first use of the system, as well as other characteristics. Then this datum will change with time. (Actually the system asks for the acquisition date of the lamp. This datum does not need to change itself, but induces different probabilities for consequences according to the current computer's date and time.)

According to the evolution of these special data, some events' probabilities will change. The expert system will manage this evolution.

5. Unfolding a typical scenario

Let us come back to the problem exposed in Section 2, and suppose that in the search process the user gave the following information to the system: the wavelength of excitation (340 nm) and the position of the "local defect" (or "unexpected band" as it is known in the program) at 383 nm. In answer to these data, the program displays a new semantic network were the node "solvent" is activated and a list of solvents is displayed (Fig. 2). As soon as the user selects "water", the program determines that the position of the unexpected band, which is as we said the local defect observed by the user, corresponds to that of the Raman scattering of the solvent in use.

Indeed, Raman scattering (RS) results from the interaction of the exciting radiation with the sample. The intensity of RS is very weak, therefore in a dilute solution of a fluorescent compound, it can only be detected for the solvent, in a fluorimeter. To describe RS in the simplest way amounts to say that in its interaction with the solvent molecules, the energy in the exciting radiation is reduced by a vibrational energy quantum of the solvent.

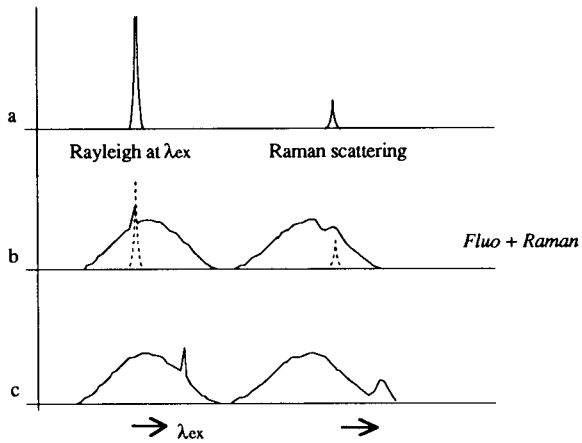

Fig. 4. Correspondence between Raman and Rayleigh shifts.

This has two consequences:

– this quantum of energy depends only on the solvent.

– the energetic separation between Rayleigh scattering and Raman scattering is constant for a given solvent.

So Raman scattering is red-shifted with respect to Rayleigh scattering. This explains why RS may overlap an emission spectrum (Fig. 4a,b)

Because the energy separation between Rayleigh and Raman scattering is constant in a given solvent, shifting excitation results in shifting Raman (Fig. 4c).

The constant difference in energy between excitation (and Rayleigh) and Raman scattering may be expressed as:

$$\bar{\nu}(\mathrm{cm}^{-1}) = \frac{10^7}{\lambda_R} - \frac{10^7}{\lambda_{ex}} = 10^7(1/\lambda_R - 1/\lambda_{ex})$$

So this shift is linked to the inverse in energy. But in a narrow range of ± 10 to ± 20 nm, in the traditional nm scale displayed by instruments, if λ_{ex} is shifted by a given amount, then RS is shifted by nearly the same amount. This feature allows for easy identification of RS.

So the system turns off the previous screen and displays a new network (Fig. 5) with the node "Raman" activated and the following comment in a message window:

``The feature at 383 nm is probably due to the Raman spectrum of water. To confirm, move the excitation to 330 nm. The un-expected band should appear at 370 nm ''.

At the same time, another window displays a textual explanation about the Raman of a solvent in fluorescence measurements. This window can

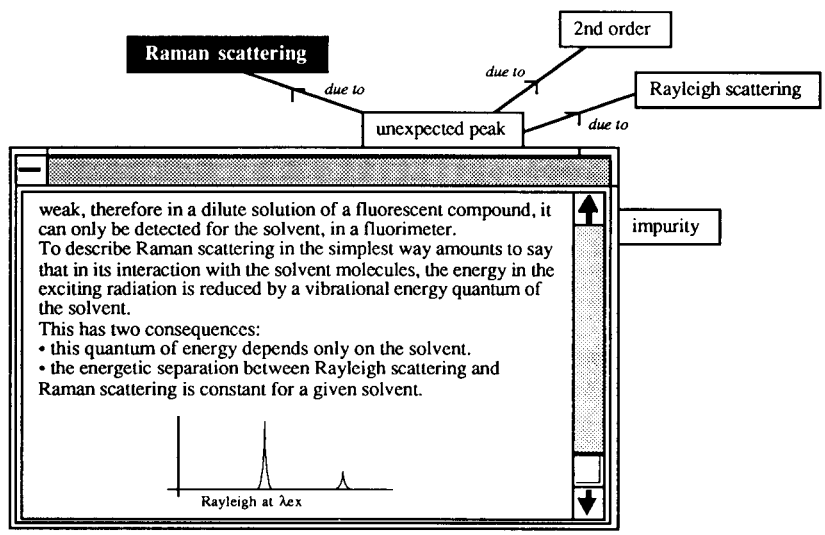

Fig. 5. Sometimes the expert system opens a particular node according to the precise deduction context.

be scrolled like any similar comment windows corresponding to the nodes of any network in the program.

If the user is not familiar with this type of interference, he will find there all the information he requires. He will then carry out the test on the fluorimeter. If the "unexpected band" shifts indeed to 370 nm, the explanation is found and a cure may be looked for. If not, the user may continue requesting help from the program.

6. Conclusion

It is clear that the first object of the program is to help a scientist or technician succeed in completing the experiment he got started. But it must also be recognized that the flexible browsing offered among a vast corpus of information related to the instruments and accessories as well as to the fundamentals of molecular luminescence is a strong incentive to learn more about this field. The variety of shapes taken by knowledge which appears in messages, pictures, explanatory texts, graphs, etc. prevents learning to become boring. The user may stop at any time and resume later, review forgotten items. So this software is also a remarkable tool for learning and teaching about experimental molecular fluorescence and phosphorescence. In our laboratory we spend a tremendous amount of time teaching graduate students these techniques and we realize now how much time we will save with this tool without any risk for the equipment. So the benefits are that time is saved, less experiments flunked, and more time is available for the advisors.

Acknowledgement

This work was presented in part at the International Symposium on Biomedical Optics '93, Los Angeles, 16–22 January 1993. Support from the French National Agency for Research Valorization (ANVAR) is acknowledged by the authors.

References

[1] S. Udenfriend, Fluorescence Assay in Biology and Medecine, Vol. II, Academic Press, New York, 1969, p. 592.
[2] C.A. Parker, Photoluminescence of Solutions, Elsevier, New York, 1968.
[3] Fluorescence Papers in the Proceedings of the Conference on Accuracy in Spectrophotometry and Luminescence Measurements, NBS Special Publication 378, 1973.
[4] J.A. Van Leeuwen, B.G.M. Vandeginste, G. Kateman, M. Mulholland and A. Cleland, Anal. Chim. Acta, 228 (1990) 145.
[5] J. Smeyers-Verbeke, M.R. Detaevernier and D.L. Massart, Anal. Chim. Acta, 191 (1986) 181.
[6] W.R. Browett, T.A. Cox and M.J. Stillman, in B.A. Hohne and T.H. Pierce (Eds.), Expert Systems Applications in Chemistry (ACS Symposium Series, Vol. 408), American Chemical Society, Washington, DC, 1989, p. 210.
[7] M. Moors and D.L. Massart, Trends Anal. Chem., 9 (1990) 164.
[8] M. Nanard, J. Nanard and P.B. Pingand, in Proceedings of the International Conference on Systems Integration, Morristown, NJ, April 1990.
[9] P.B. Pingand and J. Sallantin, in Proceedings of the Hawaii International Conference on System Sciences, Koloa, HI, January 1991.
[10] M. Esteban, I. Ruisanchez, M.S. Larrechi and F.X. Rius, Anal. Chim. Acta, 268 (1992) 95.

ELSEVIER

Analytica Chimica Acta 293 (1994) 311–318

ANALYTICA CHIMICA ACTA

Spectrophotometric determination of iron(II) in sea water after preconcentration by sorption of its 3-(2-pyridyl)-5,6-bis(4-phenylsulphonic acid)-1,2,4-triazine complex with poly(chlorotrifluoroethylene) resin

Li-Ping Zhang, Kikuo Terada *

Department of Chemistry, Faculty of Science, Kanazawa University, Kanazawa 920-11, Japan

(Received 25th September 1993; revised manuscript received 25th February 1994)

Abstract

A simple and selective method was established for the spectrophotometric determination of iron(II) in sea water after preconcentration by sorption of its 3-(2-pyridyl)-5,6-bis(4-phenylsulphonic acid)-1,2,4-triazine (ferrozine) complex with poly(chlorotrifluoroethylene) resin (PCTFE). The iron(II)–ferrozine complex was quantitatively retained as an ion-associate complex with tetrabutylammonium cation on PCTFE resin in the pH range 4.8–7.0. The retention capacity of the resin was 29 μg Fe(II) g^{-1} at a maximum flow-rate of 25 cm^3 min^{-1}. Iron(II) retained on the resin column was completely eluted with 5 cm^3 of methanol and the eluate was directly submitted to spectrophotometric measurement at 562 nm. The recovery and detection limit of iron(II) from sea water were 97 $\pm$2% and 88 ng dm^{-3} (1.6 nmol dm^{-3}), respectively.

Key words: UV–Visible spectrophotometry; Complexation; Ferrozine; Iron; Preconcentration; Sea water; Waters

1. Introduction

The determination of iron species in sea water is important because of its biological and geochemical behaviour related to phytoplankton nutrition and the possible limiting role in primary production in some ocean areas [1–3]. Dissolved iron concentrations have been evaluated to range from < 1 nmol kg^{-1} in surface offshore waters to μmol kg^{-1} levels in bay waters [1–6]. Although various methods have been proposed for the determination of iron in sea water, no sensitive method is available for direct measurements of iron in open ocean water. In general, preconcentration is required prior to its determination. Liquid–liquid extraction, e.g., with APDC or DDDC–chloroform, has been employed with graphite furnace atomic absorption spectrometry (AAS) [1,4,5], and chelating ion-exchange methods using quinolin-8-ol immobilized on Fractogel [6] and quinolin-8-ol-5-sulphonic acid immobilized on controlled-pore glass [7] have been combined with flow-injection analysis (FIA).

* Corresponding author.

SSDI 0003-2670(94)00110-8

The occurrence of iron(II) has been demonstrated in plumes of hydrothermal solution that spread over the midocean ridges (Juan de Fuca Ridge) [7]. In addition, iron(II) has been detected in anoxic basins [8], in near-bottom waters [5,9] and in surface waters, presumably owing to photochemical reduction of iron(III) [9,10].

Therefore, the redox speciation determination of iron in sea water seems very important with regard to the solubility, photochemistry, bioavailability and colloid chemistry of the element, so the availability of a selective method of preconcentration and determination of iron(II) in the presence of iron(III) has become increasingly important. The methods described above, however, are not selective for preconcentrating iron(II), so it is difficult to apply them in a simple spectrophotometric determination of the element. This paper reports a simple, selective and inexpensive spectrophotometric method for the determination of iron(II).

The chromogenic reagent ferrozine (FZ) [3-(2-pyridyl)-5,6-bis(4-phenylsulphonic acid)-1,2,4-triazine] (Fig. 1) has been used extensively for the determination of iron(II) in natural waters [11,12]. Iron(II) forms a purple complex with FZ, $Fe^{II}(FZ)_3$, with a molar absorptivity of ca. 28 600 at 562 nm in dilute aqueous solution [13], but iron(III) does not react with the reagent [7,12,13]. However, the detection limit obtained in direct spectrophotometric measurements is not low enough for the determination of oceanic iron(II).

Poly(chlorotrifluoroethylene) (PCTFE) resin has been widely used as a reversed-phase chromatographic column packing [14]. It has been reported that PCTFE can effectively adsorb some metal complexes and that the metal retained on the polymer can be easily eluted with dilute hydrochloric acid or methanol [15–17]. Recently, this method has been satisfactorily applied to the determination of quinolin-8-ol–Cu (fungicide) in environmental water [18]. The advantages of the resin are as follows: it has excellent chemical and mechanical resistance, so it can be used repeatedly as a metal complex sorbent; the ability to treat large volumes of samples in a closed system free from contamination; owing to its mechanical strength and chemical inertness, PCTFE resin does not swell in any solvent, and therefore a high flow-rate of sample solution is attainable; and by the use of an appropriate complexing agent, selective separation of metals from matrix components becomes possible. These advantages suggest its utility as a preconcentration column packing in FIA.

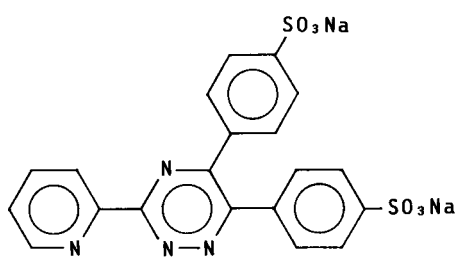

Fig. 1. Structure of ferrozine.

This paper describes a basic investigation of a simple and selective method for the preconcentration of iron(II) in sea water samples by loading $Fe(II)(FZ)_3$–tetrabutylammonium ion-associate complex on PCTFE resin, elution with a small volume (5 cm^3) of methanol and determination by spectrophotometry.

2. Experimental

2.1. Equipment

A Shimadzu UV-160 UV–visible spectrophotometer internally equipped with a data processor including a recorder and a display, using a 1.0-cm glass cell, a Hitachi Z-6100 polarized Zeeman atomic absorption spectrometer, a Tokyo Rikakikai Model MP-3 peristaltic pump and a Toyo Model SP-160K balance-operated fraction collector were used. A Shibata Type P-850 surface area measurement apparatus was used for measurement of the specific surface area of PCTFE resin by the BET method.

All glassware and tubing (Teflon and Tygon) were cleaned by dipping them in 3 mol dm^{-3} nitric acid containing hydrogen peroxide for 3

days and washing with distilled, deionized water just before use.

2.2. Reagents

All chemicals and solvents were of analytical-reagent or PMA (poisonous metal analysis) grade.

Distilled, deionized water (DDW) was prepared with a Barnstead NANO-pure system, and used in all experiments. Methanol was brand high-purity solvent from Nacalai Tesque.

A 100 mg dm^{-3} iron(II) stock standard solution was prepared by dissolving 0.707 g of ammonium iron(II) sulphate hexahydrate in 1000 cm^3 of 0.5 mol dm^{-3} sulphuric acid. The solution was diluted to the required concentration with 0.2 mol dm^{-3} sulphuric acid just before use.

A 0.13 mmol dm^{-3} ferrozine (Tokyo Kasei) solution was prepared by dissolving 0.075 g of the reagent in 50 cm^3 of DDW containing 2 cm^3 of 5.0 mol dm^{-3} hydrochloric acid and diluting to 100 cm^3 [13].

A 0.1% tetrabutylammonium chloride (TBAC) (Tokyo Kasei) solution was prepared by dissolving the reagent in DDW.

Acetate buffer solution was prepared by dissolving 473 g of sodium acetate trihydrate (Wako) in 500 cm^3 of DDW with warming, adding with 115 cm^3 of anhydrous acetic acid (Wako) and diluting to 1000 cm^3. To the solution were added 10 cm^3 of the ferrozine solution and 5 cm^3 of the TBAC solution, then the mixture was passed through a PCTFE column to remove iron(II) contained in the reagents.

2.3. Preparation of PCTFE resin

A commercially available poly(chlorotrifluoroethylene) moulding powder (Neoflon; Daikin Industrial) was sieved to sizes of 80–100 mesh and finer than 100 mesh. These powders were purified by washing with hydrochloric acid–methanol (1 + 1, v/v), to remove metals and other impurities, then rinsed with DDW until free from chloride, and finally dried under reduced pressure. The resin purified in this way was stored in methanol prior to use.

2.4. Column preparation

The column used in the study was a glass tube (20 mm i.d.) equipped with a coarse sintered-glass disc and stopcock. PCTFE powder was slurried with methanol in a 10-cm^3 measuring cylinder by mixing with an ultrasonic vibrator for 5 min (under these conditions, 1.00 g of 100-mesh resin became 2.2 cm^3) and poured into the column, then washed with DDW. Finally, the water was sucked to the top of the column bed in order to avoid channel formation.

2.5. General procedure

An aliquot of iron(II) solution (250 or 500 cm^3) was placed in a Pyrex glass bottle and 2 cm^3 of 0.13 mmol dm^{-3} ferrozine solution, 1 cm^3 of acetate buffer solution and 1 cm^3 of TBAC solution as an ion-association reagent were added sequentially. The bottle was connected to the PCTFE column with Teflon and Tygon tubing (3 mm i.d.). The resulting solution (pH $\approx$ 5) was passed through the PCTFE column at flow-rates of 3–25 cm^3 min^{-1} with the aid of a peristaltic pump. The iron(II) retained on the column as the ferrozine–TBAC ion-associate complex was eluted with 5 cm^3 of methanol. The absorbance of the eluate was determined with the spectrophotometer at 562 nm using methanol as a reference. For sea water, the pH was adjusted to ca. 5 with hydrochloric acid and acetate buffer solution. The resin can be used repeatedly after washing with DDW.

3. Results and discussion

3.1. Effect of pH on the retention of iron(II)–ferrozine complex

The retention of the $Fe^{II}(FZ)_3$ complex on a column packed with 1.0 g of PCTFE was studied as a function of pH. A 100-cm^3 volume of $Fe^{II}(FZ)_3$ complex solution (Fe concentration 10 μg dm^{-3}) adjusted to various pH values with hydrochloric acid, acetate buffer or aqueous ammonia and with 1 cm^3 of TBAC solution added,

was passed through the column (1.0 g of resin). The retained $Fe^{II}(FZ)_3$ was eluted with 5 cm^3 of methanol and the absorbance of the eluate was measured with a spectrophotometer.

Fig. 2 shows the effect of pH on the retention of $Fe^{II}(FZ)_3$. The shape of the curve resembles that for the formation of $Fe^{II}(FZ)_3$ reported by Stookey [11]. The complex was quantitatively retained from aqueous solutions in the pH range 4.8–7.0. The optimum pH of the solution was selected as 5, because the lower the pH, the lower is the interference from other metals, such as copper, cobalt and nickel, which may interfere with the absorbance measurement of iron(II) at higher pH [13,19].

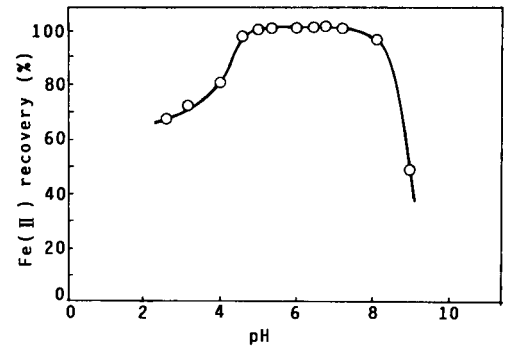

Fig. 2. Effect of pH on retention of $Fe^{II}(FZ)_3$ complex.

3.2. Blank and limit of detection

A typical reagent blank was determined by passing each DDW added reagent solution other than iron(II) through the PCTFE column as described in Section 2.5. The absorbance of the methanol eluate was measured at 562 nm. The reagent blank was found to have an absorbance of 0.003 ± 0.0008 ($n = 5$).

The limit of detection (three times the standard deviation of the blank) was 88 ng dm^{-3} (1.6 nmol dm^{-3}) for 500 cm^3 of sea water sample (concentration factor 100). The sensitivity is higher than that obtained with flame atomic absorption spectrometry.

3.3. Effect of ion association reagent

As $Fe^{II}(FZ)_3$ exists as a complex anion, it might not interact completely with non-polar PCTFE resin [16]. In fact, the complex ion was incompletely retained on PCTFE when its concentration was below 1 μg dm^{-3}. However, with the addition of TBA^+ cation, which is a bulky organic molecule, to the complex solution, the complex could be quantitatively retained on PCTFE resin. This indicates the formation of an ion pair between $[Fe^{II}(FZ)_3]^{4-}$ and TBA^+ cation leading to increased retention.

Therefore, the effect of TBAC concentration on the retention of the complex was investigated using 500 cm^3 of 1 μg dm^{-3} iron(II) solution at pH 5, which was adjusted with acetate buffer. Fig. 3 shows that the retention of $Fe^{II}(FZ)_3$ was about 70–75% at TBAC concentrations in the range 10^{-5}–10^{-3} mmol dm^{-3}, and then increased with increasing TBAC concentration up to 36 μmol dm^{-3}, at which the recovery became quantitative.

From these results, the mechanism of the sorption may be explained as follows. At very low concentrations of TBA^+, the bulky complex anion may be retained on the PCTFE column as an ion pair with sodium ion which is contained in the acetate buffer used, and with increase in TBA^+ concentration the following reaction become preferential to control the retention:

$$[Fe(FZ)_3]^{4-} + nTBA^+ \rightleftharpoons [Fe(FZ)_3(TBA)_n]^{(4-n)-}$$

$$[Fe(FZ)_3(TBA)_n]^{(4-n)-}{}_{(S)} \rightleftharpoons [Fe(FZ)_3(TBA)_n]^{(4-n)-}{}_{(R)}$$

where (S) and (R) indicate the solution and resin phases, respectively. In this case, it is assumed that as the ion-associate complex produced may become more hydrophobic than the $Fe^{II}(FZ)_3$ complex, the adsorbability on the hydrophobic polymer is significantly increased.

In a previous paper [16], it was reported that the copper (II)–quinolin-8-ol-5-sulphonic acid complex anion, $[Cu(SO_x)_2]^{2-}$ was retained on PCTFE resin as an ion-associate complex with TBA^+ cation in a ratio of 1:1. Further, it has been found that the Co–nitroso R complex anion

(charge -3) was associated with TBA^+ in a ratio of 1:2 and effectively adsorbed on PCTFE in sodium acetate–acetic acid buffer solution where the sodium ion seemed to be another counter ion which associates to the above-mentioned bulky anion [17]. In the present instance, the formation of ion pairs between the $Fe^{II}(FZ)_3$ complex anion and the TBA^+ cation also gave less polar ion-associate complexes, leading to increased retention.

3.4. Effect of ferrozine concentration

Although the use of an excess amount of FZ will ensure complete complexation with iron(II), a large excess of the reagent may cause a reagent blank. Therefore, it is preferred to minimize the amount of FZ to be used. Fig. 4 shows that the amount of FZ needed for the determination of 10 μg dm^{-3} Fe^{II} is about 12 μmol dm^{-3}, which is equivalent to 67 times the iron(II) concentration. It was also found that this amount of the reagent gave little blank absorbance.

3.5. Sorption capacity

The sorption capacity of PCTFE for the $Fe^{II}(FZ)_3$ complex was determined by a breakthrough method using 0.1 mg dm^{-3} iron(II) solution and a column packed with 1.0 g of PCTFE at a flow-rate of 5 cm^3 min^{-1}. Each 5 cm^3 of the effluent was collected with the use of a fraction collector, and the iron concentration in each fraction was determined by spectrophotometry. The

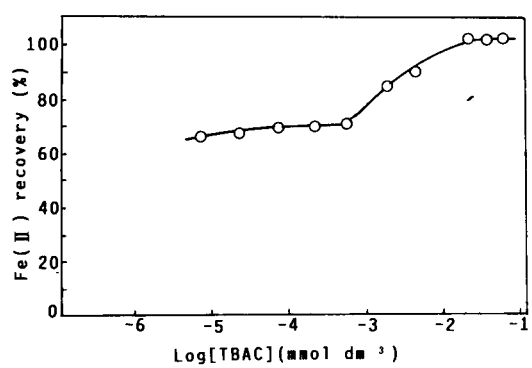

Fig. 3. Effect of TBAC concentration on retention of $Fe^{II}(FZ)_3$ complex.

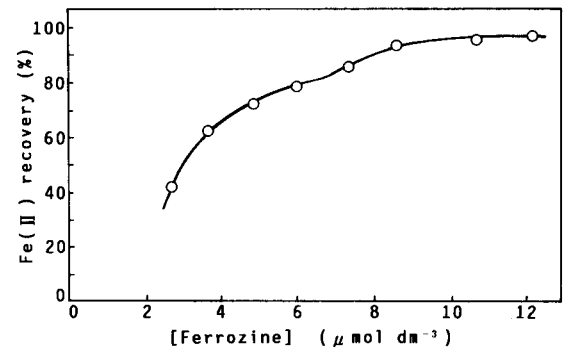

Fig. 4. Effect of ferrozine concentration on retention of $Fe^{II}(FZ)_3$ complex.

sorption capacity was calculated from the breakthrough curve and was found to be 29 μg g^{-1} (0.52 μmol g^{-1}) resin. This value was half those for Cd–SO_x, Cu–SO_x and Zn–SO_x complexes (0.8, 1.0 and 1.0 μmol g^{-1}, respectively [16]). This relatively low capacity may be attributed to the larger molecule of the complex than the latter three complex molecules and the small surface area of PCTFE resin (3.27 m^2 g^{-1}), but is considered to be sufficient for the preconcentration of traces of iron(II) in sea water.

The small surface area of the resin is also favourable for minimizing the volume of eluent to be used, so that a higher concentration factor might be attainable. Thus, 5 cm^3 of methanol could quantitatively elute $Fe^{II}(FZ)_3$ complex from the column.

3.6. Effect of flow rate

The retention of the $Fe^{II}(FZ)_3$ complex was examined by passing 500 cm^3 of the complex solution (10 μg dm^{-3} Fe) through a column packed with 1.0 g of PCTFE at various flow-rates. Quantitative and reproducible retention of the complex was attained at flow-rates between 4 and 25 cm^3 min^{-1}.

3.7. Effect of foreign ions

As described later, the recovery of iron(II) from a sea water sample to which the iron(II) standard was added was found to be quantitative

Table 1
Effect of foreign ions on the determination of Fe(II)

Ion	Concentration	Absorbance at 562 nm	Error (%)
None	–	0.106	–
Co(II)	0.10 mg dm^{-3}	0.109	+2.8
Ni(II)	0.10 mg dm^{-3}	0.107	+0.9
Cu(II)	0.50 mg dm^{-3}	0.106	0.0
NO_3^-	0.10 mmol dm^{-3}	0.106	0.0
NO_2^-	0.10 mmol dm^{-3}	0.105	−0.9
PO_4^{3-}	0.10 mmol dm^{-3}	0.106	0.0
CN^-	0.10 mmol dm^{-3}	0.105	−0.9
Tartrate	0.10 mmol dm^{-3}	0.106	0.0
Citrate	0.10 mmol dm^{-3}	0.106	0.0

Sample volume used, 250 cm^3; Fe(II) concentration, 10 μg dm^{-3}.

using the present method (see Table 3). Therefore, major elements in sea water, such as sodium, potassium, magnesium, calcium, chloride, sulphate and fluoride ions, have no influence on the determination of iron(II).

Interference with the spectrophotometric determination of iron(II) as its ferrozine complex has been reported for copper, cobalt and nickel [12,20]. The effect of the above metal ions was investigated using iron(II) standard solution to which each ion was added. The results are given in Table 1.

As can be seen, at pH 5 only cobalt gave a slightly higher value at 0.1 mg dm^{-3}, but nickel and copper had no influence at concentrations of 0.1 and 0.5 mg dm^{-3}, respectively. In natural sea water, the concentrations of copper, cobalt and nickel are not high enough to cause a detectable interference.

In Table 1, the effects of some anionic species are also shown. Nitrate, nitrite, phosphate, cyanide, tartrate and citrate ions did not interfere up to a concentration of 0.1 mmol dm^{-3}, which is rarely found in sea water.

Concerning the redox speciation determination of iron(II), the method should be highly selective for iron(II) over iron(III). The selectivity of the method for iron(II) was confirmed by determining iron(III) and iron(II) + iron(III) solutions throughout the entire procedure. As shown in Table 2, iron(III) did not give an absorbance greater than the blank value. These results indicate that the present method is highly selective for iron(II) in sea water.

Table 2
Effect of Fe(III) on determination of Fe(II)

Fe(II) added (μg dm^{-3})	Fe(III) added (μg dm^{-3})	Mean absorbance at 562 nm ($n = 4$)
10.0	–	0.106
10.0	10.0	0.106
10.0	100.0	0.106
–	100.0	0.003

Sample volume used, 100 cm^3 of aqueous solution.

3.8. Calibration

In Fig. 5, the calibration graphs are illustrated for an aqueous solution and sea water spiked with iron(II) at various concentrations. Both graphs are well fitted. Beer's law is obeyed up to ca. 1 mg dm^{-3} Fe(II).

3.9. Recovery of iron(II) spikes from sea water

The recovery of iron(II) spikes from the sample was determined with Fe(II)-free sea water. A coastal sea water was adjusted to pH 5 by adding hydrochloric acid and acetate buffer, and FZ and TBAC solutions were added as described in Section 2.5, then the solution was passed through the PCTFE column. The Fe(II)-free sea water obtained was spiked with iron(II) at 10 μg dm^{-3}.

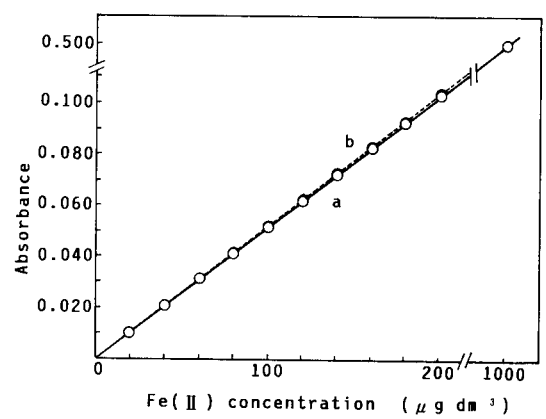

Fig. 5. Calibration graphs for iron(II) determination: (a) Fe(II) standard solution; (b) sea water.

Table 3
Recovery of traces of iron(II) from sea water

Fe(II) added [a] (μg dm^{-3})	Fe(II) found (μg dm^{-3})		Recovery (%)	
	Spectro-photometry	Flame AAS	Spectro-photometry	Flame AAS
10.0	9.7	9.7	97	97
10.0	9.6	9.5	96	95
10.0	9.9	9.8	99	98
10.0	9.6	9.7	96	97
10.0	9.7	9.6	97	96
Average			97 ± 2	97 ± 2

Sample volume used, 100 cm^3; Fe(II) concentration, 10 μg dm^{-3}.
[a] Fe(II) was determined by graphite furnace AAS.

After the preconcentration procedure had been carried out as described above, the column was washed with DDW in order to prevent the precipitation of magnesium and calcium ions in the methanol eluate. The methanol elution and the absorbance measurement were then performed.

In addition, another 1.0-cm^3 portion of the methanol eluate was submitted to one-drop flame atomic absorption measurement in order to confirm independently the recovery of iron(II). As can be seen from Table 3, a satisfactory recoveries were obtained with an average of 97 ± 2% for both measurements.

3.10. Analysis of sea water for iron(II)

The concentration of iron(II) in sea water collected from Tukumo Bay in Noto Peninsula National Park, about 130 km north of Kanazawa City, was determined using the proposed method.

FZ reagent was immediately added to the surface water, the pH was adjusted to 5 and the sample was filtered through a membrane filter (0.45-μm pore size) after bringing it to Noto Marine Laboratory, Kanazawa University, which is located on the coast of Tsukumo Bay. A 250-cm^3 volume of the sample was passed through the PCTFE column and processed as described above. The results are given in Table 4. The average concentration of iron(II) in the sample was 0.87 ± 0.05 μg dm^{-3}. This relatively high concentration of iron(II) may be attributed to the dissolution of iron from the many fishing vessels that are usually moored in the bay in the winter season.

Table 4
Analysis of coastal sea water for Fe(II)

Sample No.	Fe(II) concentration (μg dm^{-3})	Deviation from mean value
1	0.87	0.00
2	0.91	+0.04
3	0.81	−0.06
4	0.83	−0.04
5	0.93	+0.06
6	0.85	−0.02
7	0.92	+0.05
8	0.81	−0.06
Average	0.87	±0.05

Sample volume used, 250 cm^3.

Acknowledgements

The authors thank Mr. M. Miyamoto, Industrial Research Institute, Ishikawa, for help with the measurement of the specific surface area of PCTFE resin. This work was partially supported by a Grant-in-Aid for General Scientific Research, No. 03453041, from the Ministry of Education, Science and Culture of Japan.

References

[1] G.C. Anderson and F.M.M. Morel, Limnol. Oceanogr., 27 (1982) 789.
[2] L.E. Brand, W.G. Sunda and R.R.L. Guillard, Limnol. Oceanogr., 28 (1983) 1182.
[3] R.M. Gordon, J.H. Martin and G.A. Knauer, Nature, 299 (1982) 611.
[4] J.H. Martin and R.M. Gordon, Deep-Sea Res., 35 (1988) 177.
[5] W.M. Landing and K.W. Bruland, Geochim. Cosmochim. Acta, 51 (1987) 29.
[6] V.A. Elrod, K.S. Johnson and K.H. Coale, Anal. Chem., 63 (1991) 893.
[7] A.A. Alwarthan, K.A.J. Habib and A. Townshend, Fresenius' J. Anal. Chem., 337 (1990) 848.
[8] W.M. Landing and S. Westerlund, Mar. Chem., 23 (1988) 329.
[9] H. Hong and D.R. Kester, Limnol. Oceanogr., 31 (1986) 512.
[10] T.L. Theis and P.C. Singer, Environ. Sci. Technol., 8 (1974) 569.

[11] L.L. Stookey, Anal. Chem., 42 (1970) 779.
[12] M.M. Gibbs, Water Res., 13 (1978) 295.
[13] C.R. Gibbs, Anal. Chem., 48 (1976) 1197.
[14] C.M. Josefson and B. Johnston, Anal. Chem., 56 (1984) 764.
[15] C. Akita, K. Matsumoto and K. Terada, Anal. Sci., 3 (1987) 473.
[16] T. Yamaguchi, Z. Liping, K. Matsumoto and K. Terada, Anal. Sci., 8 (1992) 851.
[17] L.-P. Zhang and K. Terada, Anal. Sci., 10 (1994) 161.
[18] N. Yamada, B. Tomita, K. Chaya and N. Murakami, Eisei Kagaku, 38 (1992) 188.
[19] S.K. Kundra, M. Katyal and R.P. Singh, Anal. Chem., 46 (1974) 1605.

ELSEVIER

Analytica Chimica Acta 293 (1994) 319–324

ANALYTICA CHIMICA ACTA

Spectrophotometric determination of gold and palladium in anode slimes after separation with Amberlite XAD-7 resin

Latif Elçi *, Seval Işıldar, Mehmet Doğan

Department of Chemistry, Faculty of Art and Sciences, Erciyes University, 38039 Kayseri, Turkey

(Received 4th October 1993; revised manuscript received 29th November 1993)

Abstract

A procedure is described in which gold and palladium are quantitatively recovered from anode slimes using a short column with Amberlite XAD-7 resin, followed by their spectrophotometric determination as bromo complexes. Their separation was carried out in 0.4 M NaBr, 0.01 M KSCN and 0.05 M HNO_3 media. The gold and palladium concentrations in the samples were found to be 996 ± 5 and 3.7 ± 0.2 $\mu g\ g^{-1}$, respectively. The relative standard deviation of the combined dissolution, separation and determination method was ca. 5% ($n = 7$).

Key words: Spectrophotometry; Gold; Palladium; XAD-7

1. Introduction

Many elements are present in various concentrations in anode slimes obtained during the electrolytic purification of raw copper [1–3]. Because of its great monetary value, gold is usually determined in the slimes. Palladium, however, is frequently not determined. Analysis of anode slime for Au and Pd is difficult due to high concentrations of widely varying matrix elements such as Cu, Ag, Se, Sb, As and Pb, etc. Also, the determination of Au and Pd presents difficulties because the analyte concentrations are low. For the analysis of these precious metals from the matrix elements concentration and separation steps have to be incorporated.

This paper describes the spectrophotometric determination of Au and Pd as their bromo complexes in anode slimes after preconcentration or/and separation with a solid state extraction procedure using a short column filled with Amberlite XAD-7 resin in the presence of a mixture containing 0.4 M NaBr, 0.01 M KSCN and 0.05 M HNO_3.

2. Experimental

2.1. Instrumentation

A Hitachi Model 150-20 UV–visible spectrophotometer with a 10-mm quartz cell was used for absorbance measurements. The wavelengths used for Au and Pd in 0.4 M NaBr solution prepared with 0.05 M HNO_3 were 377.4 and

* Corresponding author.

SSDI 0003-2670(94)00114-2

332.7 nm, respectively. The atomic emission measurements were performed in a Jarrell Model Ash-SS-7 direct current plasma spectrometer; the elements were determined at their most sensitive lines (242.795 nm for gold, 363.470 nm for palladium).

2.2. Reagents and solutions

All chemicals were of analytical grade. Water, redistilled in a quartz apparatus, was used in all experiments. Stock solutions of Au (1000 mg l^{-1} in 5% (w/v) HCl) and Pd (1000 mg l^{-1} in 5% (w/v) HCl) were obtained from Sigma. Other stock solutions were prepared by dissolving a suitable salt of each element in water or acidic solution. Standards and model solutions were prepared by diluting stock solutions prior to use.

The resin used in the column was Amberlite XAD-7 (Merck, Darmstadt). It was purchased as 20–40 mesh, and was ground and sieved to 60–80 mesh. The resin was washed successively with methanol, water, 1 M HNO_3 in acetone, water, 1 M NaOH and water in order to remove organic and inorganic contaminants [4].

The slime samples were obtained from two copper factories in Kayseri (Turkey).

2.3. Column preparation

The stopcock of the glass column (100×10 mm) was covered with a fritted glass disc. The resin column was prepared by aspirating a water slurry of XAD-7 (400 mg) into the glass column. It was conditioned with a mixture of 0.4 M NaBr, 0.01 M KSCN and 0.05 M HNO_3. After this procedure the sample solution (< 100 ml) was passed through the column. After elution, the resin was regenerated with a large volume of acetone.

2.4. Extraction

The column was tested with model solutions (2–10 μg of Au and Pd in 25–50 ml) before starting with the analysis of anode slime samples. The model solutions were prepared with a mixture of 0.4 M NaBr and 0.01 M KSCN in 0.05 M HNO_3. It was loaded to the top of the prepared column and percolated under water aspirator vacuum at 8–10 ml min^{-1}. The adsorption can be observed by the appearance of a coloured zone at the top of the column. The column was washed with the solution used for preparation of the model solution and the retained metals were eluted into a 25 ml beaker with 8–10 ml of acetone at 3–4 ml min^{-1}. The effluent was evaporated to 1–2 ml and cooled. It was transferred into a volumetric flask and made up to 5 ml with 0.4 M NaBr in 0.05 M HNO_3. Au and Pd were determined spectrophotometrically at 377.4 and 332.7 nm, respectively. For their determination using a direct current plasma emission spectrometer, the effluent was evaporated to 1–2 ml and diluted to 5 ml with 2 M HCl.

2.5. Determination of Au and Pd in anode slime

The anode slime samples were dried at 110°C for 2 h. A 50–100 mg amount of the slime was decomposed with 10–15 ml of aqua regia and the solution was evaporated to dryness. The process was repeated twice. 10–15 ml of a mixture containing 0.4 M NaBr, 0.01 M KSCN and 0.05 M HNO_3 was added to the residue. The suspension was filtered through a filter paper, and the insoluble part was washed with the NaBr–KSCN–HNO_3 mixture. The filtrate and washings (final volume $\leqslant 100.0$ ml) in the receiving vessel were passed through the column and the analytes were determined as described above.

3. Results and discussion

3.1. Spectrophotometric determinations

The simultaneous spectrophotometric determination of palladium and gold as chloro or bromo complexes is proposed. For this purpose, the spectral characteristics of these complexes were investigated both in acetone and aqueous media. The absorption spectra of various mixtures of Au and Pd as their chloro complexes has only one maximum (338.0 nm in acetone and 286.0 nm in aqueous solution).

According to our results and those of previous workers [5–9], the determination of palladium and gold as their bromo complexes was appropriate in dilute nitric acid, because the absorption spectrum of Au and Pd bromo complex mixtures has two absorption maxima (377.4 nm for Au and 332.7 nm for Pd). At these wavelengths, absorbance values for gold and palladium were almost constant over a nitric acid concentration range of 0.03–0.06 M and over a sodium bromide concentration range of 0.20–0.50 M, decreasing at the extremes of the upper and lower concentration ranges of NaBr and HNO_3 for Au and Pd. In 0.4 M NaBr prepared in 0.05 M HNO_3, Beer's law was obeyed between 1.5×10^{-5} and 1.2×10^{-4} M Au and between 1.5×10^{-6} and 1.2×10^{-5} M Pd. The apparent molar absorptivities were 9.6×10^4 l mol^{-1} cm^{-1} for Au and 5.1×10^3 l mol^{-1} cm^{-1} for Pd in the analytical range above. The Sandell's sensitivity indexes for gold and palladium were 1.1 ng cm^{-2} and 39 ng cm^{-2}, respectively.

3.2. Effect of diverse ions on the spectrophotometric determination of gold and palladium

The influence of Cu(II) in the 0–10 g l^{-1} range and Ag(I), Se(IV), As(III), Pb(II), Sb(III) and Te(IV) in the 0–5 g l^{-1} range on the direct determination of 5×10^{-5} M Au and 5×10^{-6} M Pd was examined. These elements and their upper concentration limits were selected according to the possible composition of anode slimes [1,2]. It was found that the concentration range of 200–250 mg l^{-1} for Pb, Te, As and Sb, and the concentration values of 800 mg l^{-1} for Ag and Cu are upper limits for interferences. Below these values, interferences were observed. Selenium did not interfere up to 5 g l^{-1}. Therefore, it can be understood that the separation of gold and palladium from the matrix is necessary prior to their spectrophotometric determinations. For this purpose, a column separation method was investigated and used.

3.3. Column separation method

Au and Pd have been extracted from dilute HCl solutions or a mixed solution of HCl, KSCN, HBr and NaI by using a column filled with XAD-7 resin [9–13]. In this work, their separation was proposed from a mixture of KSCN and NaBr in dilute HNO_3. The method was optimized for various parameters such as reagent composition, sample volume, foreign ion and sample amount.

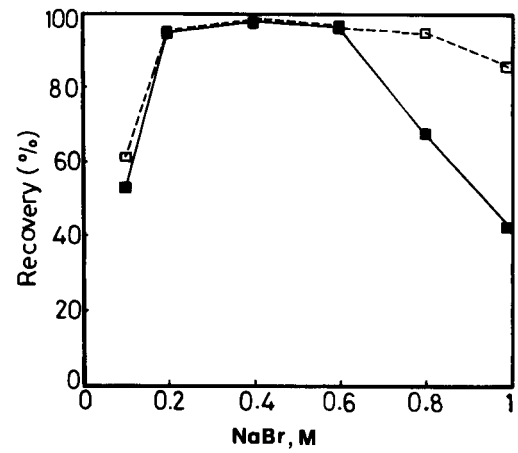

Fig. 1. Effect of NaBr concentration on the recoveries of Au (■) and Pd (□). (KSCN: 0.01 M, HNO_3: 0.05 M).

The recovery of Au and Pd was studied as a function of NaBr, KSCN and HNO_3 concentration. The results are shown in Figs. 1–3. As can be seen, quantitative recoveries ($\geqslant 95\%$) for Au and Pd were obtained with a mixture of 0.20–0.60 M NaBr, 0.005–0.050 M KSCN and 0.04–0.06 M

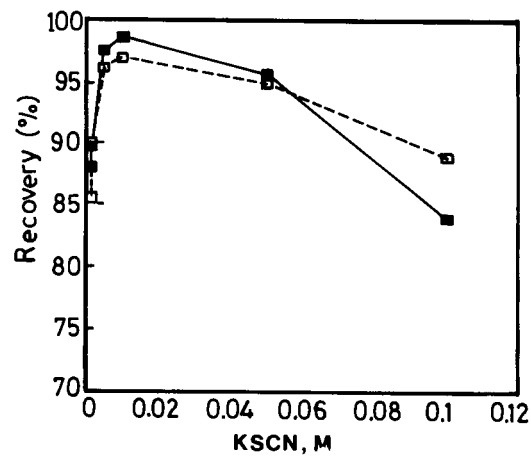

Fig. 2. Effect of KSCN concentration on the recoveries of Au (■) and Pd (□). (NaBr: 0.4 M, HNO_3: 0.05 M).

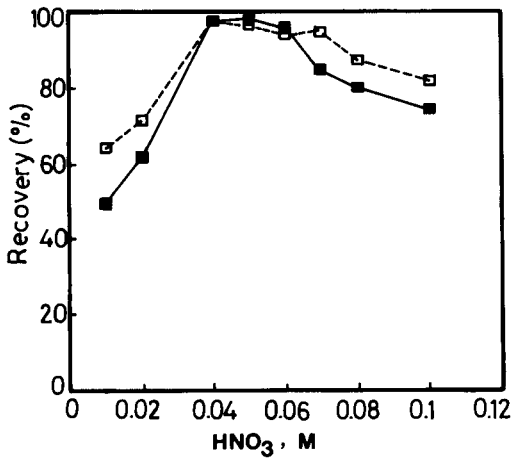

Fig. 3. Effect of HNO_3 concentration on the recoveries of Au (■) and Pd (□). (NaBr: 0.4 M, KSCN: 0.01 M).

HNO_3. The optimum conditions were taken as 0.40 M NaBr, 0.01 M KSCN and 0.05 M HNO_3.

In addition, the effect of amount of resin was examined. With increasing amount of resin up to 400 mg, the recoveries increased. The recoveries obtained with 350–400 mg of resin were approximately the same. Fig. 4 shows that quantitative retention does not occur below 350 mg of resin. If the amount is more than 450 mg, the retained metal complexes cannot be eluted completely with 10 ml of acetone. However, the gold and palladium complexes could be eluted with > 10 ml of eluent for 450 mg resin.

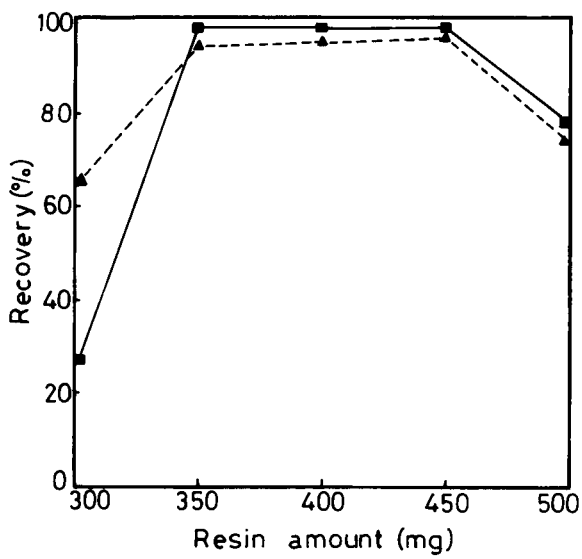

Fig. 4. Effect of amount of resin on the recoveries of Au (■), and Pd (▲) (eluent volume: 10 ml), with the optimized reagent concentration.

Table 1
Effect of sample volume on the recovery of Au and Pd (resin amount: 400 mg)

Sample volume (ml)	Recovery (%) [a]	
	Au	Pd
25.0	99±2	97±1
50.0	97±2	98±2
75.0	96±1	95±3
100.0	96±2	96±2
150.0	86±3	80±3
200.0	83±1	73±2
500.0	72±3	66±3

[a] Mean ± 95% confidence interval, $n = 7$.

The recoveries were also determined with solutions of various volumes (Table 1). Quantitative recoveries for Au and Pd were obtained with sample volumes ⩽ 100 ml.

3.4. Effect of co-existing ions on the column method

To evaluate the possibility of selective recoveries of Au and Pd in the presence of major and minor components of anode slimes, fixed amounts of Au and Pd were taken with various amounts of matrix elements following the recommended procedure. The results are summarized in Table 2. The recoveries for Au and Pd are > 95% up to the maximum tolerable concentrations of matrix

Table 2
Effect of matrix ions on the determination of Au and Pd by the recommended method

Ions	Max. tolerable conc. ($g\ l^{-1}$)	Conc. in effluent [a] ($mg\ l^{-1}$)
Cu(II)	10	22
Se(IV)	5	78
Pb(II)	5	98
Ag(I)	5	120
Te(IV)	1	50
As(III)	1	70
Sb(III)	1	65

[a] Mean of four results.

Table 3
Recoveries of Au and Pd as a function of amount of gold (Pd: 5 mg l^{-1}, sample volume: 50.0 ml)

Gold amount (μg)	Recovery (%) [a]	
	Au	Pd
100	99	96
250	97	98
500	96	95
1000	98	100
2500	97	95
5000	98	99

[a] Mean of four results.

Table 5
Recovery of Au and Pd added to sample 1 (sample amount: 75 mg)

Analyte	Amount (μg)		Error (%)
	Added	Found [a]	
Au	20.0	20.2	+1.0
	40.0	39.8	−0.5
	60.0	60.2	+0.3
	80.0	80.1	+0.1
Pd	2.0	2.0	0.0
	4.0	4.1	+2.5
	6.0	5.9	−1.7
	8.0	7.7	−3.8

[a] Mean of three results.

ions in Table 2. As can be seen, Cu, Se, Pb, Ag, Te, As and Sb did not affect the recoveries of Au and Pd even when present in large amounts. In addition, the concentrations of matrix ions in the effluent were much lower than their maximum tolerable concentrations (given above) for the direct spectrophotometric determination of gold and palladium.

Determination of Pd at trace level in the presence of a large excess of gold is important since anode slimes show relatively high gold concentrations. The results in Table 3 indicate the possibility of determining palladium in the presence of large quantities of gold. Also, the recovery of Au at these high concentrations is quantitative.

3.5. Anode slime analysis

The introduced method was applied to the determination of gold and palladium in anode slime samples. The results given in Table 4 are the mean values of determination for different sample amounts (25–100 mg). For comparison, Au and Pd in the slimes were also determined by the d.c. plasma atomic emission spectrometric technique described in the Experimental section. The results were in good agreement with the spectrophotometrically obtained concentrations. The accuracy of the results was verified by separation after addition of known amounts of gold and palladium to a sample before decomposition. The results are shown in Table 5. The added amounts of gold and palladium were recovered quantitatively.

Table 4
Gold and palladium contents of slime samples

Analyte No.	Sample	Results (μg g^{-1}) [a]	
		Spectrophotometric	DCP-AES [b]
Au	1	996 ± 5	986 ±13
	2	2801 ±12	2782 ±18
Pd	1	3.7± 0.2	3.4± 0.3
	2	n.d [c].	n.d.

[a] Mean ± 95% confidence interval, $n = 8$.
[b] d.c. plasma atomic emission spectrometry. [c] Not detectable.

4. Conclusions

The Amberlite XAD-7 column provides a simple, fairly rapid and reliable technique for the separation and determination of gold and palladium from anode slime samples. The relative standard deviations for seven experiments were 0.5–7%. The results in Tables 4 and 5 indicate a relative error of $< 4.0\%$ for both gold and palladium determinations using this method.

Acknowledgement

The authors are grateful to HES Cable Co. (Kayseri, Turkey) for supplying anode slime samples and for DCP-AES measurements.

References

[1] B. Butts, The Science and Technology of the Metal, its Alloys and Compounds, Reinhold, New York, 1984.
[2] H. Aydın and G. Somer, Talanta, 36 (1989) 723.
[3] G. Yıldırım and F.Y. Bor, Erzmetall, 4 (1985) 196.
[4] L. Elçi, M. Soylak and M. Doğan, Fresenius' J. Anal. Chem., 342 (1992) 175.
[5] Z. Marczenko, Separation and Spectrophotometric Determination of Elements, Wiley, Chichester, 1986.
[6] E.B. Sandell and H. Onishi, Photometric Determination of Traces of Metals, General Aspects, Wiley, New York, 4th edn., 1978.
[7] W.A.M. McBryde and J.H. Yoe, Anal. Chem., 20 (1948) 1094.
[8] A. Diamantatos, Anal. Chim. Acta, 63 (1973) 220.
[9] S. Işıldar, MSc Thesis, Erciyes University, Kayseri, 1992.
[10] J.S. Fritz and W.G. Millen, Talanta, 18 (1971) 323.
[11] E. Jackwerth, X.G. Yang and X.C. Xu, Fresenius' Z. Anal. Chem., 334 (1989) 514.
[12] X.G. Yang, PhD Thesis, Ruhr University, Bochum, 1989.
[13] L. Elçi, Anal. Lett., 26, (1993) 1025.

ELSEVIER

Analytica Chimica Acta 293 (1994) 325–330

ANALYTICA CHIMICA ACTA

Liquid–liquid extraction of manganese(II), copper(II) and zinc(II) with acyclic and macrocyclic Schiff bases containing bisphenol A subunits

Shigeki Abe *, Kazuhito Fujii, Tyo Sone

Department of Materials Science and Engineering (Applied Chemistry Section), Yamagata University, 992 Yonezawa, Japan

(Received 30th November 1993; revised manuscript received 31st January 1994)

Abstract

Acyclic and macrocyclic Schiff bases containing bisphenol A subunits were synthesized and the effect of ligand atoms on the liquid–liquid extraction of manganese(II), copper(II) and zinc(II) was studied. The phenol groups in the Schiff base moiety led to a large increase in the percent extraction of transition metal ions. The substitution of methoxy groups for phenolic OH ligands resulted in a marked decrease in the extractability of metal ions. Compared with a macrocyclic Schiff base, the corresponding acyclic counterpart was found to have a reasonable reactivity toward metal ions and a better solubility in organic solvents. The copper(II) complexes with acyclic Schiff bases were quantitatively extracted into nitrobenzene without the presence of bulky counter anions. Mutual separation of zinc(II), copper(II) and manganese(II) can be achieved by a proper selection of pH and extractant.

Key words: Acyclic Schiff base; Copper; Liquid–liquid extraction; Macrocyclic Schiff base; Manganese; Schiff bases; Zinc

1. Introduction

Interest in the extraction of metal ions with macrocyclic compounds has increased over the past years. Thus the extraction of alkaline earth metal ions and 'soft' metal ions are well documented in the crown ether and thiacrown ether systems, respectively. The use of nitrogen-containing macrocycles has also extended the analytical applications of extractants. Among the polyaza crown ethers studied, tetraaza and hexaaza crown ethers are the most popular extractants, which have been utilized for the extraction and spectrophotometric determination of silver(I), copper (II), zinc(II), cadmium(II), lead(II) and mercury (II) [1–3]. A major feature of metal ion extraction with hexacyclene, a nitrogen-containing analogue of 18-crown-6, was the slow complexation; it was necessary to preheat the solution for quantitative extraction purposes [3]. Besides these polyaza crown ethers, polyoxa–polyaza crown ethers [4,5], macrocyclic formazans [6] and macrocyclic Schiff bases [7–10] have also been investigated as analytical extractants. In the design of such extraction systems, the geometry and micro-environ-

* Corresponding author.

SSDI 0003-2670(94)00103-S

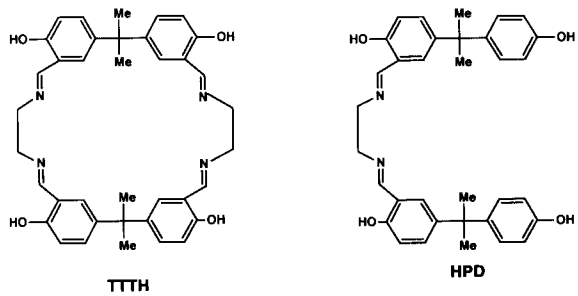

Fig. 1. Macrocyclic and acyclic Schiff bases used as extractants.

ments of the extractants are important factors for metal ion extraction processes.

In a recent study, we have introduced new types of macrocyclic Schiff bases containing either thiophene or phenol subunits as useful extractants for doubly charged transition metal ions, including zinc(II) [11]. These ligand molecules are effective for the ion-pair extraction of various metal ions. The successful applications of macrocyclic Schiff base extractants led to widespread interest in developing new mixed donor macrocyclic extractants. As a continuation of our work, some novel acyclic and macrocyclic Schiff bases were designed (as shown in Fig. 1) and their enhanced extractability was examined for manganese(II), copper(II) and zinc(II). An acyclic Schiff base containing bisphenol A subunits showed the good extractability for these metal ions and quantitative extraction of copper(II) was attained without the presence of specific counter anions.

2. Experimental

2.1. Reagents and apparatus

All reagents used were of analytical grade. Solutions of extractants were prepared by dissolving appropriate amounts of acyclic or macrocyclic Schiff bases in nitrobenzene. Tetraphenylborate (sodium salt, 1.2×10^{-2} M) was used as a counter anion. Acetate buffer (pH 3–6) and borate buffer solutions (pH 7–11) were used. The ionic strength (0.1 M) was adjusted by sodium sulphate solution.

A Hitachi Model 180-80 atomic absorption spectrometer (acetylene/air flame) was used to determine the concentration of metal ions. Spectrophotometric measurements were done with a Hitachi Model 226 spectrophotometer. A Toa HM-26S pH meter was used to measure the pH of aqueous solutions.

2.2. Preparation of macrocyclic Schiff bases

A macrocyclic Schiff base containing bisphenol A subunits, i.e., 13,13,30,30-tetramethyl-9,17,26,34-tetrahydroxy-3,6,20,23-tetraazapentacyclo-[29.3.1.$1^{8,12}$.$1^{14,18}$.$1^{25,29}$]octatriaconta-1(35),2,6,8,10,12(36),14,16,18(37),19,23,25,27,29(38),31,33-hexadecaene (TTTH), was synthesized in our laboratory according to the non-plate method [11]. Briefly, 2,2-bis(3-formyl-4-hydroxyphenyl)propane and 1,2-diaminoethane were simultaneously added to chloroform solution over a period of 12 h while stirring under nitrogen atmosphere at room temperature and the solution was further stirred for 30 h. The crude product was recrystallized from benzene and dried. The yield of TTTH was 81%; pale yellow powder, m.p. 231–234°C. Mass spectra (70 eV) m/z 616 (M^+, 7%); ^{1}H NMR ($CDCl_3$, 90 MHz) = 1.55 (12H,s), 3.82 (8H,s), 6.7–7.3 (12H,m), 8.32 (4H,s). IR (KBr), 3420, 2960, 1630, 1600, 1500, 1370, 1290, 1240, 1190 and 830 cm^{-1}. Anal. calcd. for $C_{38}H_{40}N_4O_4 \cdot H_2O$; C, 74.01%, H, 6.53%, N, 9.09%: Found; C, 73.78%, H, 6.51%, N, 8.95%.

A macrocyclic Schiff base containing methoxybenzene subunits, i.e., 13,13,30,30-tetramethyl-9,17,26,34-tetramethoxy-3,6,20,23-tetraazapentacyclo[29.3.1.1^{8,12}.1^{14,18}.1^{25,29}]octatriaconta-1(35),2,6,8,10,12(36),14,16,18(37),19,23,25,27,29(38),31,33-hexadecaene (TMTH), was prepared by [2 + 2] cyclization between 2,2-bis(3-formyl-4-methoxyphenyl)propane and 1,2-diaminoethane [12]. The crude product was recrystallized from chloroform–hexane (1:2) to give TMTH, a colourless powder, m.p. 236–238°C. Mass spectra (70 eV) m/z 672 (M, 100%); ^{1}H NMR ($CDCl_3$, 90 MHz) = 1.72 (12H,s), 3.75 (12H,s), 3.95 (8H,s), 6.50–7.20 (8H,m), 7.80–8.00 (4H,m), 8.75 (4H,s). IR (KBr), 2960, 2900, 2840, 1640, 1600, 1500, 1250, 1180, 1130 and 810 cm^{-1}. Anal. calcd. for $C_{42}H_{48}N_4O_4$

$\cdot H_2O$; C, 73.01%, H, 7.30%, N, 8.11%: Found; C, 73.19%, H, 7.11%, N, 7.66%.

2.3. Preparation of acyclic Schiff base

An acyclic Schiff base containing bisphenol A subunits, i.e., 1,6-bis{2-hydroxy-5-[2-(4-hydroxyphenyl)propane-2-yl}2,5-diazahexa-1,5-diene (HPD), was prepared according to the method described by Sone et al. [12]. The crude product was recrystallized from benzene–hexane (1 : 1) to give a yellow powder, m.p. 168–170°C. Mass spectra (70 eV), m/z 536 (M^+, 80%); ^1H NMR ($CDCl_3$, 60 MHz) = 1.58 (12H,s), 3.83 (4H,s), 6.5–7.5 (14H,m) and 8.23 (2H,s); IR (KBr), 3400, 2960, 2850, 1630, 1490, 1440, 1380 and 1360 cm^{-1}.

2.4. Extraction procedures

To 1.00 ml of the sample solution (less than 50 μg of metal ion) in a 10 ml glass-stoppered tube, the following solutions were added: 1 ml of 0.05 M buffer solution, 1 ml of 0.167 M sodium sulphate solution, 1 ml of 1.2×10^{-2} M tetraphenylborate and 1 ml of water. Then 5 ml of 1.5×10^{-3} M TTTH (or HPD) in nitrobenzene solution was added and the mixture was shaken mechanically for 20 min at room temperature. After phase separation, samples of the organic and aqueous phases were taken and the pH of the aqueous phase was measured. The metal complexes extracted in nitrobenzene were treated with concentrated nitric acid; the mixture was evaporated to dryness (three times) and the residue was dissolved in water. The metal ion concentration in organic and aqueous phases was determined by atomic absorption spectrometry.

3. Results and discussion

3.1. Comparison of acyclic and macrocyclic extractants

The extraction behaviour of typical transition metal ions, i.e., manganese(II), copper(II) and zinc(II) was studied in detail. The extraction parameters were optimized as described previously [11]. The major factors responsible for the ion-pair extraction of transition metal ions are the nature of the counter ion and of the solvent. Because of the limited solubility of the macrocyclic Schiff bases used, common solvents such as chloroform and dichloroethane were impractical. The combination of tetraphenylborate counter anion and nitrobenzene solvent provided the most efficient system for the extraction study. The organic solubility of the extractant was greatly modified by the use of the acyclic Schiff base.

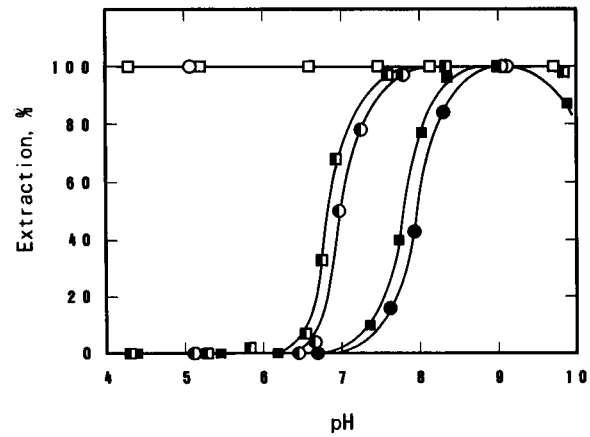

Fig. 2. Effect of pH on the extraction of Mn(II), Cu(II) and Zn(II). HPD system: ● = Mn(II); ○ = Cu(II); ◐ = Zn(II);. TTTH system: ■ = Mn(II); □ = Cu(II); ◧ = Zn(II).

The extraction curves for manganese(II), copper(II) and zinc(II) with acyclic HPD as a function of the equilibrium pH of the solution are shown in Fig. 2. For comparison, data reported for the corresponding macrocycle TTTH are included. The extraction curves of individual metal ions showed similar patterns for both extraction systems. The extraction of copper(II) with HPD was complete over a wide pH range (4–10). The extraction curve for zinc(II) lay between those of manganese(II) and copper(II). The extraction of zinc(II) became appreciable at pH > 6.5, whereas that of manganese(II) increased rapidly at pH > 7.5. Quantitative extraction was attained for zinc(II) at pH 8–10 and manganese(II) at pH 9. The slightly increased extractability observed with the macrocyclic Schiff base could be a result of stronger bonding by the nitrogen donor groups in

TTTH due to its relatively fixed sterochemistry compared with the more flexible HPD molecule. This is in agreement with previous results for the extraction with Schiff bases containing thiophene subunits [11].

In order to study the mechanism of macrocycle-based extraction, the dependence of distribution ratio (D) of copper(II) on Schiff base concentration was examined at pH 5.0. The plot of log D versus log [HPD] in the organic phase is shown in Fig. 3. In the presence of tetraphenylborate counter ions, the slope changed from 1 to 2 with increasing HPD concentrations. In contrast the slope remained 2 when tetraphenylborate counter ion was absent. As the slope corresponds to the number of HPD ligands associated with the metal ion, it is most probable that 1:2 copper(II) complexes were extracted into the organic phase. Similar results were obtained for TTTH extractant [11]. The sequence of increasing extractability ($Mn^{2+} < Co^{2+} < Ni^{2+} < Cu^{2+} > Zn^{2+}$) in the TTTH system [11] was also valid in the HPD system. Peculiarly, iron(II) extraction with TTTH or HPD was poor and about 30% of iron(II) was extracted from the aqueous solution

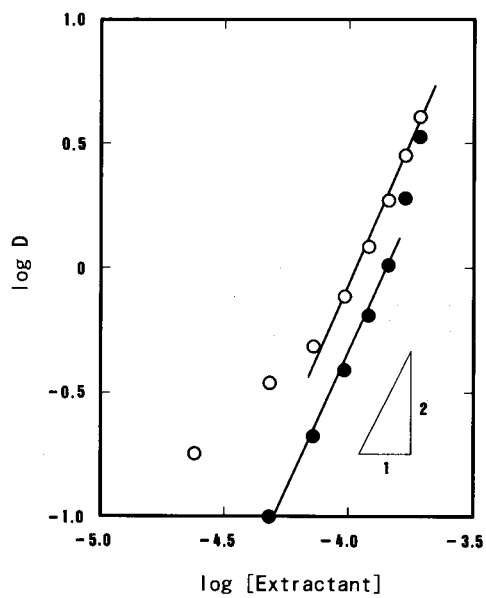

Fig. 3. Dependence of Cu(II) distribution ratio on the concentration of HPD extractant. ○ = 2.4×10^{-3} M tetraphenylborate; ● = no tetraphenylborate.

Table 1
Extraction of manganese(II), copper(II) and zinc(II) with macrocyclic TTTH and TMTH

Extractant	%Extraction (pH 9)	
	TTTH	TMTH
Metal ion		
Manganese(II)	> 99 (6)	0(0)
Copper(II)	> 99(90)	> 99(2)
Zinc(II)	> 99(74)	> 99(0)

[Extractant] = 1.5×10^{-3} M in nitrobenzene; [M^{2+}] = 50 μg/5 ml, [TPB] = 2×10^{-3} M. Values in parentheses denote the percent extractions in the absence of tetraphenylborate counter anion.

containing trichloroacetate buffer (pH 6.7); quantitative extraction of iron(II) was not attained in the pH range between 3–9. To understand the extraction behaviour of iron(II), more detailed studies are in progress.

3.2. Comparison of ligand atoms

Structural variations within macrocycles are known to affect markedly the extraction efficiency of metal ions. To clarify the role of phenol groups in the Schiff base moiety, a new macrocyclic ligand having methoxybenzene subunits (TMTH) was designed. It contains the same 26-membered rings as TTTH and has a fixed cavity of same size. TMTH also acted as an extractant, although it is less effective for the extraction of transition metal ions. The results are shown in Table 1.

The dependence of copper(II) extraction on the TTTH and TMTH concentrations is shown in Fig. 4. A large difference in the coordinating ability of these ligands was obvious. Copper(II) was extracted with less excess of extractant in the TTTH system. Thus the extraction of copper(II) with TTTH was quantitative above 3×10^{-4} M TTTH, whereas no copper(II) was extracted at this TMTH concentration, indicating that TTTH binds with copper(II) more strongly than TMTH; the latter has no available coordinating oxygen atom. TMTH alone showed no ability to extract manganese(II) and zinc(II) under the experimental conditions. In the presence of tetraphenylborate, the zinc(II)–TMTH complex was quantita-

tively extracted from weakly alkaline solution. In contrast, the least stable manganese(II) complex was not extracted (cf. Table 1). When the pH of aqueous phase was lowered to 5, only copper(II) continued to show quantitative results. Mutual separation of manganese(II), copper(II) and zinc(II) can be achieved with the use of TMTH extractant.

The importance of nitrogen ligand atoms and phenolic oxygen donor groups in the Schiff base moiety is clearly seen by comparing TTTH with its reduced analogue (13,13,30,30-tetramethyl-9,17,26,34-tetrahydroxy-3,6,20,23-tetraazapentacyclo-[29.3.1.1^{8,12}.1^{14,18}.1^{25,29}]octatriaconta-1(35),2,6,8,10,12(36),14,16,18(37),19,23,25,27,29(38),31,33-hexadecane, TTTO). This tetraaza crown ether was prepared by the reduction of TTTH with lithium aluminium hydride. Both extractants showed a marked difference in the extractability of metal ions. The disappearance of double bonded nitrogen (–N=CH–) led to a large decrease in the percent extraction of metal ions. Thus copper(II) was not quantitatively extracted by TTTO even in the presence of bulky counter anions. A tetraoxo analogue of TTTH has also been designed; this compound, however, did not extract manganese(II), copper(II) and zinc(II) at all. These facts agreed with the previous finding

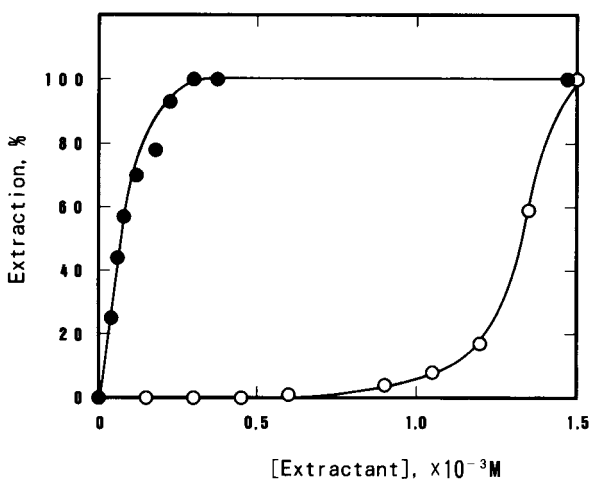

Fig. 4. Effect of extractant concentration on Cu(II) extraction. ○ = TMTH system (pH 5.0); ● = TTTH system (pH 5.0).

Table 2
Effect of coexisting anions on copper(II) extraction [a]

Cu(II) salt	Anion/Cu (mole ratio)	% Extraction	
		HPD	TTTH
Chloride	2	> 99	92
	20 [b]		93
Nitrate	2	> 99	92
	20 [b]		> 99
Sulphate	1	> 99	88
	10 [b]		98
Acetate	2	> 99	> 93

[a] [Extractant] = 1.5×10 M^{-3} in nitrobenzene; [Cu^{2+}] = 1.57×10^{-4} M, pH of aqueous phase after equilibrium = 3.7–4.0.
[b] Excess of anions was added as Na salt.

that crown ethers have no tendency for coordinating to transition metal ions.

Extraction systems that do not require specific counter anions have been reported for some ionizable crown ethers [13] and thiacrown ethers [14]. In previous work, we found that about 90% of copper(II) was extracted by TTTH alone. Preliminary experiments showed that 74 and 90% of zinc(II) were extracted by TTTH and HPD, respectively, in the absence of tetraphenylborate (cf. Table 1). To confirm the extraction mechanism, a range of less bulky counter anions has been examined, e.g. Cl^-, NO_3^- and SO_4^{2-}. Almost all copper(II) was extracted by HPD regardless of the anion present, even at the stoichiometric amount of copper(II) and anion as shown in Table2. In the more rigid TTTH extraction system, the presence of less bulky counter anions was also effective for copper(II) extraction. The use of acetate did not depress the results obtained in the tetraphenylborate anion system. These facts indicated that the phenolic OH groups in the Schiff base moiety contributed to the ion-pair extraction of metal ions, eliminating the need for addition of bulky counter anions. The coordination of pendant phenolate groups to metal ions has been proved in an earlier study of extraction with monoaza-15-crown derivatives [15].

3.3. Extraction spectrophotometry of manganese(II)

The coloured manganese(II)–HPD complexes were useful for the extraction spectrophotometric

determination of manganese. A 1:2 stoichiometry has been confirmed by the log D versus log [HPD] plot. The apparent molar absorptivity of manganese(II) complexes with acyclic Schiff base HPD was 5.4×10^3 l mol^{-1} cm^{-1} at the absorption maximum of 435 nm. Beer's law was obeyed over the range from 1–7 μg ml^{-1} manganese(II). The absorbance of the organic phase was found to remain constant by maintaining the measuring cell at 37°C. The organic extracts, however, became appreciably turbid on standing at room temperature. Application to real samples is under progress.

4. Conclusions

Extraction of manganese(II), copper(II) and zinc(II) with acyclic and macrocyclic Schiff base has been examined. Mixed donor types of Schiff bases containing bisphenol A subunits are very useful extractants for transition metal ions. The tendency of coordination by the nitrogen atom was most important for the extraction of metal ions; the phenolic OH groups in the Schiff base moiety additionally contributed to the complexation and extraction of transition metal ions. Compared with macrocyclic Schiff bases, the acyclic counterpart is characterized by easy preparation, reasonable reactivity toward metal ions and better solubility in organic solvents. The coloured Schiff base–manganese(II) complex is useful for the extraction spectrophotometry of manganese.

Acknowledgement

The authors acknowledge the technical assistance of Kazuaki Sato in synthesizing the macrocyclic and acyclic Schiff bases.

References

[1] W. Szczepaniak, B. Juskowiak and W. Ciszewska, Anal. Chim. Acta, 156 (1984) 235.
[2] Z. Brzozka and Z. Trybulowa, Anal. Chim. Acta, 172 (1985) 257.
[3] S. Arpadjan, M. Mitewa and P.R. Bontchev, Talanta, 34 (1987) 953.
[4] T. Kumamaru, Y. Nitta, H. Matsuo and E. Kimura, Bull. Chem. Soc. Jpn., 60 (1987) 1930.
[5] M.K. Beklemishev, L.I. Gorodilova, N.I. Shevtsov, L.M. Kardivarenko and N.M. Kuzmin, Zh. Anal. Khim., 44 (1989) 1058.
[6] N.V. Isakova, Yu.A. Zolotov and V.P. Ionov, Zh. Anal. Khim. 44 (1989) 1045.
[7] M. Fujiwara, T. Matsushita and T. Shono, Polyhedron, 3 (1984) 1357.
[8] E.I. Morosanova, Yu.A. Zolotov, V.A. Bodnya and A.A. Formanovskii, Mikrochim. Acta [Wien], III (1984) 389.
[9] Yu.A. Zolotov, E.I. Morosanova, S.G. Dmitrienko, A.A. Formanovskii and G.V. Ivanov, Mikrochim. Acta [Wien], III (1984) 399.
[10] N.V. Isakova, Yu.A. Zolotov and V.P. Ionova, Zh. Anal. Khim. 44 (1989) 859.
[11] S. Abe, T. Sone, K. Fujii and M. Endo, Anal. Chim. Acta, 274 (1993) 141.
[12] T. Sone, Y. Ohba, F. Nishino and S. Yamanami, Supramolecular Chem., 2 (1993) 47.
[13] J. Tang and C.M. Wai, Anal. Chem., 58 (1986) 3233.
[14] M. Muroi, A. Hamaguchi and E. Sekido, Anal. Sci., 2 (1986) 351.
[15] Y. Katayama, R. Fukuda and M. Takagi, Anal. Chim. Acta, 185 (1986) 295.

ELSEVIER

Analytica Chimica Acta 293 (1994) 331–333

ANALYTICA CHIMICA ACTA

AUTHOR INDEX

Analytical Applications of Circular Dichroism

Edited by **N. Purdie** and **H.G. Brittain**

Techniques and Instrumentation in Analytical Chemistry Volume 14

Circular dichroism is a special technique which provides unique information on dissymmetric molecules. Such compounds are becoming increasingly important in a wide variety of fields, such as natural products chemistry, pharmaceutics, molecular biology, etc. The content of this book has been selected in order to feature the unique aspects of circular dichroism, and how these strengths can be of assistance to workers in the field.

Substantial discussions have been provided regarding the particular phenomena associated with dissymmetric compounds which give rise to the circular dichroism effect. Reviews are also given of the type of instrumentation available for the measurement of these effects. A number of chapters cover the wide range of applications illustrating the power of the method.

Owing to its broad appeal, the book will be of interest to workers in all areas of chemistry and pharmaceutical science.

Contents:

© 1994 360 pages Hardbound
Price: Dfl. 355.00 (US $ 202.75)
ISBN 0-444-89508-6

ORDER INFORMATION

For USA and Canada
ELSEVIER SCIENCE INC.
P.O. Box 945
Madison Square Station
New York, NY 10160-0757
Fax: (212) 633 3880

In all other countries
ELSEVIER SCIENCE B.V.
P.O. Box 330
1000 AH Amsterdam
The Netherlands
Fax: (+31-20) 5862 845

US$ prices are valid only for the USA & Canada and are subject to exchange rate fluctuations; in all other countries the Dutch guilder price (Dfl.) is definitive. Customers in the European Community should add the appropriate VAT rate applicable in their country to the price(s). Books are sent postfree if prepaid.

ELSEVIER SCIENCE B.V.

Experimental Design: A Chemometric Approach

Second, Revised and Expanded Edition

By **S.N. Deming** and **S.L. Morgan**

Data Handling in Science and Technology Volume 11

Now available is the second edition of a book which has been described as
"...an exceptionally lucid, easy-to-read presentation... would be an excellent addition to the collection of every analytical chemist. I recommend it with great enthusiasm."
(Analytical Chemistry).
N.R. Draper reviewed the first edition in Publication of the International Statistical Institute
"...discussion is careful, sensible, amicable, and modern and can be recommended for the intended readership."

The scope of the first edition has been revised, enlarged and expanded. Approximately 30% of the text is new. The book first introduces the reader to the fundamentals of experimental design. Systems theory, response surface concepts, and basic statistics serve as a basis for the further development of matrix least squares and hypothesis testing. The effects of different experimental designs and different models on the variance-covariance matrix and on the analysis of variance (ANOVA) are extensively discussed. Applications and advanced topics (such as confidence bands, rotatability, and confounding) complete the text. Numerous worked examples are presented.

The clear and practical approach adopted by the authors makes the book applicable to a wide audience. It will appeal particularly to those with a practical need (scientists, engineers, managers, research workers) who have completed their formal education but who still need to know efficient ways of carrying out experiments. It will also be an ideal text for advanced undergraduate and graduate students following courses in chemometrics, data acquisition and treatment, and design of experiments.

Contents:

© 1993 454 pages Hardbound
Price: Dfl. 310.00 (US$ 177.25)
ISBN 0-444-89111-0

ELSEVIER SCIENCE

ORDER INFORMATION
ELSEVIER SCIENCE B.V.
P.O. Box 330
1000 AH Amsterdam
The Netherlands
Fax: (+31-20) 5862 845
For USA and Canada
P.O. Box 945
Madison Square Station
New York, NY 10159-0945
Fax: (212) 633 3680

US$ prices are valid only for the USA & Canada and are subject to exchange rate fluctuations; in all other countries the Dutch guilder price (Dfl.) is definitive. Customers in the European Union should add the appropriate VAT rate applicable in their country to the price(s). Books are sent postfree if prepaid.

PUBLICATION SCHEDULE FOR 1994

	J	F	M	A	M	J	J	A	S	O	N	D
Anal. Chim. Acta	284/3 285/1–2 285/3	286/1 286/2 286/3	287/1–2 287/3 288/1–2	288/3 289/1 289/2	289/3 290/1–2 290/3	291/1–2 291/3 292/1–2	292/3 293/1–2 293/3	294/1 294/2 294/3	295/1 295/2 295/3	296/1–2 296/3 297/1–2	297/3 298/1 298/2–3	299/1 299/2–3 300/1
Vib. Spec.	6/2		6/3		7/1		7/2		7/3		8/1	

INFORMATION FOR AUTHORS

Detailed "Instructions to Authors" for *Analytica Chimica Acta* was published in Volume 289, No. 3, pp. 381–384. Free reprints of the "Instructions to Authors" of *Analytica Chimica Acta* and *Vibrational Spectroscopy* are available from the Editors or from: Elsevier Science B.V., P.O. Box 330, 1000 AH Amsterdam, The Netherlands. Telefax: (+31-20) 5862459.

Manuscripts. The language of the journal is English. English linguistic improvement is provided as part of the normal editorial processing. Authors should submit three copies of the manuscript in clear double-spaced typing on one side of the paper only. *Vibrational Spectroscopy* also accepts papers in English only.

Rapid publication letters. *Letters* are short papers that describe innovative research. Criteria for letters are novelty, quality, significance, urgency and brevity. Submission data: max. of 2 printed pages (incl. Figs., Tables, Abstr., Refs.); short abstract (e.g., 3 lines); *no* proofs will be sent to the authors; submission on floppy disc; *no* revision will be possible.

Abstract. All papers and reviews begin with an Abstract (50–250 words) which should comprise a factual account of the contents of the paper, with emphasis on new information.

Figures. Figures should be prepared in black waterproof drawing ink on drawing or tracing paper of the same size as that on which the manuscript is typed. One original (or sharp glossy print) and two photostat (or other) copies are required. Attention should be given to line thickness, lettering (which should be kept to a minimum) and spacing on axes of graphs, to ensure suitability for reduction in size on printing. Axes of a graph should be clearly labelled, along the axes, outside the graph itself. All figures should be numbered with Arabic numerals, and require descriptive legends which should be typed on a separate sheet of paper. Simple straight-line graphs are not acceptable, because they can readily be described in the text by means of an equation or a sentence. Claims of linearity should be supported by regression data that include slope, intercept, standard deviations of the slope and intercept, standard error and the number of data points; correlation coefficients are optional.

Photographs should be glossy prints and be as rich in contrast as possible; colour photographs cannot be accepted. Line diagrams are generally preferred to photographs of equipment. Computer outputs for reproduction as figures must be good quality on blank paper, and should preferably be submitted as glossy prints.

Nomenclature, abbreviations and symbols. In general, the recommendations of IUPAC should be followed, and attention should be given to the recommendations of the Analytical Chemistry Division in the journal *Pure and Applied Chemistry* (see also *IUPAC Compendium of Analytical Nomenclature, Definitive Rules*, 1987).

References. The references should be collected at the end of the paper, numbered in the order of their appearance in the text (*not* alphabetically) and typed on a separate sheet.

Reprints. Fifty reprints will be supplied free of charge. Additional reprints (minimum 100) can be ordered. An order form containing price quotations will be sent to the authors together with the proofs of their article.

Papers dealing with vibrational spectroscopy should be sent to: Dr J.G. Grasselli, 150 Greentree Road, Chagrin Falls, OH 44022, U.S.A. Telefax: (+1-216) 2473360 (Americas, Canada, Australia and New Zealand) or Dr J.H. van der Maas, Department of Analytical Molecular Spectrometry, Faculty of Chemistry, University of Utrecht, P.O. Box 80083, 3508 TB Utrecht, The Netherlands. Telefax: (+31-30) 518219 (all other countries).

0003-2670/94/$07.00

(∞) The paper used in this publication meets the requirements of ANSI/NISO 239.48-1992 (Permanence of Paper).

PRINTED IN THE NETHERLANDS

Flow-Through (Bio)Chemical Sensors

By **M. Valcárcel** and **M.D. Luque de Castro**, Department of Analytical Chemistry, University of Córdoba, 14004 Córdoba, Spain

Techniques and Instrumentation in Analytical Chemistry Volume 16

Flow-through sensors are more suitable than classical probe-type sensors for addressing real (non-academic) problems. The external shape and operation of flow-through (bio)chemical sensors are of great practical significance as they facilitate sample transport and conditioning, as well as calibration and sensor preparation, maintenance and regeneration, all of which result in enhanced analytical features and a wider scope of application. This is a systematic presentation of flow-through chemical and biochemical sensors based on the permanent or transient immobilization of any of the ingredients of a (bio)chemical reaction (i.e. the analyte, reagent, catalyst or product) where detection is integrated with the analytical reaction, a separation process (dialysis, gas diffusion, sorption, etc.) or both.

The book deals critically with most types of flow-through sensors, discussing their possibilities and shortcomings to provide a realistic view of the state-of-the-art in the field. The large numbers of figures, the wealth of literature references and the extensive subject index complement the text.

Contents: 1. Sensors in Analytical Chemistry. Analytical chemistry at the turn of the XXI century. Analytical information. What is a sensor? Sensors and the analytical process. Types of sensors. General features of (bio)chemical sensors. (Bio)chemical sensors and analytical properties. Commercial availability. Trends in sensor development. **2. Fundamentals of Continuous-Flow (Bio)Chemical Sensors.** Definition. Classification. The active microzone. Flow-through cells. Continuous configurations. Regeneration modes. Transient signals. Measurement modes. The role of kinetics. Requirements for proper sensor performance. **3. Flow-Through Sensors Based on Integrated Reaction and Detection.** Introduction. Flow-through sensors based on an immobilized catalyst. Flow-through immunosensors. Flow-through sensors based on an immobilized reagent. Flow-through sensors based on an *in situ* produced reagent.

ELSEVIER SCIENCE

4. Flow-Through Sensors Based on Integrated Separation and Detection. Introduction. Integrated gas diffusion and detection. Integrated liquid-liquid separation and detection. Integrated retention and detection. Flow-through sensors for multideterminations based on integrated retention and detection. Ion-selective electrodes (ISEs) and ion-sensitive field-effect transistors (ISFETs). **5. Flow-Through Sensors Based on Integrated Reaction, Separation and Detection.** Introduction. Integration of gas-diffusion, reaction and detection. Integration of dialysis, reaction and detection. Integration of sorption, reaction and detection. **Index.**

© 1994 332 pages Hardbound
Price: Dfl. 355.00 (US$ 202.75)
ISBN 0-444-89866-2

ORDER INFORMATION
ELSEVIER SCIENCE B.V.
P.O. Box 330
1000 AH Amsterdam
The Netherlands
Fax: (+31-20) 5862 845

For USA and Canada
P.O. Box 945
Madison Square Station
New York, NY 10159-0945
Fax: (212) 633 3680

US$ prices are valid only for the USA & Canada and are subject to exchange rate fluctuations; in all other countries the Dutch guilder price (Dfl.) is definitive. Customers in the European Union should add the appropriate VAT rate applicable in their country to the price(s). Books are sent postfree if prepaid.